PASSIVITY-BASED CONTROL OF MULTIPLE QUAD-COPTERS WITH A CABLE-SUSPENDED PAYLOAD

PASSIVITY-BASED CONTROL OF MULTIPLE QUAD-COPTERS WITH A CABLE-SUSPENDED PAYLOAD

BY

KEYVAN MOHAMMADI, M.Sc., B.Sc.

A THESIS

SUBMITTED TO THE DEPARTMENT OF ELECTRICAL & COMPUTER ENGINEERING

AND THE SCHOOL OF GRADUATE STUDIES

OF MCMASTER UNIVERSITY

IN PARTIAL FULFILMENT OF THE REQUIREMENTS

FOR THE DEGREE OF

DOCTOR OF PHILOSOPHY

Doctor of Philosophy (2021) McMaster University

(Electrical & Computer Engineering) Hamilton, Ontario, Canada

TITLE:	Passivity-Based Control of Multiple Quad-Copters With A Cable-Suspended Payload
AUTHOR:	Keyvan Mohammadi M.Sc./B.Sc. (Electrical and Computer Engineering), Amirkabir University of Technology/ K.N.Toosi University of Technology, Tehran, Iran
SUPERVISOR:	Prof. Shahin Sirouspour
NUMBER OF PAGES:	xix, 165

Lay Abstract

Aerial robots can offer an effective solution to many existing transportation challenges as they do not rely on infrastructures or labour work. Battery-powered drones can autonomously transport objects with absolutely zero emissions. However, a single drone has limited lifting capacity and is highly susceptible to failures. One solution is to employ a team of quad-copters to cooperatively carry a cable-suspended payload. For such a scalable system, the number of quad-copters can be simply found based on the size and weight of the package. In this thesis, simple and robust motion controllers are proposed to safely transport a cable-suspended payload. The controllers are further extended to guarantee inter-drone collision avoidance. They are also capable of suppressing effects of disturbances such as wind. Furthermore, the design allows for arbitrary attachment points on both drones and the payload. All the control strategies have been successfully implemented and evaluated in an indoor laboratory setting.

Abstract

This thesis proposes several motion controllers to allow multiple quad-copters cooperatively carry a cable-suspended payload. The problem is motivated by a desire for developing a resilient scalable delivery vehicle that can be easily customized to its payload. The control problem poses a number of challenges that complicate its design. These include the quad-copter under-actuation, non-rigidity of the cables that connect the payload to the copters, external disturbances, potential for inter-drone collisions, and communication time-delay among the quad-copters. Simple robust controllers with guaranteed stability are highly desirable in such safety critical applications.

In this thesis, the energetic passivity property of the multi-body system combining the quad-copters, cables and payload is employed to design novel motion controllers for the system. These controllers make no assumption about the tension status of the cables since this property holds whether the cables are in tension or not. The design and stability analysis of the controllers rely on storage functions inspired by the physical energy of the system. Quad-copters are able to produce thrust force only along their propellers' axis. This under-actuation prevents direct application of passivity-based controllers to the system under study. A cascade control structure with an outer-loop position control and an inner-loop attitude control is employed to

deal with the under-actuation.

The first proposed controller assumes that the cables are attached to the quad-copters center of masses (COMs). This helps decouple the angular dynamics of the quad-copters from the rest of the dynamics. As a result, the inner-loop attitude controllers can be designed independently. First, angular controllers with exponentially stable tracking errors are considered. While this produces nice theoretical results, it requires measurements of linear acceleration and jerk, limiting its practical use. Then, a modified cascade control structure is proposed that takes into account the under-actuation and only needs measurements that are typically available in such systems. Semi-global stability of the closed-loop system is shown, where the region of attraction can be made arbitrary large by proper choice of control gains. An energy observer/compensator is proposed to estimate perturbation-induced energy and dissipate it through time-varying dampers. This helps suppress disturbance-induced oscillations in the system response.

The proposed controller is further revised to allow the cables be attached to the quad-copters and the payload at arbitrary points. This controller is augmented with an inter-drone collision avoidance term to prevent potential collisions among the drones. Another variation of the controller is developed by introducing inter-drone coupling terms meant to improve the controller ability to preserve the formation shape of the quad-copters. These coupling terms could potentially introduce time delay into some of the feedback signal paths. An analysis is carried out to establish conditions that the controller gains must satisfy in order to ensure closed-loop stability in the presence of these time delays.

The final contribution of this thesis focuses on the design of the reference positions for the quad-copters for the use in the controllers introduced earlier. In the proposed approach, the user specifies the desired position and orientation for the payload. Given this desired pose, an optimization problem is formulated to find a set of reference positions for the quad-copters that would minimize the total power consumed under quasi-static conditions.

The proposed controllers have been successfully evaluated in an indoor laboratory setting using measurements from a motion capture system and on-board IMUs. Results of the experiments are provided throughout the thesis.

To my beloved wife

Sara

&

To my dearest parents

Gity & Daryoush

Acknowledgements

I would like to express my sincerest gratitude to my supervisor, Dr. Shahin Sirouspour, for his technical guidance and continuous support throughout my Ph.D. studies. This research could not have moved forward without his insightful attitude and profound scientific vision.

My deepest appreciation goes to my Ph.D. committee members, Dr. Tim Davidson and Dr. Christopher Swartz for their constructive feedback. Their thoughts and comments significantly improved this research.

I would like to thank all my fellow colleagues in Telerobotics, Haptics and Computational Vision Laboratory from whom I learned a lot during our theoretical and experimental discussions.

To my family and friends, I am truly thankful for your support and encouragements throughout my entire education. You are always the most invaluable asset in my life and I am deeply pleased to have you.

Last but not least, I would like to thank to my beloved wife, Sara, who was always there for me with endless love. I could never have accomplished this journey without her unconditional support.

Contents

Lay Abstract **iii**

Abstract **iv**

Acknowledgements **viii**

1 Introduction **1**

1.1 Motivation 3

1.2 Problem Statement 5

1.3 Thesis Contributions 8

1.4 Thesis Organization 12

1.5 Related Publications 13

2 Literature Review **15**

2.1 Energetic Passivity 16

2.2 Passivity-Based Control 17

2.3 Position Control of Quad-Copters 20

2.4 Payload Transportation 23

2.5 Summary 30

3 System Modeling **31**

3.1 Modeling Assumptions 31

3.2 Kinematics 32

3.3 Equations of Motion 33

3.4 Energetic Passivity 35

3.5 Summary 39

4 Decentralized Passivity-Based Control **40**

4.1 The Proposed Controller 41

4.2 Stability Analysis 45

4.3 Experimental Validation 48

4.4 Summary 50

5 Modified Cascade Structure and Disturbance Attenuation **53**

5.1 Mathematical Preliminaries 54

5.2 Modified Cascade Structure 56

5.3 Stability Analysis 60

5.4 Disturbance Attenuation 63

5.5 Experimental Validation 67

5.6 Summary 76

6 Shifted Attachment Points **78**

6.1 Control Design 79

6.2 Experimental Validation 90

6.3 Summary 104

7 Cooperative Control with Time Delay **106**

7.1 Mathematical Preliminaries 107

7.2 Control Design and Stability Analysis 109

7.3 Experimental Verification 119

7.4 Summary 124

8 Formation Shape Design **126**

8.1 Optimal Formation Shape and Reference Trajectories 127

8.2 Experimental Results 134

8.3 Point Mass Payload 136

8.4 Summary 139

9 Conclusion **141**

9.1 Future Work 143

A Details on proof for Theorem 5 **146**

B Numerical Value of P Matrix **150**

List of Figures

1.1 Three quad-copters with a cable-suspended payload in a laboratory setting. 4

2.1 Feedback interconnection of two systems. 19

2.2 Cascade structure for position control of a single quad-copter 21

3.1 Schematic of the aerial transportation system with the motion variables defined. There are no restrictions on the cable attachment points, i.e., they are not limited to the COMs. 32

4.1 Experimental setup with a three-drone payload transport system. . . 49

4.2 Snapshots of different phases of the experiment. 50

4.3 The aerial transportation system moves the payload from $q_{L_0} = [0.6, -0.3, 0]$ to $q_{L_f} = [-1.15, -1.4, 0]$. 51

4.4 Payload attitude angles during the flight. Some initial swings are observed during take-off but the payload remains fairly stable throughout the entire trajectory. 51

5.1 Force error due to under-actuation: μ_i is the desired force and f_i is the actual force along the thrust direction; δ_i is the error. 59

5.2 The experimental setup with three quad-copters carrying a cable-suspended payload. 67

5.3 Trajectories of three quad-copters and payload for an M-shaped desired reference in the first experiment. The beginning and end points of UAV1 are marked by purple and orange arrows, respectively. The reference trajectory for UAV1 is depicted by a dashed gray line. . . . 69
5.4 Position tracking errors when following the M-shaped trajectory. Blue, black and green plots correspond to UAV1, UAV2 and UAV3, respectively. 70
5.5 Payload orientation during the M-shaped trajectory in the first experiment. 70
5.6 Thrust forces versus time. The first and last two-second segments correspond to the ramp-up and ramp-down phases of the propellers. . 71
5.7 The drones and payload positions in the second experiment. 71
5.8 The output of the time-domain disturbance energy observer. The energy remains nearly constant in the absence of disturbances but increases after the application of each disturbance. Five disturbances were applied to the payload in this experiment. 72
5.9 The value of disturbance attenuation damping for each quad-copter during the second experiment. 73
5.10 Graphical illustration of dissipation time T_{dis}. The red star is the nominal position q_{nom_i} and the sphere represents $\|q_i - q_{nom_i}\| \leq 0.05$. The UAV is initially at a hovering position shown by the black square. It leaves the sphere due to the application of the perturbation and eventually returns to and stays inside it because of energy dissipation by the controller. 74

5.11 Position of the first UAV in the presence of wind disturbance. The blue plot is the controller in Chapter 4 and the red plot is the proposed controller. 75

5.12 Position of the second UAV in the presence of wind disturbance. The blue plot is the controller in Chapter 4 and the red plot is the proposed controller. 75

5.13 Position of the third UAV in the presence of wind disturbance. The blue plot is the controller in Chapter 4 and the red plot is the proposed controller. 76

6.1 Block diagram of the proposed control system for n UAVs. The thick red and black lines represent the translational and angular measurements, respectively. The set N_i includes the neighbors of the ith UAV. 90

6.2 The trajectories of the drones and the payload during the flight. Note that the payload position is measured only for illustration and is not used in the controller. 92

6.3 The response of passivity observer/controller. At around $t = 7$ sec, the cables status changes from slack to taut. This is when the drones start to ascend and the payload suddenly leaves the ground. As a result, abrupt forces and moments are exerted on the quad-rotors leading to potential active behavior by the nominal controller. This is immediately remedied by the passivity observer/controller. 93

6.4 Plots of the thrust forces of the quad-rotors. The first and last four-second segments correspond to the ramp-up and ramp-down phases of the propellers. 94
6.5 Distances between drones throughout the square-shaped trajectory. The red lines represent the minimum distances which are set to $r = 0.65$ m for all the constraints. 94
6.6 Payload attitude angles throughout the square-trajectory flight. Except a few spikes, the rest of the flight has an acceptable swing range. 95
6.7 Quad-rotors position errors while following the square-trajectory. The blue, red and black belong to quad-rotor 1, 2, and 3, respectively. . . 95
6.8 The trajectories of the drones and the payload during the second set of experiments where the payload is subject to 20 perturbations. The flight is about 90 second long at a constant altitude. The ascending and landing phases are excluded from the plots to better display the response to the disturbances. 96
6.9 Distances between drones in the second scenario where the payload is subject to 20 perturbations and $k_{d_{ij}} = 0$. The red lines represent the minimum distances which are set to $r = 0.65$ m for all the constraints. Note that the minimum set distance is satisfied throughout the flight. 97
6.10 The output of the passivity observer in the second experiment scenario. This is used for introducing additional damping in the system. Note that positive values indicate active behavior which is quickly remedied by the controller. 98

6.11 The values of time-varying dampers used to compensate for active behavior in the system during the second experiment scenario. 98
6.12 The distances between the drones in the second experiment scenario using the controller in Chapter 4. Note that the distance between the second and third drones falls below the safety threshold a number of times during the experiment. 99
6.13 The distances between the drones while the payload was perturbed for 20 times by a wooden stick. The inter-drone damper $k_{d_{ij}} = 0.9$ eliminates the oscillations induced by the barrier terms. The drones maintain the minimum safety distance throughout the experiment. . . 100
6.14 Aggressive butterfly-shaped desired trajectories for the three quad-copters. 101
6.15 Desired velocity of the formation in the aggressive maneuver experiment. 102
6.16 Desired acceleration of the formation in the aggressive maneuver experiment. 102
6.17 UAV 1 - Desired and measured positions in the aggressive maneuver . 103
6.18 UAV 2 - Desired and measured positions in the aggressive maneuver . 103
6.19 UAV 3 - Desired and measured positions in the aggressive maneuver . 104
7.1 Steps taken to prove closed-loop stability using Theorem (1). 113
7.2 Positions of the UAVs and the payload with time-delayed coupling terms in control. 121
7.3 Position versus time for Quad-copter 1. The red and blue show the desired and measured signals, respectively. 122

7.4 Position versus time for Quad-copter 2. The red and blue show the desired and measured signals, respectively. 122
7.5 Position versus time for Quad-copter 3. The red and blue show the desired and measured signals, respectively. 123
7.6 The positions of the drones and the payload with the new controller with inter-drone coupling terms. The first quad-copter was pulled away from its position twice with the aid of a rope attached to it. 124
7.7 3D positions of the aerial transport system with the fully decentralized controller of Chapter 4. An extra rope attached to UAV 1 was pulled twice during the experiment. 125
8.1 Schematic of the aerial transportation system where the cables are attached to the COM of the UAVs. 131
8.2 Snapshot of experiment with the whiteboard payload. 134
8.3 Positions of the UAVs and the cable-suspended payload during a hovering. The whiteboard payload experience significant swings and never reaches an equilibrium. 135
8.4 Orientation of the whiteboard payload while hovering. 136
8.5 Positions of the UAVs and the cable-suspended payload while hovering for 25 seconds with the formation obtained from optimization. 137
8.6 Position of the payload (blue) throughout a 25 seconds hovering experiment. The reference position (red) is $q_{L_d} = [0 \;\; 0 \;\; 0.6]^{\mathrm{T}}$. 138
8.7 The optimal and three arbitrary reference formation shapes. The star, circle and cross symbols denote the reference positions for the first, second and third UAVs, respectively. 139

8.8 Power consumption of the four formation shapes over during a 25-second hovering flight. Note that since UAVs are identical, $\xi_1 = \xi_2 = \xi_3$.140

List of Tables

5.1 Average value of the dissipation time over eight applications of perturbation. 74

5.2 Maximum value of dissipation time over eight applications of perturbation. 75

6.1 Minimum distance (in meters) between the drones in the second experiment scenario. 98

6.2 The average values of the distances (in meters) between the drones in the second experiment scenario. 99

8.1 Comparison of power usage for four different formations. The last column represents an index (i.e. $\sum_{i=1}^{3} \frac{\mathcal{P}_i}{\xi} = \sum_{i=1}^{3} f_{i_{ss}}^{1.5} = \sum_{i=1}^{3} \|\mu_{i_{ss}}\|^{1.5}$) for power consumption of the system during a 25-second hovering flight. 139

Chapter 1

Introduction

Transportation is a vital component of every economy as its role is beyond shipment of goods and moving people from one place to another. An efficient transportation system would lead to significant economic growth and productivity. Hence, policy-makers are always looking into better transportation solutions that not only boost economic developments, but also meet the future needs [16, 18]. So far transportation systems have seen disruptive revolutions. From the invention of the wheel to the airplane, each technology has remarkably changed human lifestyles. Nowadays, many shipping and courier services deliver commercial, medical and food products to local stores or residential addresses and our lives rely heavily on their performance.

Although conventional means of transportation seem functional in many cases, they suffer from severe shortcomings to meet certain demands and standards. First of all, they are highly dependent on infrastructures such as roads, highways, airports and railways. This would make it difficult to access some remote and rural areas if the logistics are not available. Secondly, they are highly susceptible to congestion and traffic jams which can severely impact delivery time. Cities and metropolitan

areas are expanding exponentially and 68% of the world population will live in urban communities by 2050 [64]. This will further exacerbate the ongoing problem of traffic congestion and air pollution [26]. Thirdly, they are highly reliant on manual labour force for all phases of operation and support. During the COVID-19 pandemic, employees of shipping and delivery services had to often work in unsafe conditions to keep the supply chain open [14]. New advances and innovations in the transportation sector are required to help address these short and long-term concerns.

Unmanned Aerial Vehicles (UAVs) are flying robots that can operate either autonomously or by a teleoperator [7]. They are divided into two main categories, i.e, fixed-wing and rotary-wing UAVs. The latter has the capability to take off and land vertically whereas a fixed-wing drone requires a runway. Rotary-wing UAVs can hover and perform complex maneuvers which make them ideal for civil and robotics applications [67]. Among them, multi-rotor UAVs such as quad-copters and hexa-copters have been popular due to their low development and operation cost, simplicity and agility. There are a number of reasons that make multi-rotor UAVs particularly attractive for use in transportation, including:

- Compared with conventional ground-based goods delivery systems, multi-rotor UAVs are much less reliant on civilian infrastructure such as roads and bridges. Their vertical take-off and landing capability gives them advantage over their fixed-wing counterparts [28].

- They can significantly reduce delivery times by avoiding traffic congestion. This would ultimately decrease the energy cost.

- Battery-powered drones can reduce pollutant emissions [9].

- The operation of UAV transportation systems can be automated to a high degree in order to reduce human labour costs.

Aside from postal services and e-commerce retailers, several other sectors are also exploring the use of drones for delivery of emergency and medical supplies [92, 90, 88]. In emergency and disaster recovery scenarios, UAVs can quickly deliver vital medical and food supplies since ground access to the site is usually very limited [88].

Aerial transport vehicles use built-in containers, grippers or cables to carry their payload. A built-in container or a gripper increases the vehicle inertia and reduces its attitude agility [90] whereas carrying the payload through cable suspension preserves the vehicle agility. This thesis focuses on the motion control problem of an aerial transport system in which multiple conventional quad-copters cooperatively carry a cable-suspended payload.

1.1 Motivation

Despite its clear advantages, transporting a cable-suspended payload with a *single* quad-copter has two major shortcomings. First, the flight time is usually short due to the limited energy capacity of the battery, although this might not be a serious concern for short-range deliveries [42, 62]. The second issue concerns small payload capacity. While the payload capacity can be increased by using larger motors, propellers, and batteries, such an approach would inevitably lead to design compromises. A quad-copter with capacity to carry the heaviest payload would be very inefficient when used to deliver smaller items. Large drones are also less agile and harder to control in confined environments [62].

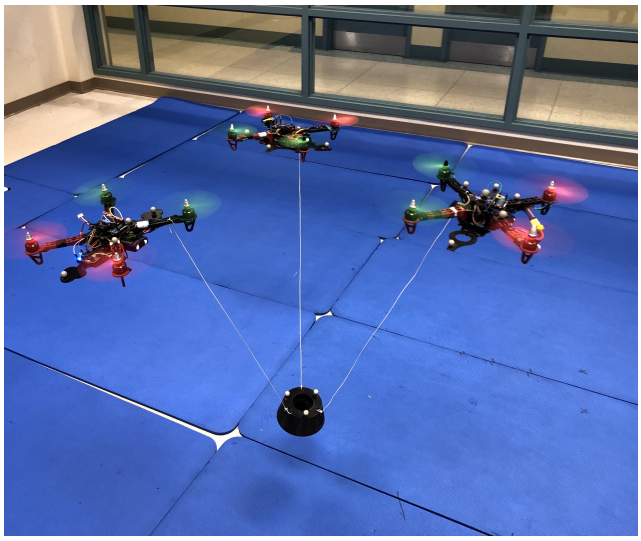

Figure 1.1: Three quad-copters with a cable-suspended payload in a laboratory setting.

The limited capacity problem can be solved by employing a number of quad-copters to cooperatively transport the payload. Figure 1.1 shows an experimental setup with three quad-copters lifting a cable-suspended payload. This approach potentially yields a number of benefits, including:

- **Scalability**: The payload capacity can be easily scaled up or down by adding or removing drones to and from the system [62, 33].
- **Fault Tolerance**: The system using multiple drones has some inherent fault tolerance as it may still be able to operate if one or more of the drones fail [57]. Obviously, this would depend on the number of functioning drones and may require some adjustments in the controller.
- **Improved Payload Control**: Having multiple attachment points on the payload allows for better control of the payload pose and its swing movements compared to the case where the payload is suspended by a single cable [59].

- **Cost Efficiency**: In general, it is more cost effective to develop and maintain multiple smaller UAVs than a larger UAV for a given desired payload capacity [4].
- **Safety**: Accidents are sometimes inevitable and smaller drones tend to pose to lower safety risk than larger ones in the event of a crash.

Cooperative systems have received much attention in the robotics community well beyond the transportation application. The system considered in this thesis can also serve more broadly as a platform for experimenting with advanced control algorithms [90]. It also has utility for research in the areas of sensing, estimation [84], path finding and trajectory planning [83].

1.2 Problem Statement

This thesis is concerned with the motion control problem of a cable-based multi-drone load transport system. This is an under-actuated mechanical system with non-rigid links connecting rigid bodies. There are significant gaps in the existing literature that need to be addressed before such transport systems can be used in practice.

The first challenge relates to the under-actuation of quad-copters. This type of UAV is typically equipped by four propellers with parallel axes. This arrangement generates torques around all three axes but a net thrust force only along the propellers main axis [34]. Cascade structures are commonly used for the position control of quad-copters. In this structure, an outer position control loop generates the desired thrust magnitude as well as angular reference commands. The attitude reference commands are passed to an inner-loop controller which would generate the required torques.

The net thrust and torques are then converted to the required thrust forces for the individual motors.

In a standard command following control problem, the reference command and its derivatives are exogenous inputs to the system. However, in a cascade control structure the references of the inner loop controller are generated from the measurements in the outer loop. So if derivatives of the references are used in the inner-loop controller, that could usually require derivatives of measurements which are not directly available. Numerical differentiation of the measurements could lead to excessive noise or lag and stability issues so it is not a preferable solution for this problem. Therefore, inner-loop attitude controllers that avoid derivatives of the angular reference commands are highly desirable [63]. The difficulty is to guarantee the stability of the closed-loop system in the absence of those derivatives. When the cable attachment points are shifted from the centre of mass (COM) of the quad-copters, the angular and translational dynamics of the vehicles become coupled, significantly complicating the controller design and stability analysis. Consequently, new or substantially-modified controllers must be devised for quad-copters with shifted attachment points.

Cable flexibility introduces another challenge in the motion control problem of the cable-based aerial transportation system. Most of the prior work on the subject inaccurately treats the cables as rigid links, assuming they are always in tension [48]. Although this assumption greatly simplifies the design and analysis of the controller, it is one that is hard to guarantee under all operating conditions. Cables may easily lose their tension due to external disturbances and aggressive maneuvering, or throughout transitory phases of the flight such as take-off and landing [62]. Thus, it is critical to eliminate this limiting assumption in the design of the controller.

External disturbances such as wind are prevalent in outdoor environments. These unwanted inputs disrupt the formation shape, and induce oscillations and payload swings [63]. Large payload swings are generally undesirable in transportation applications and must be avoided. Hence, the third challenge is to ensure robustness of the controller with respect to external perturbations. Additionally, disturbance-induced oscillations have to be sufficiently suppressed.

Given the close proximity of the drones while carrying the payload, inter-drone collisions are of concern. This issue is particularly relevant in the presence of large perturbations and during transitory phases of operation. The controller must incorporate an effective collision avoidance strategy such that a safe distance is always maintained among the quad-copters.

Inter-drone communication can help improve the performance of the controller in maintaining drones formation. In general communication among agents can lead to better stability margins and enhanced robustness to external disturbances [69]. Inter-drone communication may be subject to time delays which may compromise closed-loop control stability, if not properly addressed.

The last challenge concerns the formation shape design. Battery-powered quad-copters have notoriously short flight time. The formation shape directly impacts the amount of the thrust each quad-copter contributes to the lifting of the payload and hence its power consumption. With an ill-designed formation shape one or more quad-copters may disproportionately contribute to the lift force leading to premature depletion of their battery energy. Therefore, the formation shape must be designed in such a way to ensure that the load is equitably shared among the drones.

1.3 Thesis Contributions

The goal of this thesis is to develop stable motion controllers for a system of multiple quad-copters cooperatively carrying a cable-suspended payload. These controllers must avoid unrealistic assumptions about system model and available feedback measurements, and also be simple and robust for use in such safety-critical real-time control application. The controllers proposed here exploit the energetic passivity property of the combination of the drones, cables, and payload. Energetic passivity holds regardless of tension status of the cables, as this fundamental property is founded on the principle of energy conservation. The proposed controllers require no measurement from the payload.

The proposed controllers have a cascaded structure. Nominal outer-loop proportional-derivative (PD) controllers are considered for each drone. PD controllers establish a passive mapping from velocity to force, which is compatible with a passivity-based design philosophy. However, PD controllers cannot be fully implemented due to the quad-copters' under-actuation. In simple terms, the control force generated by the PD controller cannot be instantaneously realized since it would not be necessarily aligned with the direction of the propeller axis. Therefore, adjustments are needed to ensure the closed-loop stability.

First, assuming the cables are attached to the COM of quad-copters, an attitude controller is designed such that it aligns the direction of thrust with the desired output force of the outer-loop PD position controller with an exponentially fast convergence. The combination of the outer-loop PD and inner-loop attitude controller yields bounded tracking errors with time-varying reference positions for the quad-copters. The proposed controller is decentralized in the sense that it requires no inter-drone

communication of feedback measurements. Its closed-loop stability is shown using a Lyapunov analysis.

Although the idea of perfect attitude tracking seems a viable solution in theory, it is not realizable in practice. Exponential stability of attitude tracking errors require reference angular velocity and acceleration. These signals contain linear acceleration and jerk feedback terms making them unsuitable for practical use. Hence, a modified attitude controller is proposed to eliminate the reference angular velocity and acceleration commands. A detailed stability analysis is provided to demonstrate semi-global exponential stability of the tracking errors. The stability is shown to be robust with respect to bounded disturbance forces acting on the quad-copters and the payload. Additionally, a time-domain observer estimates the energy that perturbations may inject to the system and dissipates it through variable damping. This helps suppress disturbance-induced oscillations.

The next contribution relaxes the assumption on attaching the cables to the COM of quad-copters. In this case, it is not possible to independently analyze the stability of the attitude tracking errors as the translational and angular dynamics would become coupled. The outer-loop PD controllers are augmented with time-varying dissipative terms to account for the drones under-actuation. A storage function is defined that includes terms inspired by the kinetic and potential energies of the system components as well as virtual energy of the controller. A time-domain passivity observer is used in conjunction with an adaptive dissipative term to ensure that the value of the storage function is continuously decreased and hence, guarantees closed-loop stability. In this framework, a passivity-based controller is considered for the angular motion as well. This eliminates the need for system parameters such as the moment of inertia in the

controller.

A collision avoidance strategy is integrated in the proposed passivity-based control scheme to establish a minimum safe distance among the quad-copters. The stability of the closed-loop system with this safety constraint has been proven using a modified storage function that includes a Barrier Lyapunov candidate. The collision avoidance controller generates repulsive forces that would help maintain the safe inter-drone distances.

Simplicity and robustness are highly desirable features of passivity-based controllers. However, a fully decentralized passivity-based controller may not be very effective in preserving the formation shape in response to external perturbations. This is because each drone controller would only react to local position tracking errors and is unaware of the neighboring drones positions. A revised controller is introduced that incorporates coupling terms among the drones in order to help better preserve the formation shape. However, this requires exchange of position measurements among the drones, which could be subject to communication time delay. Lyapunov-Krasovskii functionals have been employed to derive sufficient conditions for closed-loop stability in the presence of these time delays. These conditions establish guidelines for selecting the controller gains.

The proposed controllers assume that the desired formation shape of quad-copters are provided indirectly through the reference position commands to the individual drones. Given the flexibility available in choosing these references, the question naturally arises as to how they should be selected. In this thesis, the reference positions for the quad-copters are obtained by formulating and solving an optimization problem. The objective is to minimize the total power consumption for holding the payload

under quasi-static conditions in order to maximize the flight time. This is the power that the quad-copters spend to simply balance the payload against gravity. The constraints in the optimization problem arise from the equations of static equilibrium, kinematic constraints imposed by the cables, and the inter-drone minimum safe distance requirement.

The formation optimization requires information from the payload. The load size, geometry, and the position of the attachment points directly impact the optimal formation shape. If not available, these parameters have to be estimated experimentally. A calibration process is proposed for this purpose. During the calibration, the quad-copters fly with the payload in an arbitrary formation. The position data collected from the flight is then used in a least-squares estimation of the payload parameters.

The unique features and capabilities of the proposed controllers in this thesis are summarized below:

- The controllers make no assumption about the cables being in tension as they rely on the energetic passivity property of the multi-body mechanical system. This fundamental property holds regardless of the status of the cables tension.
- Unlike most prior work, the controllers consider a rigid body payload model as opposed to a point mass model.
- The controllers require no feedback measurement from the payload.
- Both decentralized and distributed control architectures have been proposed and analyzed.
- A modified inner-loop attitude controller is proposed which eliminates reference angular velocity and acceleration commands. This helps eliminate the need for

linear acceleration and jerk measurements.

- Disturbance-induced oscillations are attenuated using an energy observer and damping injection.
- A variation of the controller is developed where the cable attachment points are not limited to the drones COMs. This provides greater flexibility in configuring the drones for carrying the payload.
- The controller is augmented with a term to avoid inter-drone collisions. This is achieved using a Barrier Lyapunov function.
- Formal proofs of stability are given for all the proposed control strategies, where the quad-copter under-actuation is taken into account.
- A method is proposed for minimizing the total power consumption by optimizing the formation shape for a given desired payload position and orientation.
- The effectiveness of the control strategies is demonstrated in several indoor experiments using a three-drone payload transport system.

1.4 Thesis Organization

The rest of this thesis is organized as follows. Chapter 2 surveys the state-of-the-art in motion control of aerial transportation systems. Chapter 3 is concerned with system modeling including kinematics, dynamics and energetic passivity property. It also outlines the assumptions made throughout the thesis. Chapter 4 presents a decentralized motion controller for the case when cables are attached to the COM of

drones. A cascade structure is considered in which the angular error dynamics of the inner-loop controller are exponentially stable. Chapter 5 improves on this decentralized controller by eliminating the need for the first and second-order derivatives of the attitude commands in the inner-loop attitude controller. The controller stability and its robustness to disturbances are analyzed. A novel centralized disturbance attenuation scheme is introduced to suppress oscillations and payload swing. In Chapter 6, the controller is revised to allow for shifted cable attachment points. The concepts of passivity observer and controller are used to deal with this problem. Safety constraints are introduced to avoid inter-drone collisions. A Lyapunov-based barrier function is added to the nominal storage function to integrate these safety constraints into the design. Chapter 7 introduces a distributed variant of the controller with possible time delays in the inter-drone communications. A detailed proof of stability is provided using a Lyapunov-Krasovskii functional. Chapter 8 introduces formation shape optimization and an experimental method to estimate the payload parameters. The thesis is concluded in Chapter 9 where some avenues for future work are also considered.

1.5 Related Publications

1.5.1 Journal Papers

- K. Mohammadi, S. Sirouspour, and A. Grivani, "Formation Shape and Control in Cable-Based Aerial Transportation Systems", *to be submitted* to IEEE Transactions on Control Systems Technology.

- K. Mohammadi, S. Sirouspour, and A. Grivani,"Passivity-Based Control of Multiple Quad-Rotors Carrying a Cable-Suspended Payload", *Accepted*, IEEE/ASME Transactions on Mechatronics.

- K. Mohammadi, S. Sirouspour, and A. Grivani. "Control of Multiple Quad-Copters With a Cable-Suspended Payload Subject to Disturbances." IEEE/ASME Transactions on Mechatronics 25.4 (2020): 1709-1718.

1.5.2 Conference Paper

- K. Mohammadi, M. Jafarinasab, S. Sirouspour, and E. Dyer. "Decentralized motion control in a cabled-based multi-drone load transport system." 2018 IEEE/RSJ International Conference on Intelligent Robots and Systems (IROS). IEEE, 2018.

Chapter 2

Literature Review

Real world autonomous delivery is not achievable unless a robust position control scheme is developed for the unmanned vehicles. The position controller must receive the desired trajectory of the system and safely transport the payload to its destination along this trajectory.

This chapter reviews the literature pertinent to the topic of thesis research. It begins by looking at the advantages of using the energetic passivity property of mechanical systems for their control. This is followed by a review of passivity-based controllers and their application. The rest of this chapter focuses on the state of the art in control of quad-copters with or without a payload. The third section explores the position control of a single quad-copter with no payload. Next, motion control of a single quad-copter with a cable-suspended payload is surveyed. This part of the review is divided into two parts as some papers have considered closed-loop control over the payload while others addressed the problem with only UAV feedback measurements. Finally, papers on motion control of multiple quad-copters with a cable-suspended payload are reviewed, where some of the deficiencies of the existing

methods have been highlighted.

2.1 Energetic Passivity

The use of inverse dynamics along with a stabilizing controller has been popular for control of fully-actuated dynamical systems. The first part of such controller cancels out the inherent dynamics of the system while the latter shapes the closed-loop characteristic to satisfy certain stability and performance requirements [36]. From a Lyapunov-based control design perspective, the inverse dynamics transforms the time-derivative of a Lyapunov function into inner product of two vectors: state variables and complementary control inputs. Although this technique has been exploited in many control systems [10, 78, 65], its practical use is limited as it requires perfect knowledge of the system dynamics.

The energetic passivity of mechanical systems opens up a path for designing simple robustly stable controllers. For the so-called *passive* systems, the maximum energy that can be extracted from the system is not more than the supplied energy [29]. In other words, the rate of change in the system total energy is less (or at most equal to) than the supplied power to it. Picking the physical storage function of the system as the Lyapunov candidate, the energy rate would be upper bounded by inner product of generalized velocity and the control inputs. This is a similar result to what was achieved after applying inverse dynamics. However, it is achieved through a natural property of the system instead of exerting any control actions. This passivity property holds irrespective of the values of the system parameters. Therefore, it provides a means for designing controllers that are robust with respect to estimation errors or changes in these parameters [47].

The energetic passivity has been an indispensable tool for the design of robot control systems [47]. These include controllers for rigid manipulators [70], teleoperation systems [68], parallel robots with elastic cables [40], spacecrafts [19] and wheeled mobile robots [46]. The design of passivity-based controllers is relatively straightforward, often utilizing energy shaping methods to achieve a desired performance while ensuring closed-loop stability [35].

2.2 Passivity-Based Control

There is a connection between the passivity concept, which is fundamentally an input/output property and Lyapunov stability, which is an internal stability concept. For a closed-loop system, the Lyapunov stability approach requires that a positive definite function of the states to decrease monotonically along the system trajectories. In passivity-based control, the system to be controlled is passive with respect to its input and output port variables. This means that the rate of change in the *physical* storage function of the plant is upper bounded by the power supplied through input-output ports.

Now, if the passive plant is connected in feedback form to an energetically passive controller, then the resulting feedback connection preserves passivity as well. To show this analytically, consider the feedback interconnection of two systems in Figure 2.1. A passive plant with input e_1 and output y_1 can be described mathematically as [39],

$$\text{Plant:} \begin{cases} \dot{x}_1 = f_1(x_1, e_1) \\ y_1 = h_1(x_1, e_1) \end{cases} \tag{2.1}$$

where there exists a positive semidefinite storage function V_1 such that [29],

$$\dot{V}_1 \leq y_1^{\mathrm{T}} e_1 \tag{2.2}$$

Similarly, a passivity-based controller can be represented as follows,

$$\text{Controller:} \begin{cases} \dot{x}_2 = f_2(x_2, e_2) \\ y_2 = h_2(x_2, e_2) \end{cases} \tag{2.3}$$

Consider V_2 as the storage function of the control action. Then, the following storage function can be defined for the whole feedback interconnection,

$$V_T \triangleq V_1 + V_2 \tag{2.4}$$

It follows from taking the time derivative of (2.4) along the system trajectories that,

$$\dot{V}_T \leq e_1^{\mathrm{T}} y_1 + e_2^{\mathrm{T}} y_2 = (u_1 - y_2)^{\mathrm{T}} y_1 + (u_2 + y_1)^{\mathrm{T}} y_2 = u_1^{\mathrm{T}} y_1 + u_2^{\mathrm{T}} y_2 \triangleq u^{\mathrm{T}} y \tag{2.5}$$

where the passivity property of each system was exploited and $u \triangleq \begin{bmatrix} u_1 \\ u_2 \end{bmatrix}$, $y \triangleq \begin{bmatrix} y_1 \\ y_2 \end{bmatrix}$. If the exogenous inputs of the system are zero, i.e. $u = 0$, then it follows from inequality (2.5) that,

$$\dot{V}_T \leq 0 \tag{2.6}$$

This implies internal stability of the feedback interconnection in Lyapunov sense.

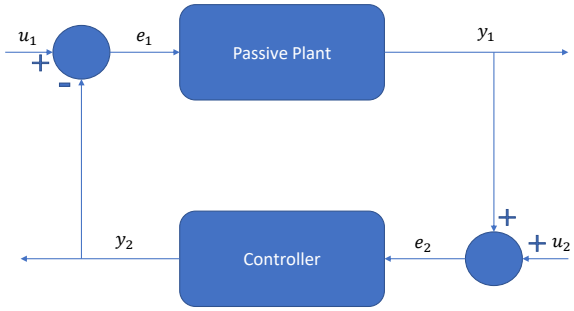

Figure 2.1: Feedback interconnection of two systems.

Hence, Lyapunov stability and passivity concept are highly correlated.

The simplest passivity-based controller that satisfies all the above conditions is the ubiquitous PD compensator. The proportional term acts as a virtual spring force to bring the system close to the desired reference command. The derivative term injects dissipation as it behaves like a damper. The first part is the negative of the gradient of a quadratic spring-type potential field. The damping term is to force the energy to reach its minimum as time tends to infinity.

Passivity-based controllers have been applied to both manipulators and mobile robots. Ortega and Spong designed an adaptive passivity-based motion controller for rigid manipulators [70]. Nuno *et al.* proved PD controllers can globally stabilize time-delayed bilateral teleoperation systems under certain gain conditions. Brogliato *et al.* applied passivity-based controllers to flexible joint manipulators to achieve global tracking performance [6]. A similar strategy has been used for underwater mobile robots considering a multiplicative input uncertainty [23]. See [29] for more applications of passivity-based controllers. Prior work on passivity-based control of UAVs will be discussed later in this chapter.

2.3 Position Control of Quad-Copters

Cascade control structures are popular whenever two feedback loops have significantly different response time. This structure allows for initial independent design of controllers for each loop without considering their interaction. Then, certain conditions can be imposed on the coupling terms to ensure closed-loop stability of the interconnected system [77]. This idea goes back to the theory of singular perturbation, mostly known as time-scale separation principle [56, 66].

The outer loop in position control of quad-copters requires translational position measurements. Motion capture system in indoor lab settings or Global Positioning System (GPS) in outdoor environments can provide this information. The inner loop is an attitude controller which typically has a higher control update rate because of the availability of high-rate IMU-based attitude measurements. This is in contrast with the lower update rates of motion capture and GPS systems. Figure 2.2 demonstrates a cascade position controller for a single quad-copter. The reference position and yaw angle trajectories are the inputs of this control system. The outer loop receives the position measurements and generates desired angles and thrust commands for the inner-loop controller. This is to generate a desired net force for the quad-copter based on the position tracking errors. The attitude measurements are fed back to the inner loop where the angular controller is implemented.

The first position control strategy accompanied with a formal proof of stability was proposed in [37] where a linear growth condition for the interconnection term was given. This term is basically the force error due to under-actuation. In this work, PD controllers with feedforward terms are designed separately for both loops.

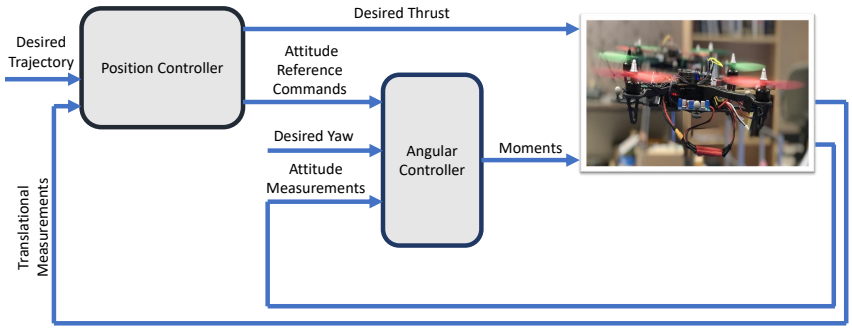

Figure 2.2: Cascade structure for position control of a single quad-copter

In [93], the performance of PD controllers was improved by augmenting online estimation of parametric uncertainty and the external disturbance upper-bound. In particular, aerodynamic coefficients were considered constant or slow-varying and were estimated by adaptation laws. In [75], a continuous sliding-mode control with finite-time convergence was proposed for position control of quad-copters. Although sliding-mode control is generally robust with respect to uncertainties and perturbations, it suffers from high frequency *chattering* [39]. The problem still exists even with high-order sliding mode controllers since finite-time convergence controllers include non-Lipschitzian switching functions with discontinuity in the origin [89]. In [52] another robust hierarchical strategy for position control of quad-copters was proposed. The control law consists of a nominal PD and a disturbance observer scheme. The observer employs a low-pass filter to avoid acceleration measurements. Although the proposed method is theoretically interesting, it is not generally straightforward to tune the cut-off frequency of its low-pass filter.

Aside from nonlinear control techniques, optimization-based control laws have been also considered for position control of quad-copters. In particular, researchers

have been looking into approaches such as Model Predictive Control (MPC) to minimize a certain cost function while enforcing state and input constraints. The control inputs of a quad-copter can easily hit the saturation levels due to limited throttle range. This highlights the need to impose input constraints in the control design process [41]. See [1, 5] for applications of MPC in quad-copters.

The orientation of a rigid-body can be expressed based on a variety of representations including Euler angles, quaternions and rotation matrices. Among them, Euler angles are intuitive and simple. However, they exhibit singularities in certain configurations [13]. Although Euler-angle-based attitude controllers works perfectly well for conditions near hovering or smooth trajectories, they are unsuitable for aggressive maneuvers of quad-copters. Hence, an innovative geometric tracking controller was proposed in [49] where it not only avoids singularity, but also guarantees the closed-loop system stability. Additionally, satisfactory experimental results were reported for highly aggressive trajectories [58]. Aggressive maneuvers, however, are uncommon in aerial transportation. These systems have to follow smooth reference trajectories to ensure the package is transported safely. Therefore, Euler angles representation should suffice for this particular application.

All the aforementioned cascade position controllers work based on attitude controllers with exponentially converging angular tracking errors. To achieve this, these controllers require the desired angular velocity and acceleration, which in turn include the linear acceleration and jerk of quad-copters. In practice, these signals are noisy and in the case of jerk not directly measured [63]. A controller with no use of desired angular acceleration was introduced and implemented in [58]. However, the paper provided no mathematical proof of the system stability.

2.4 Payload Transportation

Each payload has to be carried with special considerations and requirements. For instance, commercial goods are predominately in solid form and packaged in a way that can be safely transported without precise load control. For such payloads, it would be sufficient to close the feedback loop over the UAV. Since the parcel is constrained to the drone via cable attachments, its position is restricted to a close proximity of the vehicles. Once the drones arrive at their final destination, they can safely deploy their payload without the need for precise control of its position or orientation. On the other hand, the full pose of some payloads have to be constantly controlled while being transported. For instance, carrying payloads containing liquids requires direct control of position and specially orientation. While having precise control over the payload may be a nice feature, it could unnecessarily complicate the hardware and control algorithm requirements. In particular,

- It would require measuring the position and orientation of the payload. While this might be straightforward in indoor lab settings with a motion capture system, it would be far more challenging in outdoor environments. A possible solution is to use vision systems such as stereo cameras [38]. However, it would increase the processing time and computational cost.

- It would require knowledge of the payload's geometry and dynamics. While many researchers assumed a point mass model for the payload, e.g., see [50, 33], a rigid-body representation is needed for orientation control. To carefully address the load control problem for a rigid-body object, it is integral to know its parameters including mass, the moment of inertia and the centre of mass.

Moreover, the length of cables has to be known.

- It would require the cables to be always in tension in order to maintain control over the load. Slack cables cannot exert the desired forces and moments for a precise load control. Although this constraint can be considered in online trajectory planning, it is difficult to guarantee it in real world applications where the payload could be subject to wind and other disturbances.

- It would significantly complicate the control design problem. The payload position control problem would add another layer to the aforementioned cascade architecture [84, 82]. The first layer requires the payload velocity and passes the commanded payload orientation to the second stage which involves the third derivative of the payload position. The second layer generates the desired attitude for quad-copter which includes the fifth derivative of payload position. These high-order measurements are not directly available and would be excessively noisy if computed numerically.

It is therefore prudent to consider full pose control only in applications that definitely benefit from it. For delivery of commercial parcels, precise control of the payload trajectory is mostly unnecessary and is forgone in the interest of controller simplicity and robustness.

2.4.1 Indirect Payload Control - Single Quad-Copter

In this part, papers on motion control of aerial transportation systems are reviewed where the control loop is closed over the UAVs. The survey starts with the control of a single quad-copter carrying a cable-suspended payload and then expands to of

multiple quad-copter delivery systems. The goal here is mostly to guarantee safety and robustness rather than accurate trajectory following for the payload.

The authors in [12] proposed a hybrid model of a single quad-copter with a cable-suspended payload. The control design has been restricted to the planar case. An extension of this work to three dimensional space was presented later where a hybrid nonlinear controller was designed for the outer loop [11]. Although the hybrid modeling of this study is comprehensive, the control design lacks a proof of stability.

In [50], the authors obtained system dynamics using the Lagrange method. They modeled the cables as rigid links. This assumption can be easily violated particularly during the take-off and landing phases of the flight or in the presence of external disturbances [63]. Furthermore, only a constant reference position is considered in this work. The method was later extended to include adaptive compensation for aerodynamic damping coefficients [51]. Moreover, the overshoot of the vehicle was ensured to remain within a certain prescribed range.

A damping assignment passivity-based controller was proposed in [25] to suppress payload swing. The swing can be particularly problematic for a payload with a single attachment point as it may introduce oscillations and even instability in the system. While consistent with the under-actuation of the payload, the method has some notable shortcomings. It models the cables as rigid links and considers only the motion in the longitudinal plane. With similar assumptions, a feedback linearization with PD control was proposed in [24] where a small angle approximation is used near hovering condition. The controller was augmented with a state observer to estimate the swing angle and its derivative.

External disturbances and perturbations complicate stabilization of a UAV with

a cabled-based suspended load. An adaptive compensator for unknown constant was introduced in [43] where a PID-like controller was combined with a swing suppression strategy. Although the paper provides a formal proof of stability, it neglects the under-actuation force error of the vehicle. Moreover, it assumes the cables remain taut throughout the whole flight.

Increasing the number of attachment points can generally improve controllability over the payload [59]. A novel suspension mechanism was proposed in [8] where a payload is attached to a single quad-copter via four cables. The coupling forces and moments between the payload and the UAV were treated as bounded disturbances. Then, a robust sliding-mode controller was developed for both loops to overcome the adverse effects of these perturbations. The angular controller includes a signum function with arguments of angular velocity error. Such discontinuity in the control signal is generally undesirable.

Another interesting direction of research was pursued in [73] where guidance and control laws were proposed for soft landing of a point mass payload. That is to achieve zero payload velocity when a fragile cable-suspended payload touches the ground. Although shifted attachment point was initially included in the model, it was ultimately ignored in the design of the controller. A state-feedback controller based on a linearized model was developed for the outer loop. The guidance strategy was tested in both simulation and experiment.

2.4.2 Indirect Payload Control - Multiple Quad-Copters

Some of the advantages of cooperative aerial transportation were mentioned in the first chapter of this thesis. Prior work on such systems without feedback from payload

is review in this section.

A decentralized velocity synchronization scheme was proposed in [87] where the cables are modeled as rigid links. An adaptive term was added to equally distribute the payload weight among the UAVs. The stability analysis was carried out assuming fully-actuated agents. Simulation results were provided where the payload forces were modeled as spring forces.

In [44], a cooperative passivity-based control strategy was proposed to achieve a desired formation shape while carrying a suspended payload. The cables were modeled as rigid links. The formation controller is augmented with adaptation laws to compensate for point-mass payload forces. The controller was validated in outdoor experiments. A detailed stability proof was provided where the agents were considered as fully-actuated. Moreover, the cable forces were assumed to be constant throughout the whole mission. This assumption ignores the fact that the cable forces are generated through a feedback mechanism involving the drones and payload.

A full mathematical model of kinematics and dynamics of collaborative aerial transportation was obtained in [91] for a system involving multiple UAVs carrying a rigid-body payload attached with rigid rods. The system dynamics were linearized around non-equilibrium state-input pairs so that they can be exploited in a decentralized MPC framework. Unlike centralized algorithms, this controller works based on sharing predicted control inputs instead of state measurements. The proposed framework thoroughly considers physical constraints of the system including actuator and safety constraints. The objective is to minimize the quad-copters position as well as the payload attitude tracking errors.

2.4.3 Direct Payload Control - Single Quad-Copter

In the papers reviewed in the previous subsections, the desired trajectories were designed for the quad-copters. There are a number of other papers that have defined the performance requirements on the payload side. Feedback measurements from the payload are essential to achieve this objective. It is noted that some swing suppression strategies utilize load measurements to enhance internal stability while still closing the control loop over the UAV. See [22] for an example.

In [82], load position control problem was addressed for the first time where the authors considered a planar quad-rotor with a cable-suspended object. The payload was modeled as a point mass and the controller requires the payload mass and cable length. The authors showed semi-global exponential stability of the tracking errors. An extension of this work to three dimensional case was proposed later in [81]. Simulation results were reported where almost global exponential stability of the load position tracking error was demonstrated.

The load position controller in [81] requires measurement of the payload position and velocity, which can be difficult to obtain in an outdoor environment. Tang *et al.* addressed this issue using a downward-facing camera and estimated payload states using an extended Kalman filter [84]. The load position controller is structurally similar to [81]. The only difference is the addition of an integral control to the outer loop. Although the integral action generally improves steady-state performance, it requires the stability analysis to be revisited. Furthermore, both of these papers assumed the attachments point to be at the COM of the UAV. Robustness of these model-based controllers to uncertainties and attachment offset errors were not investigated.

2.4.4 Direct Payload Control - Multiple Quad-Copters

Concurrent position and attitude control for a cable-suspended payload was first considered in [48]. It was shown that at least three quad-copters are required to control both translational and rotational motion of the payload. A geometric nonlinear PID controller was developed that fully considers the nonlinear system dynamics. A rigorous stability analysis demonstrated the convergence of the tracking errors. This method has a few notable limitations. It treats the cables as rigid links and assumes they are attached to the COM of the quad-copters. Moreover, the angular controllers employ sliding mode terms to achieve finite-time stability. This introduces undesirable chattering in the control signals. Finally, high-order numerical differentiation of state measurements are required to implement the controller. In particular, the fifth derivative of the load position is needed.

The authors in [33] considered multiple quad-copters with a cable-suspended payload. They formulated the control design problem as an MPC with several constraints: control saturation, obstacle avoidance and inter-drone collision avoidance were included in the formulation. The resulting non-convex optimization was solved by a novel solver called ALTRO [31]. Similar to most existing work on the subject, the approach models the cables as rigid links. The payload is only a point mass and the cables are considered to be attached to the COM of UAVs.

Full pose manipulation of a cable-suspended payload was proposed in [76] where the cooperative aerial transportation was treated as a cable robot. Using Jacobian matrix as a mapping from payload pose to quad-copter positions, a kinematic controller was developed to satisfy a H_∞ robust stability index. The biggest advantage of the proposed controller is in its ability to achieve full pose control over the payload

without high-derivative measurements. However, kinematic controllers usually have limited bandwidth. In addition, under-actuation property of the vehicles was ignored.

2.5 Summary

In this chapter, first, the concept of energetic passivity and passivity-based control were briefly reviewed. Then, the position control of a single quad-copter with no load was studied where different existing cascade control structures were discussed. Finally, the state of the art control approaches for aerial transportation systems were surveyed.

Based on this review, the biggest gaps in the literature can be summarized as follows: i) cables have been treated as rigid links; ii) under-actuation force errors have not been considered in modeling and stability analysis; iii) Some of the proposed controllers work based on unrealistic measurements such as high-derivative of payload's velocity; iv) the payload has been considered as a point mass rather than a rigid-body with motion along six degrees of freedom; and finally v) the cable attachment points are restricted to the COM of quad-copters.

Chapter 3

System Modeling

In this chapter, a model of the multi-drone cable-based payload transport system is presented. First, the thesis assumptions on system modeling and dynamics are given. Second, the kinematic constraints of the system are derived based on geometric relations imposed by the length of the cables. Third, equations of motion are obtained using Newton-Euler methodology. Finally, the energetic passivity of drones-cables-payload system is shown. The derivations in this chapter are for a general case where the cables are attached at arbitrary points on both the UAVs and the payload.

3.1 Modeling Assumptions

The following modeling assumptions have been made throughout this thesis:

- The cables are massless and do not stretch or become disconnected during the flight.

- The payload is a rigid-body with six degrees of freedom with arbitrary attachment points.
- Drag forces are negligible unless otherwise stated.

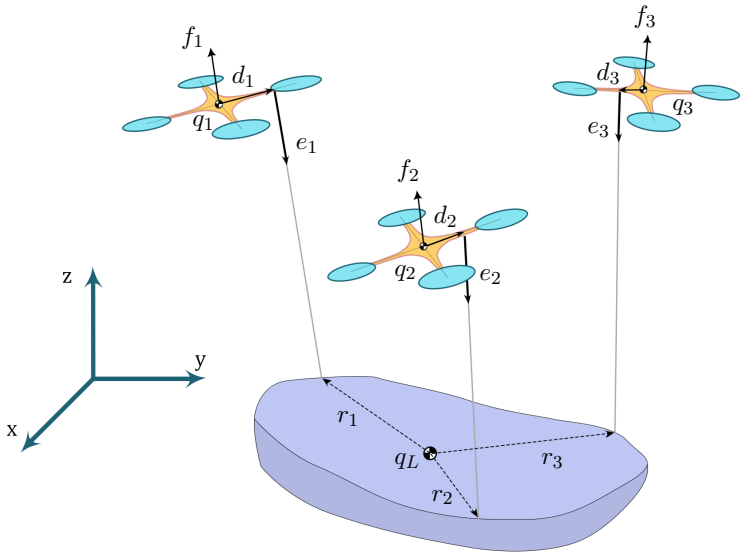

Figure 3.1: Schematic of the aerial transportation system with the motion variables defined. There are no restrictions on the cable attachment points, i.e., they are not limited to the COMs.

3.2 Kinematics

Referring to Figure 3.1, it is noted that the distance between two attachment points on a drone and the payload cannot exceed the length of the corresponding cable, i.e.,

$$\|(q_i+R_i d_i)-(q_L+R_L r_i)\| \leq l_i \quad , \quad i=1,...,n \tag{3.1}$$

where $q_i = [X_i,\ Y_i,\ Z_i]^{\mathrm{T}} \in \mathbb{R}^3$ is the position of the ith quad-rotor body-attached frame with respect to the world frame; $q_L \in \mathbb{R}^3$ denotes the position of the payload

in the world frame. The matrices R_i and $R_L \in SO(3)$ are the corresponding rotation matrices for the ith quad-rotor and the payload, respectively. Moreover, $r_i \in \mathbb{R}^3$ is the vector connecting the COM of the payload to the attachment point of the cables, and is expressed in the body-fixed frame of the payload. The vector $d_i \in \mathbb{R}^3$ connects the COM of the ith quad-rotor to the attachment point of the cable and is expressed in the body-fixed frame of the ith drone. The lengths of the cables are denoted by $l_i \in \mathbb{R}^+$ and n is the number of quad-rotors.

3.3 Equations of Motion

In this section, the dynamics of a cooperative aerial transportation system with a cable-suspended payload is presented. Consider the following equations,

$$m_i \ddot{q}_i = f_i R_i z - m_i g z + T_i R_L e_i \tag{3.2}$$

$$J_i \dot{\omega}_i + \omega_i^{\times} J_i \omega_i = \tau_i + d_i^{\times} \left(T_i R_i^T R_L e_i \right) \tag{3.3}$$

$$m_L \ddot{q}_L = -\sum_{i=1}^{n} T_i R_L e_i - m_L g z \tag{3.4}$$

$$J_L \dot{\omega}_L + \omega_L^{\times} J_L \omega_L = \sum_{i=1}^{n} r_i^{\times} (-T_i e_i) \tag{3.5}$$

Here, $m_i \in \mathbb{R}^+$ is the mass of the ith quad-rotor, $J_i \in \mathbb{R}^{3\times3}$ is its moment of inertia with respect to the body-fixed frame, and $g \in \mathbb{R}^+$ is the gravitational acceleration. Similarly, $m_L \in \mathbb{R}^+$ and $J_L \in \mathbb{R}^{3\times3}$ denote the mass and the moment of inertia of the payload. The thrust and torques in the body-fixed frames are represented by $f_i \in \mathbb{R}$ and $\tau_i \in \mathbb{R}^3$. The tension magnitude of each cable is $T_i \in \mathbb{R}^+ \cup \{0\}$ with e_i being a unit vector along the cable direction expressed in the body-fixed frame

of the payload. The angular velocity of the ith quad-rotor w.r.t the world frame is represented by ω_i which is expressed in the body-fixed frame of the ith drone. The vectors $\omega_L \in \mathbb{R}^3$ denotes the angular velocity of the payload in its body-fixed frame. Finally, the superscript $\times$ is the cross-product operator which maps a vector $a = [a_1, a_2, a_3]^{\mathrm{T}} \in \mathbb{R}^3$ to a skew-symmetric matrix

$$a^{\times} = \begin{bmatrix} 0 & -a_3 & a_2 \\ a_3 & 0 & -a_1 \\ -a_2 & a_1 & 0 \end{bmatrix} \tag{3.6}$$

The roll-pitch-yaw Euler angles are used to represent the orientation of the rigid bodies in this thesis. The angle vector $\eta_i = [\phi_i, \theta_i, \psi_i]^{\mathrm{T}} \in \mathbb{R}^3$ represents the orientation of the ith quad-rotor body-attached frame with respect to the world frame. The time derivative of the Euler angles are related to the angular velocity of the body through the matrix $\Psi(\eta_i) \in \mathbb{R}^{3\times3}$ as follows

$$\omega_i = \Psi(\eta_i)\dot{\eta}_i \tag{3.7}$$

where

$$\Psi(\eta_i) = \begin{bmatrix} 1 & 0 & -\sin(\theta_i) \\ 0 & \cos(\phi_i) & \cos(\theta_i)\sin(\phi_i) \\ 0 & -\sin(\phi_i) & \cos(\theta_i)\cos(\phi_i) \end{bmatrix} \tag{3.8}$$

As a result, the angular motion dynamics of the quad-rotors in (3.3) can be rewritten

as,

$$J_i\Big(\Psi(\eta_i)\ddot{\eta}_i + \dot{\Psi}(\eta_i)\dot{\eta}_i\Big)+\big(\Psi(\eta_i)\dot{\eta}_i\big)^{\times} J_i\Psi(\eta_i)\dot{\eta}_i = \tau_i + d_i^{\times}(T_i R_i^T R_L e_i) \tag{3.9}$$

After multplying both sides by $\Psi^T(\eta_i)$ and some algebraic manipulations, it follows that,

$$M(\eta_i)\ddot{\eta}_i + C(\eta_i,\dot{\eta}_i)\dot{\eta}_i = \Psi(\eta_i)^{\mathrm{T}}\tau_i + \Psi^T(\eta_i)d_i^{\times}(T_i R_i^{\mathrm{T}} R_L e_i) \tag{3.10}$$

where,

$$M(\eta_i) \triangleq \Psi(\eta_i)^{\mathrm{T}} J_i \Psi(\eta_i)$$
$$C(\eta_i,\dot{\eta}_i) \triangleq \Psi(\eta_i)^{\mathrm{T}} J_i \dot{\Psi}(\eta_i)+\Psi(\eta_i)^{\mathrm{T}}\big(\Psi(\eta_i)\dot{\eta}_i\big)^{\times} J_i\Psi(\eta_i)$$

This is the Euler angle representation of the attitude dynamics. Here, it is assumed that the roll and pitch angles stay in the permissible range, $\mid \phi_i \mid < \frac{\pi}{2}$ and $\mid \theta_i \mid < \frac{\pi}{2}$ which guarantees the inverse of $\Psi(\eta_i)$ to exist.

3.4 Energetic Passivity

In this section, the energetic passivity property of cable-based cooperative aerial transportation system is demonstrated. In the first subsection, the transition of the cables from slack to taut or vice versa has been considered ideal. In the second section, this transition has been modeled as an inelastic collision. Energetic passivity of the system has been shown in both cases.

3.4.1 Ideal Transition

Consider equations of motion (3.2), (3.10), (3.4) and (3.5). The total energy of the combined drones, cables, and payload system can be written as,

$$E = \frac{1}{2}\sum_{i=1}^{n} m_i \dot{q}_i^{\mathrm{T}} \dot{q}_i + \sum_{i=1}^{n} m_i g z^{\mathrm{T}} q_i + \frac{1}{2}\sum_{i=1}^{n} \dot{\eta}_i^{\mathrm{T}} M(\eta_i)\dot{\eta}_i + \frac{1}{2} m_L \dot{q}_L^{\mathrm{T}} \dot{q}_L + m g z^{\mathrm{T}} q_L + \frac{1}{2}\omega_L^{\mathrm{T}} J_L \omega_L + \beta \tag{3.11}$$

where β is a positive constant. By taking the derivative of the total energy in (3.11) with respect to time and using (3.2), (3.10), (3.4), and (3.5), it follows that

$$\begin{aligned} \dot{E} =& \sum_{i=1}^{n} \dot{q}_i^{\mathrm{T}} \big(R_i z f_i - m_i g z + T_i R_L e_i\big) + \sum_{i=1}^{n} m_i g z^{\mathrm{T}} \dot{q}_i + \sum_{i=1}^{n} \dot{\eta}_i^{\mathrm{T}} \Big(\dot{M}(\eta_i) - 2C(\eta_i, \dot{\eta}_i)\Big)\dot{\eta}_i \\ &+ \sum_{i=1}^{n} \dot{\eta}_i^{\mathrm{T}} \Big(\Psi^{\mathrm{T}}(\eta_i)\big(\tau_i + d_i^{\times}(T_i R_i^T R_L e_i)\big)\Big) - \dot{q}_L^{\mathrm{T}} \big(\sum_{i=1}^{n} T_i R_L e_i + m_L g z\big) + m_L g z^{\mathrm{T}} \dot{q}_L \\ &- \omega_L^{\mathrm{T}} \big(\omega_L^{\times} J_L \omega_L + \sum_{i=1}^{n} r_i^{\times}(T_i e_i)\big) \end{aligned} \tag{3.12}$$

After some algebraic manipulations and using the fact that the matrix $\dot{M}(\eta_i) - 2C(\eta_i, \dot{\eta}_i)$ is skew-symmetric [79], it can be shown that,

$$\begin{aligned} \dot{E} =& \sum_{i=1}^{n} \dot{q}_i^{\mathrm{T}}(R_i z f_i) + \sum_{i=1}^{n} \omega_i^{\mathrm{T}} \tau_i + \sum_{i=1}^{n} T_i (R_L e_i)^{\mathrm{T}} (\dot{q}_i - \dot{q}_L) \\ &+ \sum_{i=1}^{n} T_i (R_i^{\mathrm{T}} R_L e_i)^{\mathrm{T}} (\omega_i^{\times} d_i) - \sum_{i=1}^{n} T_i e_i^{\mathrm{T}} (R_L^{\mathrm{T}} R_L)(\omega_L^{\times} r_i) \end{aligned}$$

where the so-called scalar triple product property has been employed. Furthermore, the rotation matrix is orthogonal which implies $R_L^{-1} = R_L^{\mathrm{T}}$. Therefore,

$$\begin{aligned}\dot{E} = &\sum_{i=1}^{n} \dot{q}_i^{\mathrm{T}}(R_i z f_i) + \sum_{i=1}^{n} \omega_i^{\mathrm{T}} \tau_i \\ &+ \sum_{i=1}^{n} T_i (R_L e_i)^{\mathrm{T}} \Big(\dot{q}_i - \dot{q}_L + R_i(\omega_i^{\times} d_i) - R_L(\omega_L^{\times} r_i) \Big)\end{aligned} \tag{3.13}$$

The second line is always zero regardless of cables status. If a cable is not in tension, then $T_i = 0$. If it is in tension, then the projections of relative velocities along the cables are zero, which implies that

$$(R_L e_i)^{\mathrm{T}} \big(\dot{q}_i - \dot{q}_L + R_i(\omega_i^{\times} d_i) - R_L(\omega_L^{\times} r_i) \big) = 0 \tag{3.14}$$

Thus, it can be concluded that

$$\dot{E} = \sum_{i=1}^{n} \dot{q}_i^{\mathrm{T}}(R_i z f_i) + \sum_{i=1}^{n} \omega_i^{\mathrm{T}} \tau_i \tag{3.15}$$

which demonstrates the energetic passivity of the system.

3.4.2 Nonideal Transition

The cable goes from taut to slack when the tension becomes zero. Once the tension is re-established, there is a discrete change in the velocity. *This can be modeled as a perfectly inelastic collision* [11], [80]. In particular, the condition for the ith cable to

go from slack to taut can be mathematically formulated as [80], [83],

$$S=\{\|(q_i+R_id_i)-(q_L+R_Lr_i)\|=l_i\ ,\ \frac{d}{dt}(\|(q_i+R_id_i)-(q_L+R_Lr_i)\|)>0\} \quad (3.16)$$

Therefore, the cooperative aerial transportation system with a cable-suspended payload can be modeled as a hybrid system that has several discrete states based on the status of the cables. However, the most important feature of the proposed passivity-based approach is that it works regardless of the cables status. In fact, the passivity property always holds for all these discrete states. To show that, consider Equation (3.13),

$$\dot{E}=\sum_{i=1}^{n}\dot{q}_i^{\mathrm{T}}(R_izf_i)+\sum_{i=1}^{n}\omega_i^{\mathrm{T}}\tau_i+\sum_{i=1}^{n}T_i(R_Le_i)^{\mathrm{T}}\Big(\dot{q}_i-\dot{q}_L+R_i(\omega^{\times}d_i)-R_L(\omega_L^{\times}r_i)\Big) \quad (3.17)$$

It has been shown that the last term remains zero if the cable is either in a slack or taut status. Here, we demonstrate that the transition from slack to taut preserves passivity.

The unit vector along the ith cable, e_i, is expressed in the body-fixed frame of the payload. As a result, $l_iR_Le_i=(q_L+R_Lr_i)-(q_i+R_id_i)$ and $\frac{d}{dt}(\|(q_i+R_id_i)-(q_L+R_Lr_i)\|)=\frac{d}{dt}(\|l_iR_Le_i\|)$. It can be shown that

$$\frac{d}{dt}(\|l_iR_Le_i\|)=l_i\frac{d}{dt}\sqrt{(R_Le_i)^{\mathrm{T}}(R_Le_i)}=2l_i\frac{(R_Le_i)^{\mathrm{T}}\frac{d(R_Le_i)}{dt}}{\sqrt{(R_Le_i)^{\mathrm{T}}(R_Le_i)}} \quad (3.18)$$

It follows from (3.16) that $\frac{d}{dt}(\|l_iR_Le_i\|)>0$ which implies that

$$(R_Le_i)^{\mathrm{T}}\frac{d(R_Le_i)}{dt}=\frac{(R_Le_i)^{\mathrm{T}}}{l_i}\Big(\dot{q}_L+R_L(\omega_L^{\times}r_i)-(\dot{q}_i+R_i(\omega^{\times}d_i))\Big)>0 \quad (3.19)$$

Now going back to (3.17), it is clear that the third term exhibits a dissipative behavior once we are in a transition from slack to taut,

$$\sum_{i=1}^{n} T_i (R_L e_i)^{\mathrm{T}} \Big(\dot{q}_i - \dot{q}_L + R_i (\omega^{\times} d_i) - R_L (\omega_L^{\times} r_i) \Big) < 0 \tag{3.20}$$

Therefore, regardless of any status in cables or a transition between them, the passivity property holds.

$$\dot{E} \leq \sum_{i=1}^{n} \dot{q}_i^{\mathrm{T}} (R_i z f_i) + \sum_{i=1}^{n} \omega_i^{\mathrm{T}} \tau_i \tag{3.21}$$

3.5 Summary

In this chapter, kinematics and dynamics of cable-based cooperative aerial transportation system were obtained. In addition, energetic passivity property was mathematically demonstrated. This property holds regardless of cables status. Interestingly, the nonideal transition of cables from slack to taut has some intrinsic dissipation since it can be modeled as an inelastic collision. As a result, the energetic passivity property remains valid for all cases.

Chapter 4

Decentralized Passivity-Based Control

This chapter presents a provably stable method for decentralized motion control of multiple quad-copters carrying a cable-suspended payload. The intuition behind the approach is that the transportation application does not require very accurate motion control of the payload itself. What is important is robust stability of the control system. PD controllers are known to provide robust stable motion control for conventional robotic manipulators, when accurate tracking is not critical. This is thanks to the energetic passivity of the controller and robotic manipulator subsystems. The proposed motion control method relies on the principle that the interconnected drones-payload system is energetically passive, irrespective of the status of the cables. The control laws are derived from a Lyapunov function inspired by the passivity of

The result in this chapter was presented in the 2018 IEEE/RSJ International Conference on Intelligent Robots and Systems (IROS). See reference [62].

the system, and take into account the drones under-actuation. They can be implemented in a decentralized way on the individual drones using local position/velocity measurements, and do not require any measurement from the payload. They also make no assumption about the status of the cables tension.

Throughout this chapter, it is assumed that the cables are attached to the COM of the aerial vehicles. This assumption would decouple angular motion of the drones from the rest of the system and allow for independent control design.

To realize the proposed passivity-based idea, an exponentially stable trajectory tracking controller is designed for the angular motion of quad-rotors. This ensures fast alignment of the thrust with the desired PD force. Although this approach cannot be exactly implemented in the given format, it provides good insight into a rather simple approach to the control of this multi-body mechanical system.

The rest of this chapter is organized as follows. First, the control design process is presented. Next, the stability of the closed-loop system is investigated. Finally, experimental results are given to demonstrate the effectiveness of the proposed passivity-based controller.

4.1 The Proposed Controller

Consider the attitude dynamic of a quad-copter in (3.10) with no offset in the attachment point, i.e. $d_i = 0$. Then, the attitude motion can be described as,

$$M_i(\eta_i)\ddot{\eta}_i + C_i(\eta_i, \dot{\eta}_i)\dot{\eta}_i = \Psi(\eta_i)^{\mathrm{T}}\tau_i \tag{4.1}$$

The development of the control laws takes advantage of the decoupling of the

translational and angular dynamics and begins with the attitude control of the individual drones. Assuming $\det(\Psi(\eta_i)) \neq 0$, the following feedback linearizing control law is employed,

$$\tau_i = (\Psi(\eta_i)^{\mathrm{T}})^{-1}(M_i(\eta_i)v_i + C_i(\eta_i, \dot{\eta}_i)\dot{\eta}_i) \tag{4.2}$$

where $v_i \in \mathbb{R}^3$ is defined as,

$$v_i = \ddot{\eta}_{d_i} - K_v\dot{e}_{\eta_i} - K_c e_{\eta_i} \tag{4.3}$$

Here $e_{\eta_i} = \eta_i - \eta_{d_i}$ and η_{d_i} is the desired attitude to be defined later. Moreover, $K_v, K_c \in \mathbb{R}^{3\times3}$ are positive definite design parameters. The proposed control law results in the following attitude error dynamics,

$$\ddot{e}_{\eta_i} + K_v\dot{e}_{\eta_i} + K_c e_{\eta_i} = 0,\ t \geq 0 \tag{4.4}$$

which in turn yields,

$$\|e_{\eta_i}(t)\| \leq k_1 \exp(-\alpha t), \quad t \geq 0 \tag{4.5}$$

where $k_1, \alpha \in \mathbb{R}^+$.

The goal of the aerial transportation system is to carry the payload from point A to point B. To achieve this objective, a reference virtual point is assigned to each drone. Control laws are going to be derived such that the drones would follow the trajectory of the virtual points from the origin to destination. If the drones were fully actuated, simple PD controllers acting as virtual spring-damper couplings between

the drones and the reference virtual points would have accomplished the control objective. The control laws presented here are built on this simple concept by taking into consideration the drones under-actuation.

The trajectory of the reference virtual points are denoted by $q_{v_i}(t) \in C^2[0, \infty)$, where C^2 is the space of continuous real-valued functions with first and second continuous derivatives [45]. The following assumptions are made for the reference virtual points,

$$\dot{q}_{v_i} \triangleq \dot{q}_v \in \mathcal{L}_\infty, \quad i \in \{1, ..., n\}$$
$$\ddot{q}_{v_i} \triangleq \ddot{q}_v \in \mathcal{L}_\infty, \quad i \in \{1, ..., n\}$$

The above assumptions simply imply that the reference virtual points retain their spatial configuration during the flight. This would help reduce the possibility of collisions among the drones. Also, the acceleration of reference virtual points are selected such that $\ddot{q}_v \in \mathcal{L}_1$ and $\lim_{t\to\infty} \ddot{q}_v = 0$. See [15] for more details about $\mathcal{L}_p$ spaces. The drones desired thrust force is chosen as

$$\mu_i \triangleq [\mu_x \quad \mu_y \quad \mu_z]_i^{\mathrm{T}} = m_i \ddot{q}_v - K_d \dot{\tilde{q}}_i - K_p \tilde{q}_i \tag{4.6}$$

where $\tilde{q}_i \triangleq q_i - q_{v_i}$ and $K_p,\ K_d \in \mathbb{R}^{3\times 3}$ are positive definite matrices representing the stiffness and damping coefficients of the virtual springs-dampers. However, given the under-actuation of the drones, the actual thrust force may not exactly follow the

desired one, i.e.,

$$f_i R(\eta_i) z = f_i R(\eta_{d_i} + e_{\eta_i}) z \triangleq f_i R(\eta_{d_i}) z + f_i H(\eta_{d_i}, e_{\eta_i}) \tag{4.7}$$
$$= \mu_i + f_i H(\eta_{d_i}, e_{\eta_i})$$

Here $H(\eta_{d_i}, e_{\eta_i}) \in \mathbb{R}^3$ and $H(\eta_{d_i}, 0) = 0$. The left side of the above equation represents the actual thrust force. The first term on the right-hand side is the desired thrust from (4.6) and the second term is the thrust force error. It can be shown that $\|H(\eta_{d_i}, e_{\eta_i})\| \leq k_2 \|e_{\eta_i}\|$, $k_2 \in \mathbb{R}^+$ [37]. The set of three nonlinear equations

$$f_i R(\eta_{d_i}) z = \mu_i = [\mu_{x_i} \quad \mu_{y_i} \quad \mu_{z_i}]^{\mathrm{T}} \tag{4.8}$$

involve four unknowns, i.e., the magnitude of the thrust force f_i, and the three desired Euler angles in the vector $\eta_{d_i} = [\phi_{d_i},\ \theta_{d_i},\ \psi_{d_i}]^{\mathrm{T}}$. These equations can be solved for f_i and two of the desired Euler angles ϕ_{d_i} and θ_{d_i}. The remaining desired Euler angle ψ_{d_i} can be chosen independently of the linear motion. Note that it follows from (4.6) that the thrust magnitude satisfies the inequality,

$$\|\mu_i\| = \|f_i\| \leq \mathcal{M} \|\ddot{q}_v\| + K_d \|\dot{\tilde{q}}_i\| + K_p \|\tilde{q}_i\| \tag{4.9}$$

where $\mathcal{M} \triangleq \max_{i \in \{1,\ldots,n\}} m_i$ is the maximum drone mass.

4.2 Stability Analysis

The following storage function is defined for the aerial transportation system,

$$E \triangleq E_1 + E_2 \tag{4.10}$$

$$\begin{aligned} E_1 =& \frac{1}{2}\sum_{i=1}^{n} m_i \dot{\tilde{q}}_i^T \dot{\tilde{q}}_i + \frac{1}{2}\sum_{i=1}^{n} \dot{e}_{\eta_i}^T \dot{e}_{\eta_i} + \frac{1}{2}\sum_{i=1}^{n} e_{\eta_i}^{\mathrm{T}} K_c e_{\eta_i} + \frac{1}{2}\omega_L^{\mathrm{T}} J_L \omega_L \\ &+ \frac{1}{2} m_L (\dot{q}_L - \dot{q}_v)^{\mathrm{T}} (\dot{q}_L - \dot{q}_v) \end{aligned} \tag{4.11}$$

$$E_2 = \sum_{i=1}^{n} m_i g z^{\mathrm{T}} \tilde{q}_i + m_L g z^{\mathrm{T}} (q_L - \frac{\sum_{i=1}^{n} q_{v_i}}{n}) + \sum_{i=1}^{n} \tilde{q}_i^{\mathrm{T}} K_p \tilde{q}_i + \kappa \tag{4.12}$$

where $\kappa \in \mathbb{R}^+$ adjusts the reference point for the gravitational energy. It is obvious that $E_1 \geq 0$. Given the boundedness of q_{v_i}, it can also be shown that E_2 is lower bounded and can be made non-negative by a proper selection of κ.

Regardless of the status of the cables, that passivity of the combined drones-cables-payload can be exploited to show (see Chapter 3)

$$\dot{E} = -\sum_{i=1}^{n} \dot{\tilde{q}}_i^{\mathrm{T}} K_d \dot{\tilde{q}}_i - \sum_{i=1}^{n} \dot{e}_{\eta_i}^{\mathrm{T}} K_v \dot{e}_{\eta_i} + \sum_{i=1}^{n} \dot{\tilde{q}}_i^{\mathrm{T}} f_i H(\eta_{d_i}, e_{\eta_i}) - m_L \big(\dot{q}_L - \dot{q}_v\big)^{\mathrm{T}} \ddot{q}_v \tag{4.13}$$

Note that the third term is due to the system under-actuation. Next the boundedness of the storage function E is demonstrated. In view of (4.9) and given that

$\|H(\eta_{d_i}, e_{\eta_i})\| \leq k_2\|e_{\eta_i}\|$,

$$\dot{E} \leq \sum_{i=1}^{n} \|\dot{\tilde{q}}_i\|(\mathcal{M}\|\ddot{q}_v\| + K_d\|\dot{\tilde{q}}_i\| + K_p\|\tilde{q}_i\|)k_2\|e_\eta\| + m_L\|\dot{q}_L\|\|\ddot{q}_v\| + m_L\|\dot{q}_v\|\|\ddot{q}_v\| \quad (4.14)$$

For any $\|\dot{q}_L\| \geq 1$, it follows from (4.5) and Young's inequality [61],

$$\begin{aligned}\dot{E} \leq & \sum_{i=0}^{n} k_1 k_2 \exp(-\alpha t) \times \left(\dot{\tilde{q}}_i^{\mathrm{T}}(\mathcal{M}\mathcal{I}_3 + K_d + K_p)\dot{\tilde{q}}_i + \tilde{q}_i^{\mathrm{T}} K_p \tilde{q}_i + \mathcal{M}\ddot{q}_v^{\mathrm{T}}\ddot{q}_v\right) \\ & + m_L\dot{q}_L^{\mathrm{T}}\dot{q}_L\|\ddot{q}_v\| + m_L\|\dot{q}_v\|\|\ddot{q}_v\|\end{aligned} \quad (4.15)$$

where $\mathcal{I}_3$ denotes the identity matrix. It can be shown that constants $\mathcal{K}_1,\ \mathcal{K}_2 \in \mathbb{R}^+$ exist such that the quadratic terms on the right hand side of (4.15) are upper bounded by the storage function E. Consequently,

$$\dot{E} \leq \mathcal{K}_1 \exp(-\alpha t)E + \mathcal{K}_2 \exp(-\alpha t)\ddot{q}_v^{\mathrm{T}}\ddot{q}_v + \mathcal{K}_3\|\ddot{q}_v\|E + m_L\|\dot{q}_v\|\|\ddot{q}_v\| \quad (4.16)$$

It follows from the Gronwall-Bellman Lemma [3],

$$E(t) \leq \exp(\int_0^t f(\tau)d\tau) + \int_0^t \exp(\int_r^t f(\tau)d\tau)g(r)dr,\ t \geq 0$$

where $f(t) \triangleq \mathcal{K}_1 \exp(-\alpha t) + \mathcal{K}_3\|\ddot{q}_v\|$ and $g(t) \triangleq \mathcal{K}_2 \exp(-\alpha t)\ddot{q}_v^{\mathrm{T}}\ddot{q}_v + m_L\|\dot{q}_v\|\|\ddot{q}_v\|$. Since $\ddot{q}_v \in \mathcal{L}_1$, $\int_0^t f(\tau)d\tau$ converges and the first term on the righthand side is bounded. For the second term,

$$\int_0^t \exp(\int_r^t f(\tau)d\tau)g(r)dr \leq \mathcal{M}_1\mathcal{M}_2(\mathcal{K}_2 + m_L)\int_0^t \|\ddot{q}_v(r)\|dr$$

where $\mathcal{M}_1 \triangleq \sup_{[0,\infty)} \exp(\int_\tau^t f(\tau)d\tau)$ and $\mathcal{M}_2 = \sup_{[0,\infty)} \Big(\exp(-\alpha t)\|\ddot{q}_v\| + \|\dot{q}_v\| \Big)$. This proves the boundedness of the storage function in (4.10). As a result, the signals $\dot{\tilde{q}}_i,\ (\dot{q}_L - \dot{q}_v),\ \Omega_L,\ \tilde{q}_i$ are all bounded and belong to $\mathcal{L}_\infty$. Now, it is clear that $\dot{E} \leq W_1 + W_2$ with

$$W_1 \triangleq -\sum_{i=1}^{n} \dot{\tilde{q}}_i^{\mathrm{T}} K_d \dot{\tilde{q}}_i - \sum_{i=1}^{n} \dot{e}_{\eta_i}^{\mathrm{T}} K_v \dot{e}_{\eta_i}$$

$$W_2 \triangleq (\mathcal{K}_1 \exp(-\alpha t) + \mathcal{K}_3 \|\ddot{q}_v\|)E + m_L \|\dot{q}_v\| \|\ddot{q}_v\| + \mathcal{K}_2 \exp(-\alpha t) \ddot{q}_v^{\mathrm{T}} \ddot{q}_v$$

Using the *Modified Invariance Principle* for nonautonomous systems [3, Th. 2.11], [74], it can be shown that

$$\lim_{t\to\infty} \dot{\tilde{q}}_i, \ddot{\tilde{q}}_i, (\ddot{q}_L - \ddot{q}_v), (\dot{q}_L - \dot{q}_v), \dot{\Omega}_L, \Omega_L = 0, \quad \forall i \in \{1, ..., n\}$$

In summary, the drones and the payload arrive at a resting steady-state configuration at the end of the trip. This configuration can be determined as a function of the final positions of the reference virtual points, the masses of the drones, and the control gain K_p,

$$\sum_{i=1}^{n} K_p \tilde{q}_i = -(\sum_{i=1}^{n} m_i + m_L) g z \tag{4.17}$$

where shows static balance of the control actions with the gravity forces.

4.3 Experimental Validation

Experiments with a three-drone payload transport system are conducted to investigate the effectiveness of the proposed controller. A video demonstrating the experiments is available at `https://youtu.be/nBM3OmAN9gI`. The payload with mass $m_L = 0.23$ kg is connected to the drones via cables. The weight of each drone with battery is $m_i = 0.75$ kg. The goal is to transport the payload between two points.

Figure 4.1 shows the experimental setup. The operator selects the trajectories of the reference virtual points and the desired yaw angles of the drones. The drones positions are measured with the Optitrack motion capture system using eight Flex 13 cameras at a rate of 120 Hz. The data is streamed to a ground computer through USB cables, where parts of the control computations are performed. The thrust force and desired attitude angles of each quad-copter are computed and transmitted wirelessly to on-board flight controllers via Lairdtech embedded wireless transceivers at a rate of 100 Hz. The attitude controller is implemented on the on-board STM32 F3 microcontroller. The flight control boards are also equipped with Inertial Measurments Units (IMU). The IMU measures the angular velocities as well as the roll and pitch angles of the quad-copters. The flight control board also issues resulting low-level PWM commands to the Electronic Speed Controllers (ESC)s of the motors. As Figure 4.1 demonstrates, the system operates in a decentralized manner since there is no inter-drone communication.

The desired trajectories of the three reference virtual points are designed as vertices of a fixed triangle moving parallel to the ground at fixed orientation. The trajectory involves three distinct phases. First, the triangle moves up vertically so the drones can lift up the payload. Next it travels laterally parallel to the x-y plane

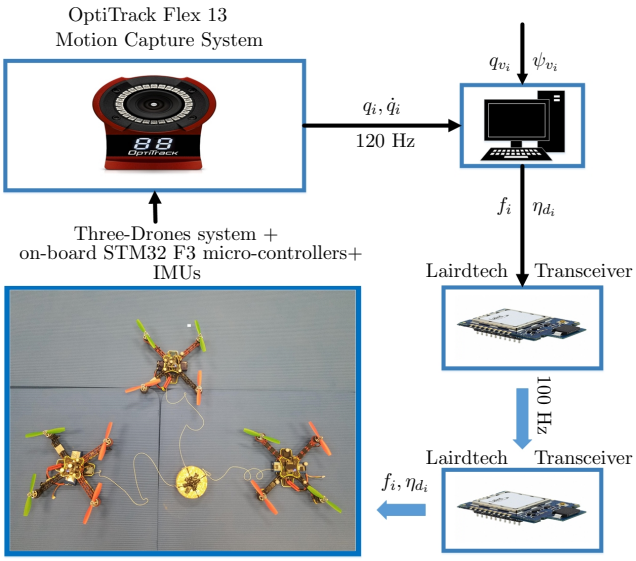

Figure 4.1: Experimental setup with a three-drone payload transport system.

(ground) to move the payload directly above its destination. In the final phase, the triangle of the reference virtual points descends vertically to land the payload at its destination. The desired yaw angles are set to zero for all the drones. The high-level control design parameters of all the quad-copters are as follows:

$$K_p = \text{diag}\Big\{8, 5, 8\Big\}, \;\; K_d = \text{diag}\Big\{5, 7, 2.5\Big\},$$

The low-level design parameters for all the drones are set as,

$$K_c = \text{diag}\Big\{44, 58, 45\Big\}, K_v = \text{diag}\Big\{30, 35, 70\Big\}$$

Figure 4.2 depicts snapshots of the system during different phases of the experiment. Interestingly, there are times at which not all three cables are in tension but system still behaves stably, as the controller is expected to perform normally irrespective

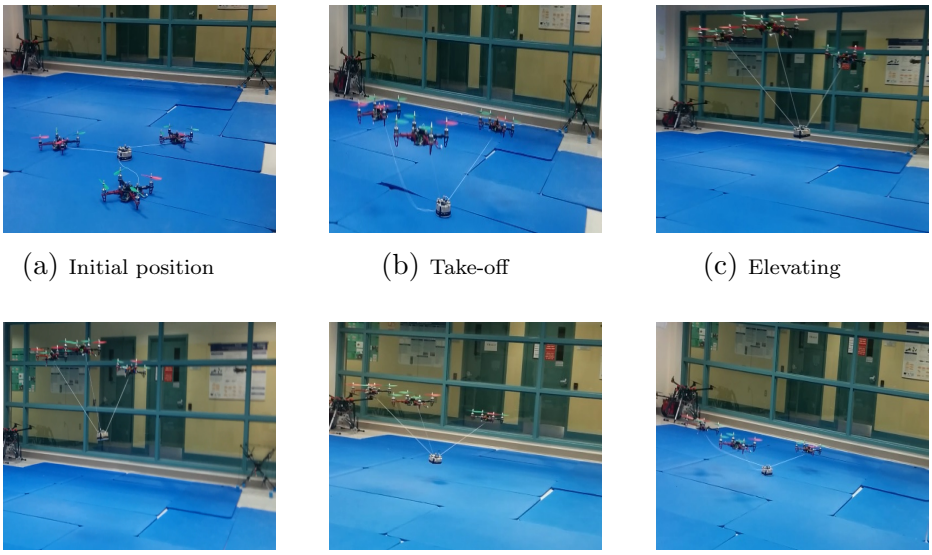

(a) Initial position (b) Take-off (c) Elevating

(d) Moving laterally (e) Descending (f) Landing

Figure 4.2: Snapshots of different phases of the experiment.

of the cable tensions. The drones and payload position trajectories are given in Figure 4.3, which show that the system preserves its spatial configuration during the flight. Moreover, the cargo's weight is distributed among the three quad-copters, allowing for the transport of heavier payloads by scaling the number of the drones.

Figure 4.4 shows the attitude of the payload during flight. While some payload swings are apparent during the initial take-off phase of the trajectory, these are well within an accepted range for reliable transportation. The attitude angles of the payload remain fairly stable during most of the flight, demonstrating the controller ability to safely transport the payload.

4.4 Summary

In this chapter, a method was proposed for the motion control of a cable-based multi-drone load transport system. The approach makes no assumption about the cables

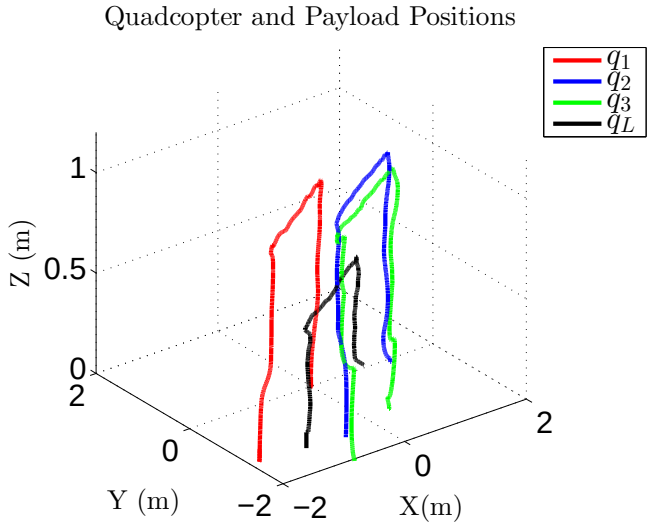

Figure 4.3: The aerial transportation system moves the payload from $q_{L_0} = [0.6, -0.3, 0]$ to $q_{L_f} = [-1.15, -1.4, 0]$.

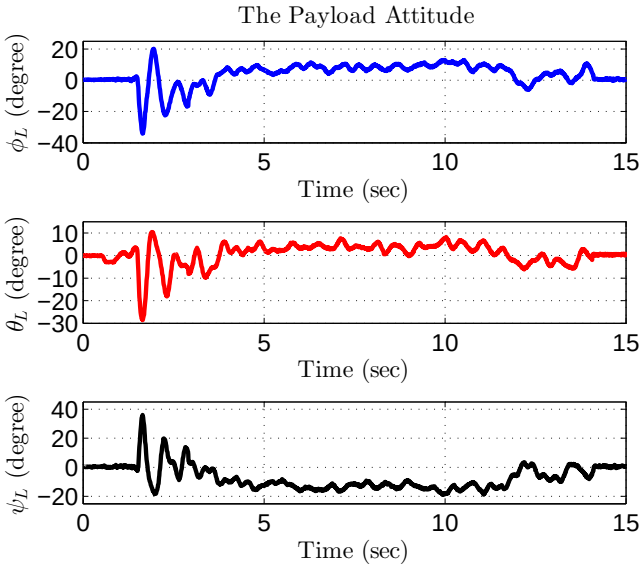

Figure 4.4: Payload attitude angles during the flight. Some initial swings are observed during take-off but the payload remains fairly stable throughout the entire trajectory.

tension status in the the development of the control laws and stability analysis. The control algorithm exploits the fundamental property of energetic passivity of the combined drone-cable-payload system to stably move the payload from its origin to destination. No measurement from the payload is required in the control algorithm, which can be implemented in a decentralized way among the drones. The stability of the motion control system was demonstrated analytically. Results of experiments with a three-drone system using the new controller were provided to support the conclusions of the theoretical analysis.

In the current format, the proposed angular controller contains linear acceleration and jerk. This can be seen by twice differentiation of (4.8) as reference angular velocity and acceleration commands include first and second derivatives of the translational velocity. In practice, this can be avoided by removing the desired angular acceleration and velocity from the attitude controller. However, the effect of this change on the system performance should be analyzed further. In the next chapter, stability analysis of the system with the modified angular controller will be revisited.

Chapter 5

Modified Cascade Structure and Disturbance Attenuation

In the previous chapter, a cascade control strategy was introduced and its stability was shown. The inner-loop of this controller requires the desired angular velocity and acceleration. The desired angular position is the output of the outer-loop controller and contains the linear velocity of the quad-copters. Therefore, linear acceleration and jerk appear in the inner-loop controller. Acceleration is measured by the on-board IMU but it is a highly noisy signal; the jerk is not measured. In this chapter, a modified inner-loop angular controller is proposed which works without the derivatives of the desired attitude and hence avoids this issue. Although a controller with no use of desired angular acceleration was previously introduced and implemented in [58], the paper provided no mathematical proof of system stability.

The result in this chapter was published in the IEEE/ASME Transactions on Mechatronics 25.4 (2020). See reference [63]

In this chapter, a storage function inspired by the mechanical energy of the system is introduced and used to derive the control laws that achieve semi-global exponential stability. The stability is shown to be robust with respect to bounded disturbance forces acting on the quad-copters and the payload. Additionally, a time-domain observer estimates the energy that perturbations may inject to the system and dissipates it through variable damping. This helps suppress disturbance-induced oscillations. The effectiveness of the control strategy is demonstrated in several experiments.

5.1 Mathematical Preliminaries

Definition 1 ([72]) *Consider the nonlinear parametrized system,*

$$\dot{x} = f(x, \kappa) \tag{5.1}$$

where $x \in \mathbb{R}^{\mathfrak{n}}$ *and* $\kappa \in \mathbb{K} \subset \mathbb{R}^{\mathfrak{m}}$ *is a constant vector of user-defined controller gains and* $f(0, \kappa) = 0$. *The system is Semi-global Exponential Stable if for any* $r > 0$, *there exists a controller gain vector* $\kappa^*(r) \in \mathbb{K}$ *and some positive constants* k_r, λ_r, *such that* $\forall x_0 \in \mathcal{B}_r = \{x \in \mathbb{R}^n \mid \|x\| \leq r\}$,

$$\|x(t)\| \leq k_r \|x_0\| \exp(-\lambda_r t) \quad , \quad t \geq 0 \tag{5.2}$$

Hence, for a given compact set $\mathcal{B}_r$, $\kappa^*(r)$ *is a stabilizing gain of the controller such that the region of attraction contains the compact set* $\mathcal{B}_r$.

Theorem 1 ([77]) *Assume that for the system*

$$\dot{x} = f(x) + g(x)u$$

a continuous control law $u = \alpha(x)$ achieves Global Asymptotic Stability (GAS) and also Local Exponential Stability (LES) of $x = 0$ and consider the augmented system,

$$\dot{x} = f(x) + g(x)\zeta$$
$$\ddot{\zeta} = v$$

Let $p(s) = s^2 + ka_1 s + k^2 a_0$ be an arbitrary Hurwitz polynomial. Then the feedback,

$$v = -ka_1\dot{\zeta} - k^2 a_0(\zeta - \alpha(x)) \tag{5.3}$$

achieves semi-global exponential stabilization of $(x, \zeta) = (0, 0)$, that is, for any compact neighborhood $\bar{\Omega}^*$ of $(x, \zeta) = (0, 0)$, there exists k^* such that for all $k \geq k^*$, the region of attraction contains $\bar{\Omega}^*$.

Proof: It follows from the proof in [77] that any compact set $\bar{\Omega}^* = \{(x, \zeta) \mid \|(x, \zeta)\| < R\}$, $R > 0$, can be included in the region of attraction as long as the gain condition $R \leq \sqrt{ck}$ is satisfied, where $c > 0$ is the local exponential convergence rate of $\dot{x} = f(x) + g(x)\alpha(x)$. See [77] for the details and [72] for equivalent theorems.

Corollary 1 *Consider the perturbed system defined over $[0, \infty) \times D$, where $D =$*

$\{(x,\zeta) \mid \|(x,\zeta)\| < \sqrt{ck}\}$,

$$\dot{x} = f(x) + g(x)\zeta + W_1(t)$$
$$\ddot{\zeta} = v + W_2(t)$$

and $\|[W_1^T(t)\ W_2^T(t)]^T\| < \Delta \in \mathbb{R}^+$. *Assume the conditions of Theorem (1) holds. Then, the origin is robust to some perturbations if the parameters c and k are sufficiently large.*

Proof: The result is the direct consequence of [39, Lemma 9.2]. Since the nominal system is exponentially stable with respect to the compact region $\|(x,\zeta)\| < \sqrt{ck}$, then the solution of the system remains uniformly ultimately bounded with a bound proportional to the perturbation size Δ. Increasing c and k can accommodate larger perturbations

5.2 Modified Cascade Structure

In this section, first, a nominal passivity-inspired controller is designed for the cable-based aerial transportation system. The controller is simple and inherently robust, uses very little knowledge of the system model, and makes no assumption about the rigidity of the cables. It improves on the previous results by eliminating the need for the derivative of the desired angular position in the inner-loop attitude controller, hence linear acceleration feedback. The proposed controller guarantees semi-global exponential stability of the closed-loop system. Moreover, uniform ultimate boundedness [39] of the tracking errors are shown in the presence of external disturbances.

Consider the equations of motion in (3.2), (3.3), (3.4) and (3.5). They turn into

the following dynamical equations if: I) it is assumed that cables are attached to the COM of the quad-copters (i.e. $d_i = 0$) and II) the system experiences exogenous perturbations:

$$m_i \ddot{q}_i = f_i R(\eta_i) z - m_i g z + T_i R_L e_i + \mathcal{D}_{i1}(t) \tag{5.4}$$

$$M(\eta_i)\ddot{\eta}_i + C(\eta_i, \dot{\eta}_i)\dot{\eta}_i = \Psi(\eta_i)^{\mathrm{T}} \tau_i + \mathcal{D}_{i2}(t) \tag{5.5}$$

$$m_L \ddot{q}_L = -\sum_{i=1}^{n} T_i R_L e_i - m_L g z + \mathcal{D}_3(t) \tag{5.6}$$

$$J_L \dot{\omega}_L + \omega_L^{\times} J_L \omega_L = \sum_{i=1}^{n} r_i^{\times}(-T_i e_i) + \mathcal{D}_4(t) \tag{5.7}$$

The vectors $\mathcal{D}_{i1}(t), \mathcal{D}_{i2}(t) \in \mathbb{R}^3$ denote disturbances acting on the translational and angular motion of ith quad-copter. Similarly, $\mathcal{D}_3(t),\ \mathcal{D}_4(t) \in \mathbb{R}^3$ represent disturbance forces and torques on the payload, respectively. It is assumed that $\mathcal{D}_{i1}(t)$, $\mathcal{D}_{i2}(t)$, $\mathcal{D}_3(t)$, and $\mathcal{D}_4(t) \in \mathcal{L}_\infty$, i.e., the disturbances have bounded magnitude.

The goal is to carry the payload to a predetermined destination. As the payload and quad-copters are mechanically constrained through the cables, it would be sufficient to design reference trajectories for the drones. Let the continuously differentiable signal $q_{d_i}(t) \in \mathbb{R}^3,\ i = 1, ..., n$ be the reference trajectory of the ith quad-copter. Throughout this chapter, it is assumed that $\dot{q}_{d_i}(t) = \dot{q}_d(t)$ and $\ddot{q}_{d_i}(t) = \ddot{q}_d(t)$. This should preserve the spatial formation of the drones and reduce the possibility of inter-drone collision. It is also assumed that $\lim_{t\to\infty} \ddot{q}_d(t) = 0$, which is quite reasonable as the drones are expected to come to rest at the end of their flight.

If the quad-copters were fully-actuated, then a control force $\mu_i \in \mathbb{R}^3$ of the following form could be employed for their position control,

$$\mu_i \triangleq -k_{p_i}(q_i - q_{d_i}) - k_{d_i}(\dot{q}_i - \dot{q}_d) + m_i \ddot{q}_d \tag{5.8}$$

where $k_{p_i}, k_{d_i} \in \mathbb{R}^{3\times 3}$ are positive definite matrix gains. However, under-actuation prevents generating control forces with an arbitrary direction, unless they are aligned with the drones thrust directions. Figure 5.1 shows the resulting force error $\delta_i(\eta_i, \eta_{d_i}, f_i) \in \mathbb{R}^3$ due to the under-actuation, where

$$\delta_i(\eta_i, \eta_{d_i}, f_i) = f_i R(\eta_i) z - \mu_i \triangleq f_i \big(R(\eta_i) - R(\eta_{d_i})\big) z \tag{5.9}$$

and $\eta_{d_i} = [\phi_{d_i} \ \theta_{d_i} \ \psi_{d_i}]^{\mathrm{T}} \in \mathbb{R}^3$ are the reference attitude commands. An attitude controller is now required to align the thrust with the desired force direction in (5.8),

$$f_i R(\eta_{d_i}) z \triangleq \mu_i \tag{5.10}$$

The thrust magnitude f_i, as well as the roll and pitch reference commands ϕ_{d_i}, θ_{d_i} are obtained from (5.10). Moreover, since Equation (5.10) is underdetermined, the yaw motion would be free and can be controlled independently. Now consider the attitude dynamics of quad-copters in (5.5). A feedback linearizing inverse-dynamic control law can be applied,

$$\tau_i = \big(\Psi(\eta_i)^{\mathrm{T}}\big)^{-1} \Big(M(\eta_i) v_i + C(\eta_i, \dot{\eta}_i)\dot{\eta}_i \Big) \tag{5.11}$$

where $v_i \in \mathbb{R}^3$ is a stabilization controller yet to be designed. By substituting (5.11)

in (5.5), it follows that

$$\ddot{\eta}_i = v_i + \mathcal{W}_{i2} \tag{5.12}$$

where $\mathcal{W}_{i2} \triangleq M^{-1}(\eta_i)\mathcal{D}_{i2}$. Since the inertia matrix is positive definite, $\mathcal{W}_{i2}$ inherits the $\mathcal{L}_\infty$ property of $\mathcal{D}_{i2}$. Similarly, substituting (5.8) and (5.9) in the translational dynamics (5.4) yields,

$$m_i\ddot{\tilde{q}}_i + k_{d_i}\dot{\tilde{q}}_i + k_{p_i}\tilde{q}_i = \delta_i(\eta_i, \eta_{d_i}, f_i) - m_i g z + T_i R_L e_i + \mathcal{D}_{i1} \tag{5.13}$$

In addition, the translational dynamics of the payload (5.6) can be rewritten as,

$$m_L\ddot{\tilde{q}}_L = -\sum_{i=1}^{n} T_i R_L e_i - m_L g z + \mathcal{W}_3 \tag{5.14}$$

where $\dot{\tilde{q}}_L \triangleq \dot{q}_L - \dot{q}_d$ and $\mathcal{W}_3 \triangleq -m_L\ddot{q}_d + \mathcal{D}_3$.

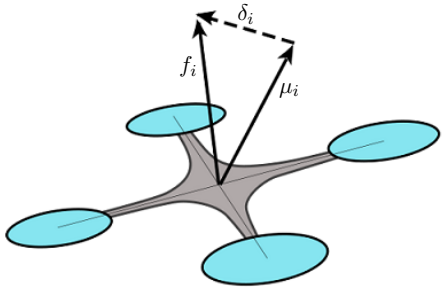

Figure 5.1: Force error due to under-actuation: μ_i is the desired force and f_i is the actual force along the thrust direction; δ_i is the error.

5.3 Stability Analysis

In the absence of external disturbances, $\mathcal{D}_{i1}, \mathcal{D}_4$ and $\mathcal{W}_{i2}, \mathcal{W}_3$ are all set to zero. In such cases, the unforced dynamics (5.12) have the structure of ζ-subsystem in Theorem (1). The variable η_i can be considered as a virtual control in (5.13). If $\eta_i \triangleq \eta_{d_i}$ is picked, then $\delta_i(\eta_{d_i}, \eta_{d_i}, f_i) = 0$ is obtained. It is an immediate consequence of Theorem 1 that, if the dynamical system represented by (5.13) with $\delta_i(\eta_{d_i}, \eta_{d_i}, f_i) = 0$, (5.14) and (5.7) are GAS and LES, then the following attitude controller achieves semi-global exponential stability of the closed-loop system,

$$v_i = -KK_{v_i}\dot{\eta}_i - K^2K_{c_i}(\eta_i - \eta_{d_i}) \tag{5.15}$$

where $K, K_{c_i}, K_{v_i} \in \mathbb{R}^{3\times3}$ are positive definite gains. It is remarkable that the feed-forward reference commands $\dot{\eta}_{d_i}$ and $\ddot{\eta}_{d_i}$ are absent in (5.15).

Theorem 2 *The unforced dynamical system represented by equations (5.13) with $\delta_i(\eta_{d_i}, \eta_{d_i}, f_i) = 0$, (5.14) and (5.7) is GAS and LES.*

Proof: Consider the following storage function,

$$\begin{aligned} E = &\frac{1}{2}\sum_{i=1}^{n} m_i \dot{\tilde{q}}_i^{\mathrm{T}} \dot{\tilde{q}}_i + \frac{1}{2}\sum_{i=1}^{n} \tilde{q}_i{}^{\mathrm{T}} k_{p_i} \tilde{q}_i + \sum_{i=1}^{n} m_i g z^{\mathrm{T}} \tilde{q}_i \\ &+ \frac{1}{2} m_L \dot{\tilde{q}}_L^{\mathrm{T}} \dot{\tilde{q}}_L + \frac{1}{2}\Omega_L^{\mathrm{T}} J_L \Omega_L + m_L g z^{\mathrm{T}} (q_L - \frac{\sum_{i=1}^{n} q_{d_i}}{n}) + \beta \end{aligned} \tag{5.16}$$

where $\beta \in \mathbb{R}^+$ adjusts the reference for potential gravity. Aside from quadratic terms related to kinetic energies, the storage function (5.16) involves quadratic terms w.r.t $\tilde{q}_i$. The latter along with the kinematic constraint (3.1) implies that E is lower-bounded. The time derivative of (5.16) along the unforced system trajectories (5.13),

(5.14) and (5.7) is given as [62],

$$\dot{E} = -\sum_{i=1}^{n} \dot{\tilde{q}}_i^{\mathrm{T}} k_{d_i} \dot{\tilde{q}}_i \leq 0 \tag{5.17}$$

This shows that all the states forming the storage function are bounded ($\tilde{q}_i$, $\dot{\tilde{q}}_i$, $\dot{\tilde{q}}_L$, $\Omega_L \in \mathcal{L}_\infty$). To prove GAS, it follows from the modified invariance principle of non-autonomous systems [3, 74] that $\lim_{t\to\infty} \dot{\tilde{q}}_i = 0$ and $\lim_{t\to\infty} \ddot{\tilde{q}}_i = 0$. Now it can be deduced from the translational dynamics of the vehicles (5.13),

$$k_{p_i} \tilde{q}_i = -m_i g z + T_i R_L e_i \quad , \quad i = 1, ..., n \tag{5.18}$$

Summation over i and substituting the recent result in (5.14) yield,

$$m_L \ddot{\tilde{q}}_L = -\sum_{i=1}^{n} k_{p_i} \tilde{q}_i - (\sum_{i=1}^{n} m_i + m_L) g z \tag{5.19}$$

It follows from (5.19) that $\ddot{\tilde{q}}_L \in \mathcal{L}_\infty$. Then, it can either converge as $t \to \infty$ or oscillate forever. If it oscillates, then at least one of the $\tilde{q}_i$'s must exhibit periodic behavior. As a result, $\dot{\tilde{q}}_i$ has to oscillate as well. This contradicts the previous result of $\lim_{t\to\infty} \dot{\tilde{q}}_i = 0$. Thus, $\lim_{t\to\infty} \ddot{\tilde{q}}_L = \bar{c},\ \bar{c} \in \mathbb{R}$. Since $\dot{\tilde{q}}_L \in \mathcal{L}_\infty$, it has no choice rather than converging to zero, i.e. $\bar{c} = 0$. Moreoever, it immediately follows from the kinematic constraint (3.1) that $\dot{\tilde{q}}_L$ has to reach zero at steady state. Consequently, the system rests at the expected equilibrium,

$$\sum_{i=1}^{n} k_{p_i} \tilde{q}_i = -(\sum_{i=1}^{n} m_i + m_L) g z \tag{5.20}$$

Similar arguments can be made for (5.7) to prove $\lim_{t\to\infty} \dot{\omega}_L, \omega_L = 0$. This demonstrates the GAS property of the equilibrium. Next, local exponential convergence of the errors is proven. To this end, the following two scenarios are considered:

I) $T_i = 0$ (cables not in tension): Consider the dynamical system (5.13) and let $V(\mathcal{X}) = \mathcal{X}^{\mathrm{T}} P \mathcal{X}$ where $P \in \mathbb{R}^{6\times 6}$ is a positive definite matrix that satisfies the Lyapunov equation of $A^{\mathrm{T}}P + PA = -Q$ and $\mathcal{X} \triangleq [k_{p_i}^{-1}(\tilde{q}_i - m_i g z) \quad k_{p_i}^{-1}\dot{\tilde{q}}_i]^{\mathrm{T}}$. The time derivative of the proposed Lyapunov function along the trajectory of $\dot{\mathcal{X}} = A\mathcal{X},\ A = \begin{bmatrix} 0 & I \\ -k_{p_i} & -k_{d_i} \end{bmatrix}$ is given as,

$$\dot{V} = -\mathcal{X}^{\mathrm{T}} Q \mathcal{X} \tag{5.21}$$

where $Q \in \mathbb{R}^{6\times 6}$ is a positive definite matrix. This proves exponential stability.

II) $T_i \neq 0$ (cables in tension): a state vector can be defined as $\bar{\mathcal{X}} \triangleq [k_{p_i}^{-1}\big(\tilde{q}_i - (m_i g z + \xi_i)\big) \quad k_{p_i}^{-1}\dot{\tilde{q}}_i]^{\mathrm{T}}$ where the constant vector $\xi_i \in \mathbb{R}^3$ is the share of ith drone in transportation of the payload. It follows from the GAS property of the system that $T_i R_L e_i = -\xi_i + \mathcal{T}_i$, where $\mathcal{T}_i \in \mathbb{R}^3$ is upper bounded by $\|\mathcal{T}_i\| < \alpha \|\bar{\mathcal{X}}\|$, $\alpha > 0$, inside a compact set containing the equilibrium point. This is characterized as a vanishing term. Now pick $V(\bar{\mathcal{X}}) = \bar{\mathcal{X}}^{\mathrm{T}} P \bar{\mathcal{X}}$ where $P \in \mathbb{R}^{6\times 6}$ is a positive definite matrix that satisfies the Lyapunov equation of $A^{\mathrm{T}}P + PA = -\gamma I,\ \gamma > 0$. The time derivative of the proposed Lyapunov function along the system trajectory is given as $\dot{V} = -\bar{\mathcal{X}}^{\mathrm{T}}\Big(\gamma - \alpha\Big)\bar{\mathcal{X}}$. Proper choice of k_{p_i}, k_{d_i} would guarantee the condition $\gamma - \alpha > 0$ that implies exponential decaying rate.

It can be then concluded that the states in (5.13) are exponentially convergent. As a

result,

$$\sum_{i=1}^{n} T_i R_L e_i = m_L g z + \sum_{i=1}^{m} \mathcal{T}_i \tag{5.22}$$

where $m \leq n$ is the number of vehicles contributing to cooperation and $\|\mathcal{T}_i\| \leq \upsilon \exp(-\lambda t)$, $t \geq 0$ and $\upsilon, \lambda \in \mathbb{R}^+$. Now it follows from (5.14) and (5.22) that $\ddot{\tilde{q}}_L$ has to decay exponentially. The gains k_{p_i}, k_{d_i} determine the rate of convergence. Similar arguments can be made for the angular motion of the payload. This completes the proof. □

According to Theorem (1), the outer-loop control (5.8) and attitude controller (5.11) and (5.15) achieve semi-global exponential stability. The gain k_{p_i}, k_{d_i}, K can be used to expand the region of attraction. Furthermore, it follows from [39, Lemma 9.2] that this exponential stability is robust to bounded-amplitude disturbances. Corollary (1) states that if gains k_{p_i}, k_{d_i}, K are sufficiently large, then larger perturbations can be tolerated. Moreover, if the perturbations vanish at steady state, i.e. $\lim_{t\to\infty} \mathcal{W}_{i2}, \mathcal{W}_3 = 0$ and $\lim_{t\to\infty} \mathcal{D}_{i1}, \mathcal{D}_4 = 0,\ i = 1, ..., n$, then the states also converge to zero [39].

5.4 Disturbance Attenuation

The nominal controller maintains closed-loop stability in the presence of external disturbances, but its performance may still be impacted by these undesired forces. In this section, additional compensation is introduced to suppress any disturbance-induced oscillations.

Disturbance observers usually rely on the system dynamics to estimate and compensate for disturbances acting on it [60]. Such an approach would be difficult to apply here due to the non-rigidity of the cables connecting the payload to the drones. Instead, the method proposed in this chapter attempts to estimate and compensate for any energy added by the disturbances. First, a time-domain energy observer is introduced to estimate any energy injected by the external disturbances. Then, a time-varying damping will be employed to dissipate the extra energy.

Consider a mechanical system described by the following equation of motion in the generalized coordinates $x \in \mathbb{R}^n$,

$$H(x)\ddot{x} + V(x,\dot{x})\dot{x} + G(x) = U(t) + D(t) \tag{5.23}$$

where $H(x) \in \mathbb{R}^{n\times n}, V(x,\dot{x}) \in \mathbb{R}^{n\times n}$ denote the inertia and Coriolis matrices, respectively. The vector $g(x) \in \mathbb{R}^n$ stands for gravity forces and is related to the gravitational energy $\mathcal{U} \in \mathbb{R}$ through the following equation,

$$\int_{T_1}^{T_2} g(x)^{\mathrm{T}}\dot{x}dt = \mathcal{U}(x(T_2)) - \mathcal{U}(x(T_1)) \tag{5.24}$$

The control input and disturbance are shown by $U(t) \in \mathbb{R}^n$ and $D(t) \in \mathbb{R}^n$, respectively. Multiplying both sides of (5.23) by $\dot{x}^{\mathrm{T}}$ and adding the term $\frac{1}{2}\dot{x}^{\mathrm{T}}\big(\dot{H}(x) - 2V(x,\dot{x})\big)\dot{x} = 0$ [79], lead to the following expression,

$$\dot{x}^{\mathrm{T}}\Big(H(x)\ddot{x} + \frac{1}{2}\dot{H}(x)\dot{x} + G(x)\Big) = \dot{x}^{\mathrm{T}}\big(U(t) + D(t)\big)$$

Integrating both sides from $t = T_1$ to $t = T_2$ results in,

$$\mathcal{K}\big(x(T_2), \dot{x}(T_2)\big) + \mathcal{U}\big(x(T_2)\big) - E_{cont} + \alpha = E_{dis}$$

where $\mathcal{K}\big(x, \dot{x}\big) \triangleq \frac{1}{2}\dot{x}^{\mathrm{T}} H(x)\dot{x}$ is the kinetic energy and $\alpha \in \mathbb{R}$ can be found based on the initial conditions. The energy added by the disturbance is $E_{dis} \triangleq \int_{T_1}^{T_2} \dot{x}(t)^{\mathrm{T}} D(t) dt$ which must be dissipated instantaneously to overcome the undesired effect of disturbance. The control input has both conservative and dissipative actions governed by the relation $E_{cont} \triangleq \int_{T_1}^{T_2} \dot{x}(t)^{\mathrm{T}} U(t) dt$.

The kinetic and gravitational energy can be computed from the measurements at each sample time. One can easily determine E_{dis} as E_{cont} is always available. There might be intervals in which the disturbances do not increase the energy level of the system and hence, no extra dissipation is needed. The control input is modified as,

$$U = U_{nom} + U^* \tag{5.25}$$

where U_{nom} is the nominal controller and $U^* = -k_{dis}(t)\dot{x}$ is extra compensation for disturbances. The time-varying damping $k_{dis}[j] \in \mathbb{R}^+$ is chosen as,

$$k_{dis}[j] = \begin{cases} \frac{E_{dis}[j] - E_{dis}[j-1]}{\|\dot{x}[j]\|^2} & \text{if } \; E_{dis}[j] > E_{dis}[j-1] \\ 0 & \text{otherwise} \end{cases} \tag{5.26}$$

where j is the sample number.

Remark 1 *The formula in (5.26) may generate a large value whenever the velocities*

are small. A possible alternative is to use $k_{dis}[j] = \frac{E_{dis}[j]-E_{dis}[j-1]}{\|\dot{x}[j]\|^2+\epsilon},\ \epsilon > 0$ *to avoid division by small numbers. As it was shown in the previous section, the system remains stable in the presence of bounded disturbances. Hence, even if all the extra energy is not dissipated instantaneously, stability will always be guaranteed. The objective here is to attenuate rather than to cancel the disturbances.*

Remark 2 *Continuity in the control inputs can be preserved if instead of switching to zero dissipation in (5.26) a monotonically decreasing sequence such as* $k_{dis}[j] = a\ k_{dis}[j-1],\ 0 < a < 1$ *is used.*

The energy injected through the control actions of quad-copters over a specific interval can be expressed as,

$$E_{cont} = \sum_{i=1}^{n} \Big(\int_{T_1}^{T_2} (\dot{q}_i^{\mathrm{T}} f_i R(\eta_i) z + \omega_i^{\mathrm{T}} \Gamma \tau_i) dt \Big) \tag{5.27}$$

where $\Gamma \triangleq \mathrm{diag}\big\{1, 1, 0\big\}$ and the energy associated with the yaw motion is excluded. This is because the yaw motions are decoupled from the rest of the system and are controlled independently. The mechanical energy of the load transport system can be given as,

$$\begin{aligned} E_{mech} = \frac{1}{2}\sum_{i=1}^{n} m_i \dot{q}_i{}^{\mathrm{T}} \dot{q}_i + \sum_{i=1}^{n} m_i g z^{\mathrm{T}} q_i + \frac{1}{2}\sum_{i=1}^{n} \omega_i^{\mathrm{T}} J_i \Gamma \omega_i \\ + \frac{1}{2} m_L \dot{q}_L^{\mathrm{T}} \dot{q}_L + \frac{1}{2} \Omega_L^{\mathrm{T}} J_L \Omega_L + m_L g z^{\mathrm{T}} q_L + \beta \end{aligned} \tag{5.28}$$

and the energy introduced by disturbances is $E_{dist} = E_{mech} + E_{cont} + \alpha$, where α is determined based on the initial conditions.

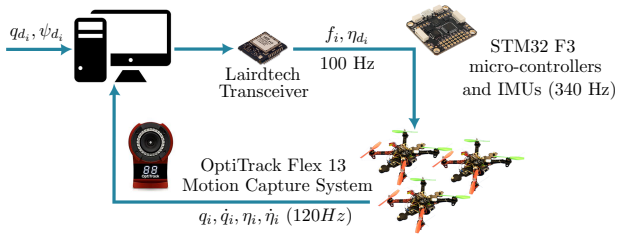

Figure 5.2: The experimental setup with three quad-copters carrying a cable-suspended payload.

The dissipative element for the system motions except yaw is given by,

$$k_{dis_i}[j] = \begin{cases} \frac{E_{dis}[j]-E_{dis}[j-1]}{\|\dot{q}_i[j]\|^2+\epsilon} & \text{if } E_{dis}[j] > E_{dis}[j-1] \\ a\ k_{dis_i}[j-1] & \text{otherwise} \end{cases}$$

The control law in (5.8) is modified to,

$$\mu_i \triangleq -k_{p_i}(q_i - q_{d_i}) - \Big(k_{d_i} + k_{dis_i}(t)\Big)(\dot{q}_i - \dot{q}_d) + m_i \ddot{q}_d \tag{5.29}$$

A dissipative gain for the yaw motion can be defined similarly.

5.5 Experimental Validation

Experiments with three quad-copters carrying a cable-suspended payload were conducted to evaluate the effectiveness of the proposed controller. Each drone weighs $m_i = 0.67$ kg including the battery. The payload mass is $m_L = 0.39$ kg. Figure 5.2 illustrates the experimental setup. The user provides the reference trajectory and desired formation for the drones as a group, and the individual trajectories for the drones are derived accordingly. The desired yaw angles are also specified by the user.

Third-order polynomials are fitted between waypoints to ensure the smoothness of these trajectories. OptiTrack Flex 13 motion capture system measures the quad-copter positions and streams to a ground station at a rate of 120 Hz. The drones velocities are computed by numerical differentiation of their positions. The outer-loop position controller runs on the ground station and computes the desired thrusts and attitude commands. These are then transmitted to the onboard flight controllers via a LairdTech wireless module at a rate of 100 Hz. The onboard flight controller of each drone is an STM32 F3 microcomputer and runs the angular control loop at a rate of 340 Hz. It generates PWM commands for the Electronics Speed Controllers (ESCs) of the propellers. The outer-loop control gains for all the quad-copters are as follows,

$$k_{p_i} = \mathrm{diag}\big\{9, 6, 9\big\},\ k_{d_i} = \mathrm{diag}\big\{3, 2.25, 1.25\big\}$$

The inner-loop control gains for all the quad-copters are selected as,

$$K_{c_i} = \mathrm{diag}\big\{10, 15, 18\big\},\ K_{v_i} = \mathrm{diag}\big\{7.5, 8.5, 10\big\}$$

and $K = 2I_3$ where $I_3 \in \mathbb{R}^{3\times 3}$ is the identity matrix.

The following scenarios were considered in the experiments. A video demonstrating the experiments is available at `https://youtu.be/aQ9rBlenekU` .

5.5.1 Trajectory Tracking

In this experiment, an M-shaped reference trajectory was considered. Figure 5.3 depicts the trajectory of three quad-copters with the payload. First, the quad-copters

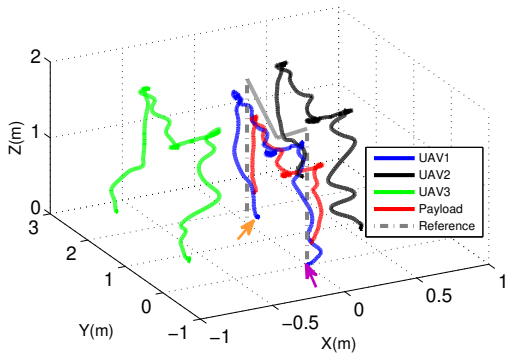

Figure 5.3: Trajectories of three quad-copters and payload for an M-shaped desired reference in the first experiment. The beginning and end points of UAV1 are marked by purple and orange arrows, respectively. The reference trajectory for UAV1 is depicted by a dashed gray line.

ascend to an altitude of about $z = 1.4$ m. Then, the system descends for a half meter while moving along the y-axis for roughly 0.8 m. In the next phase of the trajectory, the drones return to the previous altitude of $z = 1.4$ m while moving forward along y-axis for another 0.8 m. Finally, the drones descend vertically for landing. Tracking errors were observed in the altitude due to the lack of full gravity compensation in the control scheme, but this is not an issue in an aerial transportation system. The desired yaw angles were set to zero for this experiment.

Figure 5.4 illustrates position tracking errors of the three quad-copters when following the M-shape trajectory. The largest errors are in altitude due to the effect of gravity.

Large payload swings are generally undesirable in transportation applications and must be avoided. Figure 5.5 shows the payload attitude during the flight which, with the exception of some jumps in the take-off stage, exhibits an acceptable behaviour.

Figure 5.6 illustrates the time history of thrust forces of the quad-copters. With the exception of the ramp-up and ramp-down stages of the propellers, all the thrust

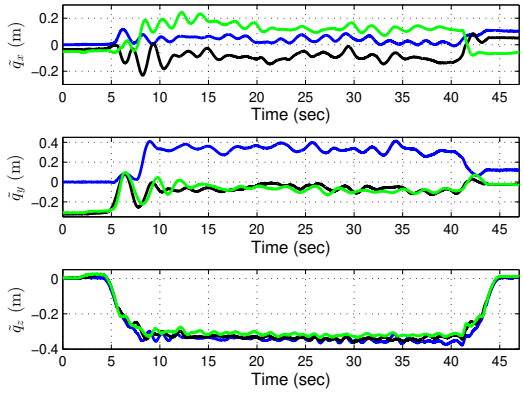

Figure 5.4: Position tracking errors when following the M-shaped trajectory. Blue, black and green plots correspond to UAV1, UAV2 and UAV3, respectively.

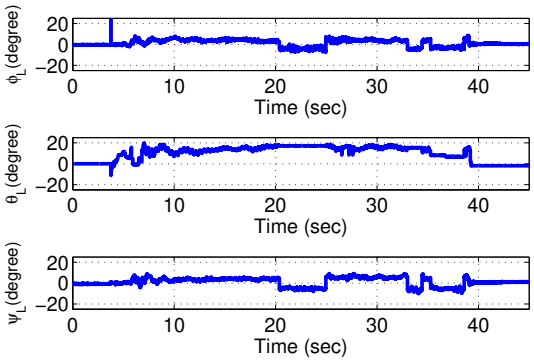

Figure 5.5: Payload orientation during the M-shaped trajectory in the first experiment.

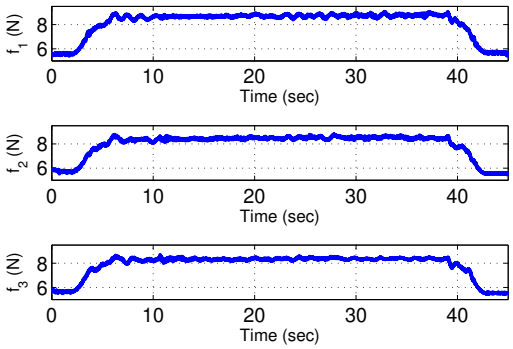

Figure 5.6: Thrust forces versus time. The first and last two-second segments correspond to the ramp-up and ramp-down phases of the propellers.

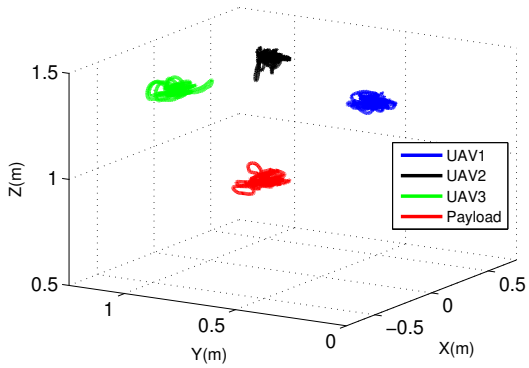

Figure 5.7: The drones and payload positions in the second experiment.

forces mostly remained close to $f_1 \approx f_2 \approx f_3 \approx (m_i + \frac{m_L}{n})g \approx 8$ N. This implies that the load is uniformly distributed among the vehicles. The result is indebted to homogeneous agents, identical rope length, and symmetric formation shape.

5.5.2 Disturbance Attenuation

In this experiment, the performance of the proposed disturbance attenuation approach was evaluated. Five perturbations were applied to the payload while the drones were hovering. The positions of the drones and payload are shown in Figure 5.7.

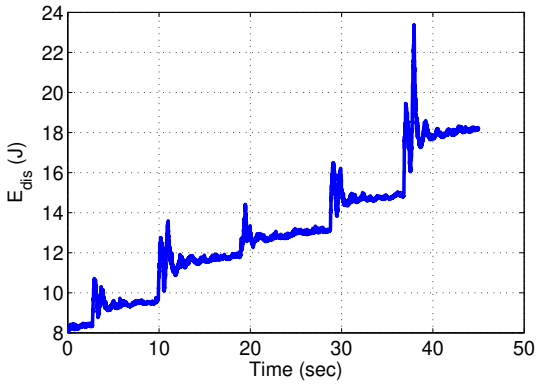

Figure 5.8: The output of the time-domain disturbance energy observer. The energy remains nearly constant in the absence of disturbances but increases after the application of each disturbance. Five disturbances were applied to the payload in this experiment.

Figure 5.8 depicts the output of the disturbance energy observer. In the beginning, there is no disturbance on the system and hence, its associated energy level is constant. At $t = 2.7$ sec, the first disturbance is applied to the system. As a result, the dissipative element k_{dis} is activated, as can be seen in Figure 5.9. The value of k_{dis} is saturated to avoid the actuation limit. The parameter $\epsilon = 0.1$ has been selected to circumvent zero divisions. After attenuation of the disturbance, the value of k_{dis} is gradually decreased in a sequence with $a = 0.99$. The next four disturbances are applied at $t = 10, 18, 27, 36$ sec approximately, and the dissipative element is triggered accordingly.

5.5.3 Comparison to a Baseline Controller

The new controller is compared to the one in Chapter 4 to investigate the effectiveness of the disturbance attenuation strategy. In the first scenario, the drones move to hovering configuration and then the payload is perturbed by a stick eight (8) times.

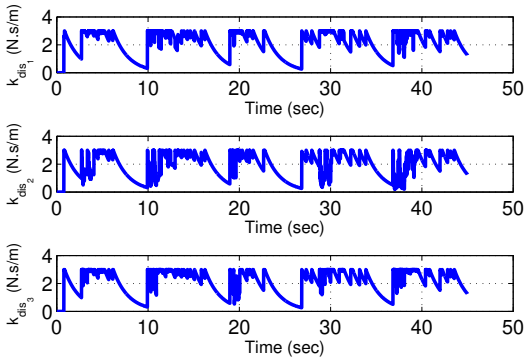

Figure 5.9: The value of disturbance attenuation damping for each quad-copter during the second experiment.

In the second scenario, the drones carry the payload for 2 m along the $y-$axis at a constant altitude while a fan blows air against them. This simulates the effect of wind on the system in outdoor settings.

- Perturbations: For the purpose of comparison, a metric named dissipation time is defined and denoted by $T_{dis} \in \mathbb{R}^+$. Suppose the system is hovering at a nominal position $q_{nom_i} \in \mathbb{R}^3$. T_{dis} denotes the time that it would take for the UAVs to return to and stay inside a ball of radius 5 cm i.e. $\|q_i - q_{nom_i}\| \leq 0.05$ centred around their nominal position after the onset of the disturbance. This is roughly the time needed by the controller to dissipate the disturbance energy and settle the system back into around its nominal position. Figure 5.10 illustrates this measure graphically.

  Table 5.1 compares the average value of dissipation time over the eight applications of perturbation. It is evident that the proposed controller (5.29) dampens the oscillations more quickly than the baseline controller. The maximum values of the dissipation times of the two controllers are also compared in Table 5.2.

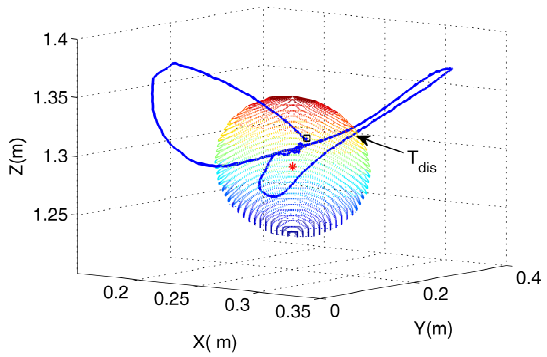

Figure 5.10: Graphical illustration of dissipation time T_{dis}. The red star is the nominal position q_{nom_i} and the sphere represents $\|q_i - q_{nom_i}\| \leq 0.05$. The UAV is initially at a hovering position shown by the black square. It leaves the sphere due to the application of the perturbation and eventually returns to and stays inside it because of energy dissipation by the controller.

Table 5.1: Average value of the dissipation time over eight applications of perturbation.

mean(T_{dis}) (sec)	Proposed Controller	Controller in Chapter 4
UAV1	3.75	4.57
UAV2	4.78	7.51
UAV3	3.27	3.34

Again, the proposed controller clearly outperforms the baseline controller.

- Attenuation of Wind Disturbance: In this scenario, the drones first elevate to an altitude of $z = 1.5$ m. Then, they move along the $y-$ axis for 2 meters while a fan blows air against them in the x direction. They finally land after completing this horizontal motion.

  The results in Figures 5.11, 5.12 and 5.13 show that the proposed controller is more effective than the baseline controller in attenuating this disturbance as there are fewer oscillations along the $x-$ axis with this controller.

Table 5.2: Maximum value of dissipation time over eight applications of perturbation.

$\max(T_{dis})$ (sec)	Proposed Controller	Controller in Chapter 4
UAV1	4.81	7.06
UAV2	6.42	10.64
UAV3	4.52	7.85

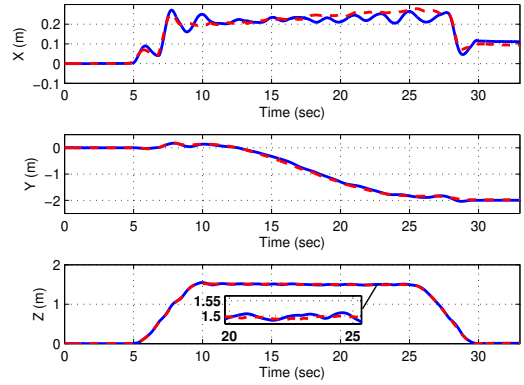

Figure 5.11: Position of the first UAV in the presence of wind disturbance. The blue plot is the controller in Chapter 4 and the red plot is the proposed controller.

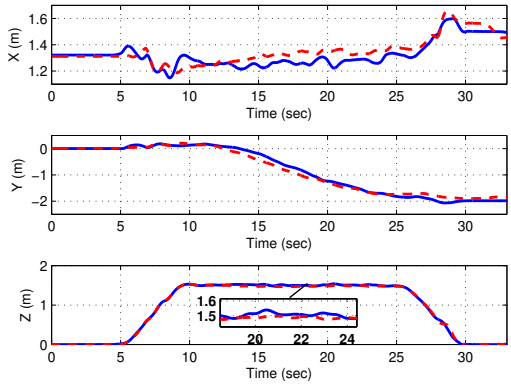

Figure 5.12: Position of the second UAV in the presence of wind disturbance. The blue plot is the controller in Chapter 4 and the red plot is the proposed controller.

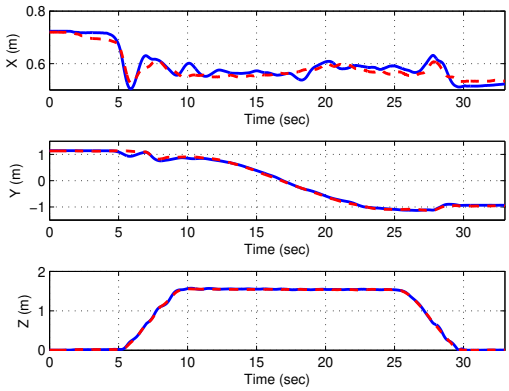

Figure 5.13: Position of the third UAV in the presence of wind disturbance. The blue plot is the controller in Chapter 4 and the red plot is the proposed controller.

5.6 Summary

In this chapter, a passivity-based cascaded controller was proposed to stably transport a cable-suspended payload with a number of quad-copters. The proposed controller made no assumption about the cables tensions as it relied on energetic passivity property of the combined drones, cables, and payload system. The attitude sub-controller only required the angular position reference command but not its first and second derivatives. This helped avoid linear acceleration or jerk measurements in the control system. Semi-global exponential stability of the system was demonstrated, where the region of attraction could be expanded arbitrarily by the choice of the controller gains. Uniform ultimate boundedness of the tracking errors in the presence of disturbances was also shown.

A disturbance attenuating term was further introduced to reduce adverse effects of external disturbances on the controller performance. A time-domain disturbance energy observer estimated any excess energy introduced into the system. This was

then removed with additional controller damping. Results of the experiments performed with a three-drone payload transport system in an indoor setting showed that the controller can perform effectively even in the presence of significant external disturbances.

Although the proposed cascaded controller has a number of practical advantages, it assumes that the cables are attached to the COM of the UAVs. In the next chapter, a passivity-based approach is introduced to allow for shifted attachment points, eliminating this limitation. In addition, a safety constraint will be added to the controller to avoid any possible inter-drone collisions.

Chapter 6

Shifted Attachment Points

In this chapter, a new passivity-based controller is proposed for stable cooperative transportation of a cable-suspended payload by a number of quad-rotors. Nominal proportional-derivative position controllers with desired acceleration feedforward are augmented with time-varying dissipative terms to account for the drones underactuation. A storage function is defined that includes terms inspired by the kinetic and potential energies of the system components as well as virtual energy of the controller. A time-domain passivity observer is used in conjunction with an adaptive dissipative term to ensure that the value of the storage function is continuously decreased and hence, guarantees closed-loop stability. Moreover, barrier Lyapunov functions are employed to avoid inter-drone collisions. The proposed controller makes no assumption about and requires no knowledge of the cables tension status. Additionally, it requires no measurement from the payload. The cables can be attached to the quad-rotors and the payload at arbitrary points. Experiments with a system of three quad-rotors and a cable-suspended payload demonstrate the effectiveness of the proposed approach.

Similar to the previous chapters, here the focus remains on delivery of cable-suspended commercial parcels using multiple unmanned aerial vehicles. Commercial goods are predominately in solid form and are packaged in a way that can be safely transported without precise load control. In our approach, the payload package is constrained to the drones via cable attachments so its position is restricted to a close proximity of the drones. Once the drones arrive at their final destination, they can safely deploy their payload without the need for precise control of its position and orientation. Precise control of the payload trajectory is unnecessary for this application and is forgone in favour of controller simplicity and robustness.

6.1 Control Design

In this section, a passivity-based controller is proposed for the cable-based multi-drone payload transportation system with shifted attachment points. The combination of drones, cables, and payload is an energetically passive system regardless of whether the cables are in tension or not. This property was exploited in previous chapters to develop controllers that guaranteed the system stability without making any assumptions about the cables tensions. However, in those schemes, it was assumed that the cables are attached to the Center Of Mass (COM) of the drones in order to decouple the attitude dynamics of the quad-rotors from the rest of the system dynamics. The assumption allowed for the development of a separate controller for the angular motion, which simplified the design process. The current controller generalizes previous strategies by allowing for arbitrary cable attachment points, hence eliminating a limitation of these earlier approaches. In this case, the control development has to account for the coupling of translational and angular dynamics of the quad-rotors.

First, PD position controllers with time-varying derivative gains and desired acceleration feedforward are introduced. These controllers produce the desired drone forces that are converted to drones thrust magnitudes and desired angles. A storage function is defined and a control correction term is computed in a way to ensure that the storage value decreases over time. A passivity observer detects any potential active behaviour and would trigger time-varying dissipative elements accordingly to dampen the extra energy introduced in the system. This will be shown to guarantee the control system stability.

Given the close proximity of the drones, a collision avoidance strategy is needed to prevent inter-drone collisions due to disturbances or during the transient phase of the response. Barrier Lyapunov functions have been used to implement state constraints in nonlinear control systems [86]. Inspired by [71], a collision avoidance strategy is integrated in the proposed control scheme. The stability of the closed-loop system with this safety constraint has been proven using a modified storage function that includes a Barrier Lyapunov function.

The features of the new controller that distinguish it from the existing literature can be summarized as follows:

- Cable attachment points are not limited to the drones COMs. This provides greater flexibility in configuring the drones for carrying the payload. However, this extra flexibility comes at the expense of coupling of the translational and angular dynamics. These dynamics have been considered decoupled in prior related work, which simplifies the control design.

- The proposed controller makes no assumptions about the tension status of the cables since it relies on the energetic passivity of the system, a property that

holds regardless of whether the cables are in tension or not.

- The controller requires no measurement from the payload.
- Unlike model-based control schemes for attitude dynamics, the passivity-based angular controller does not need system parameters such as the moment of inertia.
- Under-actuation of UAVs has been fully taken into account in the control design and stability analysis. Closed-loop stability is guaranteed using an energy-domain passivity observer and a complementary passivity-based controller.
- The controller is augmented with a term to avoid inter-drone collisions, where this capability is demonstrated through analysis.

6.1.1 Nominal Control Design

Consider the following translational controller for each drone, consisting of a PD controller, an acceleration feedforward term, and a collision avoidance control term,

$$\mu_i \triangleq m_i \ddot{q}_{d_i} - \big(K_{d_i} + \alpha_i(t)\mathcal{I}_3\big)(\dot{q}_i - \dot{q}_{d_i}) - K_{p_i}(q_i - q_{d_i}) + f_{b_i} \tag{6.1}$$

where the gains $K_{d_i}, K_{p_i} \in \mathbb{R}^{3\times 3}$ are positive definite matrices and $q_{d_i}(t) : [0, \infty) \to \mathbb{R}^3$ is the reference position for the ith drone trajectory. The time-varying gain $\alpha_i(t) : [0, \infty) \to \mathbb{R}^+$ is an additional damper and $\mathcal{I}_3 \in \mathbb{R}^{3\times 3}$ is the identity matrix. The collision avoidance term $f_{b_i} \in \mathbb{R}^3$ is assumed to be zero for now and will be designed later. Here $\mu_i \in \mathbb{R}^3$ is the control force that would have been applied if the drones were fully-actuated. Due to under-actuation, an attitude controller will be required

to align the thrust direction with the direction of the desired force in (6.1). It follows from substituting the control thrust in the translational dynamics of the ith drone in (3.2),

$$m_i\ddot{q}_i = f_i R(\eta_{d_i})z + \delta(\eta_i, \eta_{d_i}, f_i) - m_i g z + T_i R_L e_i \tag{6.2}$$

where $\delta(\eta_i, \eta_{d_i}, f_i) \triangleq f_i\Big(R(\eta_i) - R(\eta_{d_i})\Big)z$ is the force error due to the under-actuation and η_{d_i} is the reference attitude.

The requirement for the thrust direction to be aligned with the desired force can be formulated as

$$f_i R(\eta_{d_i})z \triangleq \mu_i \tag{6.3}$$

This provides reference values for the roll and pitch angles as well as the thrust magnitude; A constant reference for the yaw angle can be chosen freely as its value would not impact the direction of the thrust. The attitude controller is given by

$$\tau_i = \Big(\Psi^{\mathrm{T}}(\eta_i)\Big)^{-1}(-K_{v_i}\dot{\eta}_i - K_{c_i}(\eta_i - \eta_{d_i})) \tag{6.4}$$

where $K_{v_i}, K_{c_i} \in \mathbb{R}^{3\times 3}$ are positive definite gains. Unlike the angular controllers in [62], [63], the control law in (6.4) is not based on feedback linearization and hence makes no use of model parameters such as the moment of inertia. It is noted that the derivatives of the desired roll and pitch angles are absent in this controller. This is critical since these desired angles contain linear velocity of the drone, i.e., see (6.1) and (6.3); their derivatives, $\dot{\eta}_{d_i}$ and $\ddot{\eta}_{d_i}$, would involve linear acceleration and jerk,

respectively. Although the linear acceleration of a drone can be measured through onboard accelerometers, jerk measurements are not available directly and would be highly noisy if they were to be obtained through numerical differentiation.

6.1.2 Passivity Observer and Closed-loop Stability

The desired motion trajectories for the individual quad-rotors are denoted by $q_{d_i} : [0, \infty) \rightarrow \mathbb{R}^3, \ \forall i = 1, ..., n$. These reference trajectories are designed such that $\dot{q}_{d_i} = \dot{q}_d$, $\ddot{q}_{d_i} = \ddot{q}_d$, i.e., all quad-rotors are required to move with the same velocity and acceleration. This would ensure that the drones would preserve their spatial configuration throughout the flight, hence reducing the possibility of inter-drone collisions. It is also assumed that $\dot{q}_d, \ \ddot{q}_d \in \mathcal{L}_\infty$ and $\lim_{t\rightarrow\infty} \ddot{q}_d = 0$. The closed-loop dynamics of the system with the proposed controller in (6.1) and (6.4) and reference trajectories can be written as,

$$m_i\ddot{\tilde{q}}_i + \big(K_{d_i} + \alpha_i(t)\mathcal{I}_3\big)\dot{\tilde{q}}_i + K_{p_i}\tilde{q}_i = \delta_i(\eta_i, \eta_{d_i}, f_i) - m_i g z + T_i R_L e_i \tag{6.5}$$

$$M(\eta_i)\ddot{\eta}_i + C(\eta_i, \dot{\eta}_i)\dot{\eta}_i = -K_{v_i}\dot{\eta}_i - K_{c_i}(\eta_i - \eta_{d_i}) + \Psi^T(\eta_i) d_i^\times (T_i R_i^T R_L e_i) \tag{6.6}$$

$$m_L(\ddot{q}_L - \ddot{q}_d) = -\sum_{i=1}^{n} T_i R_L e_i - m_L g z - m_L \ddot{q}_d \tag{6.7}$$

$$J_L\dot{\omega}_L + \omega_L^\times J_L \omega_L = \sum_{i=1}^{n} r_i^\times (-T_i e_i) \tag{6.8}$$

where $\tilde{q}_i \triangleq q_i - q_{d_i}$. Consider the following storage function for the closed-loop system,

$$\begin{aligned} V =& \frac{1}{2}\sum_{i=1}^{n} m_i \dot{\tilde{q}}_i^{\mathrm{T}} \dot{\tilde{q}}_i + \frac{1}{2}\sum_{i=1}^{n} \tilde{q}_i^{\mathrm{T}} K_{p_i} \tilde{q}_i + \frac{1}{2}\sum_{i=1}^{n} \dot{\eta}_i^{\mathrm{T}} M(\eta_i)\dot{\eta}_i \\ &+ \frac{1}{2}\sum_{i=1}^{n} (\eta_i - \eta_{d_i})^{\mathrm{T}} K_{c_i} (\eta_i - \eta_{d_i}) + \sum_{i=1}^{n} m_i g z^{\mathrm{T}} \tilde{q}_i \\ &+ \frac{1}{2} m_L \dot{\tilde{q}}_L^{\mathrm{T}} \dot{\tilde{q}}_L + \frac{1}{2}\omega_L^{\mathrm{T}} J_L \omega_L + m g z^{\mathrm{T}} (q_L - \frac{\sum_{i=1}^{n} q_{d_i}}{n}) + \beta \end{aligned} \tag{6.9}$$

where $\dot{\tilde{q}}_L \triangleq \dot{q}_L - \dot{q}_d$ and $\beta \in \mathbb{R}^+$ adjusts the reference for potential gravity. Using the energetic passivity property of the system in chapter 3, it can be shown that the time derivative of (6.9) along the system trajectories (6.5), (6.6), (6.7) and (6.8) is given by,

$$\begin{aligned} \dot{V} =& -\sum_{i=1}^{n} \dot{\tilde{q}}_i^{\mathrm{T}} \big(K_{d_i} + \alpha_i(t)\mathcal{I}_3\big)\dot{\tilde{q}}_i - \sum_{i=1}^{n} \dot{\eta}_i^{\mathrm{T}} K_{v_i} \dot{\eta}_i \\ &+ \sum_{i=1}^{n} \dot{\eta}_{d_i}^{\mathrm{T}} K_{c_i} (\eta_{d_i} - \eta_i) + \sum_{i=1}^{n} \dot{\tilde{q}}_i^{\mathrm{T}} \delta_i(\eta_i, \eta_{d_i}, f_i) - \dot{\tilde{q}}_L^{\mathrm{T}} \ddot{q}_d \end{aligned} \tag{6.10}$$

Equation (6.10) can be rewritten as $\dot{V} \triangleq Q + W$ to distinguish dissipative and sign-indefinite terms where $Q, W \in \mathbb{R}$ are defined as,

$$\begin{aligned} Q \triangleq& -\sum_{i=1}^{n} \dot{\tilde{q}}_i^{\mathrm{T}} \big(K_{d_i} + \alpha_i(t)\mathcal{I}_3\big)\dot{\tilde{q}}_i - \sum_{i=1}^{n} \dot{\eta}_i^{\mathrm{T}} K_{v_i} \dot{\eta}_i \\ W \triangleq& \sum_{i=1}^{n} \dot{\tilde{q}}_i^{\mathrm{T}} \delta_i(\eta_i, \eta_{d_i}, f_i) + \sum_{i=1}^{n} \dot{\eta}_i^{\mathrm{T}} K_{c_i} (\eta_{d_i} - \eta_i) - \dot{\tilde{q}}_L^{\mathrm{T}} \ddot{q}_d \end{aligned}$$

If the UAVs were fully-actuated, the first two terms of W would not have appeared. The last term of W is due to the under-actuation of the payload. The goal is to choose the time-varying damping term $\alpha_i(t)$ such that the value of the storage function $V(t)$ is

decreased over time. Ideas from the time-domain passivity observer/controller [27] or energy monitoring appraches [21] can be employed to this end. The passivity observer can be implemented in power or energy domain. However, the power-domain observer is more conservative as it requires $\dot{V}(t) \leq 0$ without considering the time history of the two terms Q and W [2]. In this paper, an energy-domain observer is considered. The tank-based energy approach also works in the energy domain [20].

It is noted that the sign indefinite term W involves the payload velocity in $-\dot{\tilde{q}}_L^{\mathrm{T}}\ddot{q}_d$, which is not measured. The passivity observer would have to compute the time integral of W. The integral of the term involving the payload velocity can be written as,

$$-\int_0^t (\dot{q}_L - \dot{q}_d)^{\mathrm{T}} \ddot{q}_d d\xi = -q_L^{\mathrm{T}}\ddot{q}_d + \int_0^t q_L^{\mathrm{T}} \dddot{q}_d d\xi + \frac{1}{2}\dot{q}_d^{\mathrm{T}}\dot{q}_d + c$$

where integration by parts has been used and $c \in \mathbb{R}$ is a constant obtained based on initial conditions. Given the application of interest, it is safe to assume that the reference positions signals are smooth and slow-varying, hence $\dddot{q}_d \approx 0$. Furthermore, using the kinematic constraint (3.1), it can be shown that

$$-q_L^{\mathrm{T}}\ddot{q}_d \leq \|\ddot{q}_d\|\|q_L\| \leq \|\ddot{q}_d\|\Big(\|q_i\| + \max\{r_i + d_i\} + l_i\Big) \triangleq \Gamma(t, q_i) \tag{6.11}$$

It follows from the above inequality that $\int_0^t W d\xi \leq \int_0^t \bar{W} d\xi$ with

$$\bar{W} \triangleq \sum_{i=1}^{n} \dot{\tilde{q}}_i^{\mathrm{T}} \delta(\eta_i, \eta_{d_i}, f_i) + \frac{d}{dt}\Big(\Gamma(t, q_i) + \frac{1}{2}\dot{q}_d^{\mathrm{T}}\dot{q}_d\Big) + \sum_{i=1}^{n} \dot{\eta}_{d_i}^{\mathrm{T}} K_{c_i}(\eta_{d_i} - \eta_i) \tag{6.12}$$

Therefore, using (6.12) and $\dot{V} = Q + W$,

$$V(t) - V(0) \leq \int_0^t (Q + \bar{W}) d\xi \tag{6.13}$$

Let $\epsilon \in \mathbb{R}^+,\ 0 < \epsilon < 1$. Then the above inequality can be re-written as,

$$V(t) - V(0) \leq \int_0^t \Big((1-\epsilon)Q + \bar{W}\Big) d\xi + \epsilon \int_0^t Q d\xi \tag{6.14}$$

Consider the following two cases where ΔT is the sampling time of the system and $\mathtt{j}$ is the sample number:

- If $\int_0^{(\mathtt{j}-1)\Delta T} \Big((1-\epsilon)Q + \bar{W}\Big) d\xi \leq 0$, then the system is dissipating sufficient energy and there is no need for extra dissipation. In this case, $\alpha_i(\mathtt{j}\Delta T) = 0$.
- If $\int_0^{(\mathtt{j}-1)\Delta T} \Big((1-\epsilon)Q + \bar{W}\Big) d\xi > 0$, the value of the time-varying damping is computed as,

$$\alpha_i(\mathtt{j}\Delta T) = \frac{\int_0^{(\mathtt{j}-1)\Delta T} \Big((1-\epsilon)Q + \bar{W}\Big) d\xi}{n\Delta T \dot{\tilde{q}}_i^{\mathrm{T}} \dot{\tilde{q}}_i} \tag{6.15}$$

  so the quad-rotors contribute equally to the dissipation.

This would ensure that

$$\int_0^{(\mathtt{j}-1)\Delta T} \Big((1-\epsilon)Q + \bar{W}\Big) d\xi \leq 0,\ \forall t > 0 \tag{6.16}$$

Since $\epsilon \int_0^t Q d\xi \leq 0$, it can be concluded that,

$$V(t) - V(0) \leq \int_0^t \Big((1-\epsilon)Q + \bar{W}\Big) d\xi + \epsilon \int_0^t Q d\xi \leq 0 \tag{6.17}$$

It follows from (6.17) that $V(t) \leq V(0)$ which guarantees boundedness of the storage function, i.e. $V(t) \in \mathcal{L}_\infty$. Therefore, all the states in the storage function (6.9) are also bounded. Note that using (6.17),

$$V(t) - V(0) \leq \epsilon \int_0^t Q d\xi \tag{6.18}$$

and hence,

$$V(t) + \epsilon \int_0^t \Big(\sum_{i=1}^{n} \dot{\tilde{q}}_i^{\,\mathrm{T}} K_{d_i} \dot{\tilde{q}}_i + \sum_{i=1}^{n} \dot{\eta}_i^{\mathrm{T}} K_{v_i} \dot{\eta}_i \Big) d\xi \leq V(0) \tag{6.19}$$

which proves that $\dot{\tilde{q}}_i, \dot{\eta}_i \in \mathcal{L}_2$. The closed-loop dynamics can be employed to show $\ddot{\tilde{q}}_i, \ddot{\eta}_i \in \mathcal{L}_\infty$, which guarantees the uniform continuity of the velocities. Now, it follows from the Barbalat's lemma [85] that $\lim_{t\to\infty} \dot{\tilde{q}}_i, \dot{\eta}_i = 0$. Similar arguments can be made to show convergence of the acceleration signals.

Remark 3 *The sign-indefinite term in the passivity observer, $\bar{W}$, includes the derivative of the reference command for the angular position, i.e., $\dot{\eta}_{d_i}$. It follows from taking the derivative of Eq. (6.3) and the position controller in (6.1) that this command contains the linear acceleration. The proposed passivity observer works in energy domain and so it actually needs the integral of $\bar{W}$. This should filter out some of the noise typically present in the acceleration measurements.*

Remark 4 *In practice the actuator thrusts are limited, which restricts the values of $\alpha_i(\mathrm{j}\Delta T)$. In such cases, the leftover energy would be dissipated in the subsequent sample times.*

Remark 5 *The parameter ϵ determines how conservative the passivity observer behaves. It changes the portion of dissipative energy from the nominal controller coming to the passivity observer. If $\epsilon \to 0$ is picked, then the passivity observer considers all the dissipation from the nominal controller. As a result, it may need to activate the passivity controller less frequently. If $\epsilon \to 1$ is picked, then the passivity observer considers almost no dissipation from the nominal controller. As a result, it may always try to activate the passivity controller to preserve stability. If a wider and more conservative stability margin is needed, then ϵ has to be closer to unity. The price for a conservative stability margin is a more sluggish motion control system.*

6.1.3 Inter-drone Collision Avoidance

It is noted that the proposed translational controller in (6.1) with $f_{b_i} = 0$ may lead to drone-to-drone collisions during the transient phase of the response or due to disturbances such as wind depending on the reference trajectories and values of the control gains. A constraint of the form $\mathcal{C}_{ij}(t) = (q_i - q_j)^{\mathrm{T}}(q_i - q_j) - r_{ij}^2 > 0$, where $r_{ij} = r_{ji} \in \mathbb{R}^+, j \neq i$ is a distance threshold, can be imposed to maintain a safe distance between ith and jth drones. To this end, the following barrier Lyapunov function is defined,

$$V_b = \frac{1}{2} \sum_{i=1}^{n} \sum_{\substack{j=1 \\ j \neq i}}^{n} \frac{k_{b_{ij}} \tilde{q}_i^{\mathrm{T}} \tilde{q}_i}{\Big((q_i - q_j)^{\mathrm{T}}(q_i - q_j) - r_{ij}^2 \Big)^2} \tag{6.20}$$

where $k_{b_{ij}} = k_{b_{ji}} \in \mathbb{R}^+$ is a control gain. Now, consider $V_T = V + V_b$ where V is defined in (6.9), as the new closed-loop storage function. It follows from (6.20) and

the closed-loop dynamics with nonzero f_{b_i} that,

$$\dot{V}_T = \dot{V} + \sum_{i=1}^{n} \dot{\tilde{q}}_i^{\mathrm{T}} f_{b_i} + \sum_{i=1}^{n} \sum_{\substack{j=1 \\ j\neq i}}^{n} \frac{k_{b_{ij}} \dot{\tilde{q}}_i^{\mathrm{T}} \tilde{q}_i}{\left((q_i - q_j)^{\mathrm{T}}(q_i - q_j) - r_{ij}^2\right)^2} - \sum_{i=1}^{n} \sum_{\substack{j=1 \\ j\neq i}}^{n} \frac{k_{b_{ij}} \tilde{q}_i^{\mathrm{T}} \tilde{q}_i (\dot{\tilde{q}}_i - \dot{\tilde{q}}_j)^{\mathrm{T}}(q_i - q_j)}{\left((q_i - q_j)^{\mathrm{T}}(q_i - q_j) - r_{ij}^2\right)^3} \tag{6.21}$$

where $\dot{q}_{d_i} = \dot{q}_d$ has been used. By choosing the collision avoidance control term as,

$$f_{b_i} \triangleq - \sum_{\substack{j=1 \\ j\neq i}}^{n} \frac{k_{b_{ij}} \tilde{q}_i}{\left((q_i - q_j)^{\mathrm{T}}(q_i - q_j) - r_{ij}^2\right)^2} + \sum_{\substack{j=1 \\ j\neq i}}^{n} \frac{(k_{b_{ij}} \tilde{q}_i^{\mathrm{T}} \tilde{q}_i + k_{b_{ij}} \tilde{q}_j^{\mathrm{T}} \tilde{q}_j)(q_i - q_j)}{\left((q_i - q_j)^{\mathrm{T}}(q_i - q_j) - r_{ij}^2\right)^3} - \sum_{\substack{j=1 \\ j\neq i}}^{n} k_{d_{ij}} (\dot{\tilde{q}}_i - \dot{\tilde{q}}_j) \tag{6.22}$$

where $k_{d_{ij}} = k_{d_{ji}} \in \mathbb{R}^+$. It can be shown that,

$$\dot{V}_T = \dot{V} - \sum_{\substack{j=1 \\ j\neq i}}^{n} (\dot{\tilde{q}}_i - \dot{\tilde{q}}_j)^{\mathrm{T}} k_{d_{ij}} (\dot{\tilde{q}}_i - \dot{\tilde{q}}_j) \tag{6.23}$$

It follows from (6.17) and (6.23) that $V_T(t) < V_T(0)$ which demonstrates the boundedness of $V(t)$, $V_b(t)$ and the signals therein. Moreover, as $\dot{\tilde{q}}_i$ and $\dot{q}_d$ are bounded, the uniform continuity of q_i is guaranteed. Hence, the constraint $\mathcal{C}_{ij}(t)$ is continuous.

Suppose that the initial conditions are such that $\mathcal{C}_{ij}(0) > 0$. Note that $V_b(t) = \frac{1}{2} \sum_{i=1}^{n} \sum_{\substack{j=1 \\ j\neq i}}^{n} \frac{k_{b_{ij}} \tilde{q}_i^{\mathrm{T}} \tilde{q}_i}{\mathcal{C}_{ij}^2} \to \infty$ only if $\mathcal{C}_{ij} \to 0$. Therefore $\mathcal{C}_{ij}(t) > 0$ because of its continuity and $V_b(t) \in \mathcal{L}_\infty$. All these theoretical results can be summarized in the following theorem. The block diagram of the proposed control scheme has been illustrated in Figure 6.1 as well.

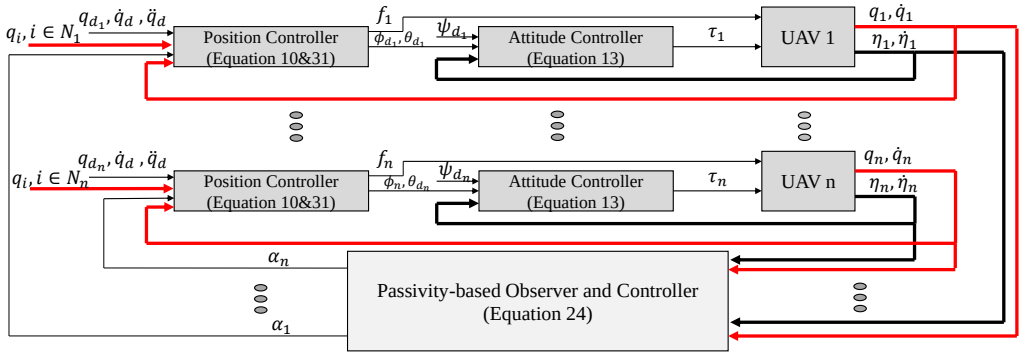

Figure 6.1: Block diagram of the proposed control system for n UAVs. The thick red and black lines represent the translational and angular measurements, respectively. The set N_i includes the neighbors of the ith UAV.

Theorem 3 *Consider the equations of motion (3.2), (3.3), (3.4), (3.5) for the cable-based aerial transportation system with shifted attachment points. Suppose the initial conditions are sufficiently small and the safety constraint $\mathcal{C}_{ij}(0) > 0$ is initially satisfied. Then, the passivity-based control force in (6.1) with time-varying gain (6.15) and the control moment (6.4) achieve the following results:*

1. *The safety constraint $\mathcal{C}_{ij}(t) = (q_i - q_j)^T(q_i - q_j) - r_{ij}^2 > 0$ is satisfied for $t \geq 0$.*

2. *The motion variables remain bounded for $t \geq 0$.*

3. *If $\lim_{t\to\infty} \ddot{q}_d = 0$, then velocities are synchronized for all the robots and the payload, i.e., $\lim_{t\to\infty} \dot{\tilde{q}}_i = 0$ and $\lim_{t\to\infty} \dot{\tilde{q}}_L = 0$.*

6.2 Experimental Validation

In the experiments, three conventional quad-rotors each weighing $m_i = 0.67$ kg cooperatively carry a cable-suspended payload with a mass of $m_L = 0.4$ kg. The cable

attachment points are intentionally placed off the COMs of the drones. The experimental setup is similar to Figure 5.2. See chapter 5 for more details on the hardwares. The outer-loop control gains for all the quad-rotors are as follows,

$$K_{p_i} = \text{diag}\{9, 6, 9\} \quad , \quad K_{d_i} = \text{diag}\{3, 2.25, 1.25\}$$

where the cuboid shape of the battery led to different control parameters along the x and y axis. In addition, there exists a trade-off in picking both of proportional and derivative terms. If the gain K_{p_i} is increased, then the system would have a smaller steady state error due to gravity and disturbances. However, a higher K_{p_i} may lead to oscillations in the system response as well as hitting the saturation limit of actuators. If the nominal damping, K_{d_i} is increased, then it may make the response sluggish as it injects dissipation. However, a very low value for K_{d_i} can also cause an oscillatory response. The inner-loop control gains for all the quad-rotors are selected as,

$$K_{c_i} = \text{diag}\{10, 15, 18\} \quad , \quad K_{v_i} = \text{diag}\{7.5, 8.5, 10\}$$

The barrier function gains are $k_{b_{ij}} = 0.15$ for all the inter-drone collision avoidance terms and $\epsilon = 0.1$ is selected for the passivity observer. The inter-drone damper coefficients, $k_{d_{ij}}$, are set to zero, unless stated otherwise. Three scenarios were considered to illustrate the effectiveness of the proposed controller. Videos demonstrating these scenarios are available at `https://youtu.be/UQTLOxcVb6w` and `https://youtu.be/1vmqre2lpCU`.

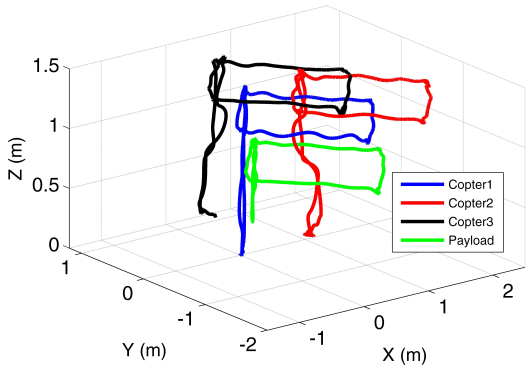

Figure 6.2: The trajectories of the drones and the payload during the flight. Note that the payload position is measured only for illustration and is not used in the controller.

6.2.1 Square-Shaped Reference Trajectory

The first experiment scenario is as follows. First, the drones fly up to an altitude of about $z = 1.4$ m. Then, they follow a square trajectory parallel to the ground in the $x-y$ plane. Once back at the same $x-y$ position, they land at their original location on the ground. The yaw angles are kept at zero for all the three quad-rotors.

Figure 6.2 shows the position trajectories of the drones as well as the payload. The drones are able to fly stably along their desired paths with some small errors mostly due to the gravity. It should be noted that the position of the payload is measured only for illustration purposes and is not used in the control.

Figure 6.3 displays the behavior of the passivity observer over time. It is notable that around $t = 7$ sec, as the quad-rotors begin to ascend, the passivity observer detects potential active behavior from the nominal controller and responds by activating the time-varying damping. This triggers extra dissipation to prevent build-up of the storage function. For the remainder of the flight, the passivity observer/controller remains inactive as no extra dissipation is needed beyond what is already provided

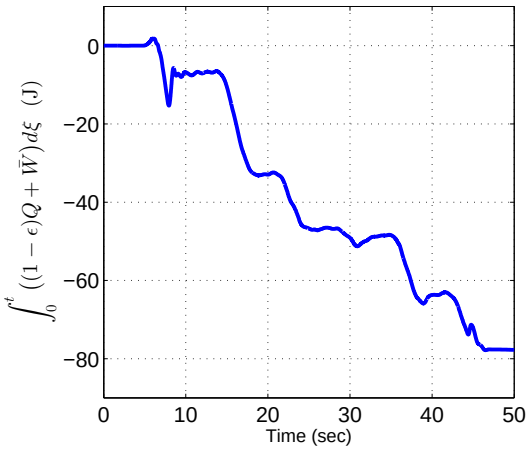

Figure 6.3: The response of passivity observer/controller. At around $t = 7$ sec, the cables status changes from slack to taut. This is when the drones start to ascend and the payload suddenly leaves the ground. As a result, abrupt forces and moments are exerted on the quad-rotors leading to potential active behavior by the nominal controller. This is immediately remedied by the passivity observer/controller.

by the nominal controller.

Figure 6.4 plots the thrust forces of the quad-rotors versus time. Note that around $t = 7$ sec, the time-varying dampers are activated to contribute to system stability. Figure 6.5 shows the euclidean norm of relative distances of quad-rotors as a function of time. All the constraints were set to $\mathcal{C}_{ij} > 0.65$ m. It is evident that the control system satisfies the collision avoidance constraints throughout the flight.

Payload swing can be a concern in aerial transportation and its reduction is desirable [62]. Figure 6.6 represents the attitude of the payload during the flight. Disregarding the take-off stage, the rest of the flight shows a satisfactory swing for the payload. The proposed controller successfully attenuates oscillations in the payload motion. Figure 6.7 depicts the position errors of the quad-rotors during the square-trajectory flight. The position errors are mainly due to effects of the cables and gravity.

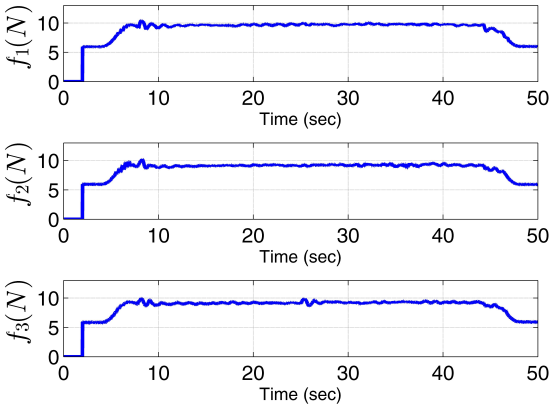

Figure 6.4: Plots of the thrust forces of the quad-rotors. The first and last four-second segments correspond to the ramp-up and ramp-down phases of the propellers.

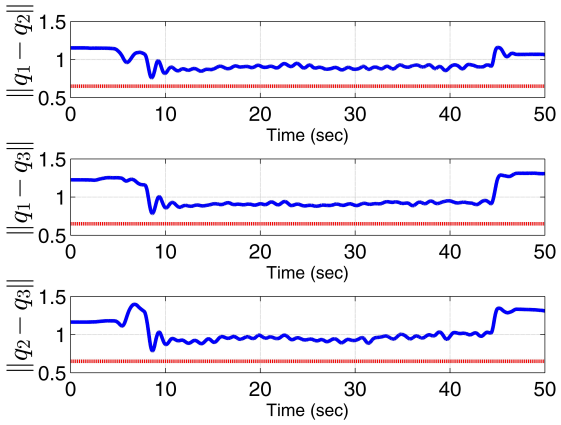

Figure 6.5: Distances between drones throughout the square-shaped trajectory. The red lines represent the minimum distances which are set to $r = 0.65$ m for all the constraints.

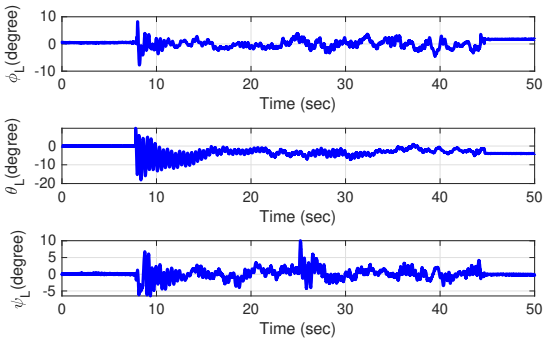

Figure 6.6: Payload attitude angles throughout the square-trajectory flight. Except a few spikes, the rest of the flight has an acceptable swing range.

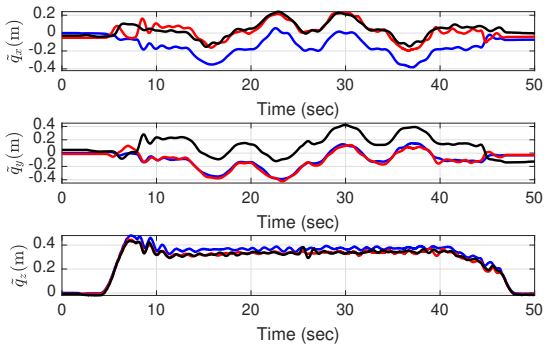

Figure 6.7: Quad-rotors position errors while following the square-trajectory. The blue, red and black belong to quad-rotor 1, 2, and 3, respectively.

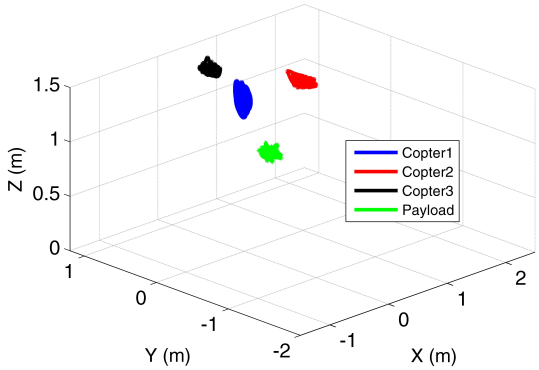

Figure 6.8: The trajectories of the drones and the payload during the second set of experiments where the payload is subject to 20 perturbations. The flight is about 90 second long at a constant altitude. The ascending and landing phases are excluded from the plots to better display the response to the disturbances.

6.2.2 Robustness to Perturbations

In this experiment, the drones hover at a constant altitude of $z = 1.4$ m for about 90 seconds. The payload is perturbed using a stick for 20 times during the flight. The perturbations propagate to the drones due to mechanical coupling. Figure 6.8 illustrates the positions of the drones and the payload in response to the perturbations. There are some deviations from the nominal positions as a result. Figure 6.9 shows that the minimum set distance between the drones are kept despite the disturbances, demonstrating the effectiveness of the collision avoidance control using a barrier function.

It is instructive to see how the passivity observer and controller manage to preserve stability of the system throughout this flight. Figure 6.10 demonstrates the time history of the passivity observer. Once the observer detects an active behaviour in the system, it instantaneously triggers the passivity controller by injecting additional damping to the system and quickly dissipating the extra energy. Figure 6.11 shows

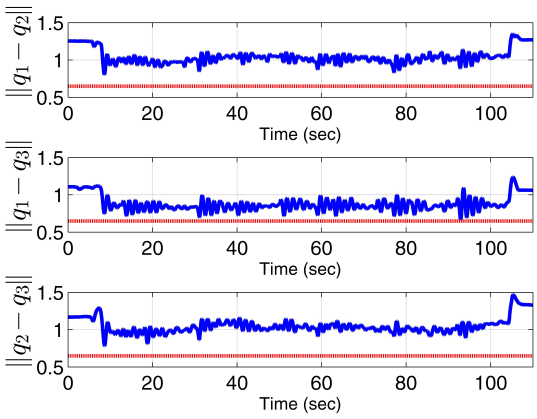

Figure 6.9: Distances between drones in the second scenario where the payload is subject to 20 perturbations and $k_{d_{ij}} = 0$. The red lines represent the minimum distances which are set to $r = 0.65$ m for all the constraints. Note that the minimum set distance is satisfied throughout the flight.

the values of time-varying dampings which respond to active behavior detected by the passivity observer.

The performance of the proposed controller in the second scenario was also compared to the controller in Chapter 4 to highlight the effectiveness of the collision avoidance strategy. Although the system remained stable during the flight with the controller in Chapter 4, the data in Tables 6.1 and 6.2 show the new controller is much more effective in keeping the drones away at a safe distance from each other. Figure 6.12 also shows that with the controller in Chapter 4, the drones would violate the minimum distant constraint a number of times as the controller obviously lacks a mechanism for enforcing such constraints.

It is instructive to compare Figure 6.9 and Figure 6.12 in terms of oscillations. The formation controller with $k_{d_{ij}} = 0$ only includes terms with respect to relative positions and lacks damping. The barrier function exerts significant repulsive forces and introduces oscillations that are damped poorly. This problem is resolved by

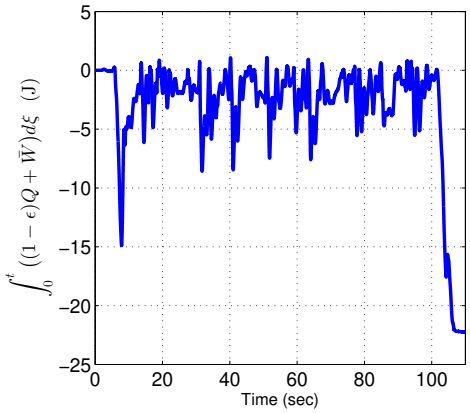

Figure 6.10: The output of the passivity observer in the second experiment scenario. This is used for introducing additional damping in the system. Note that positive values indicate active behavior which is quickly remedied by the controller.

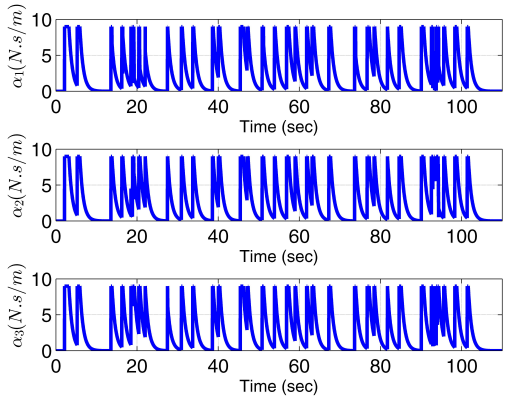

Figure 6.11: The values of time-varying dampers used to compensate for active behavior in the system during the second experiment scenario.

Table 6.1: Minimum distance (in meters) between the drones in the second experiment scenario.

$\min(\|q_i - q_j\|)$	$\|q_1-q_2\|$	$\|q_1-q_3\|$	$\|q_2-q_3\|$
Equ. 6.22 with $k_{d_{ij}}=0$	0.80	0.66	0.78
Equ. 6.22 with $k_{d_{ij}}=0.9$	0.80	0.77	0.83
The controller in Chapter 4	0.69	0.54	0.69

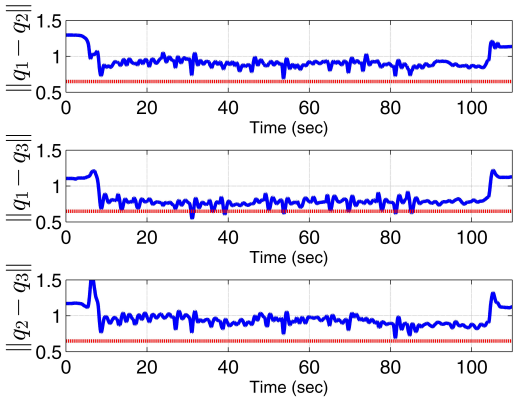

Figure 6.12: The distances between the drones in the second experiment scenario using the controller in Chapter 4. Note that the distance between the second and third drones falls below the safety threshold a number of times during the experiment.

Table 6.2: The average values of the distances (in meters) between the drones in the second experiment scenario.

mean($\|q_i - q_j\|$)	$\|q_1 - q_2\|$	$\|q_1 - q_3\|$	$\|q_2 - q_3\|$
Equ. 6.22 with $k_{d_{ij}} = 0$	1.01	0.84	1.02
Equ. 6.22 with $k_{d_{ij}} = 0.9$	0.98	0.90	0.94
The controller in Chapter 4	0.89	0.77	0.92

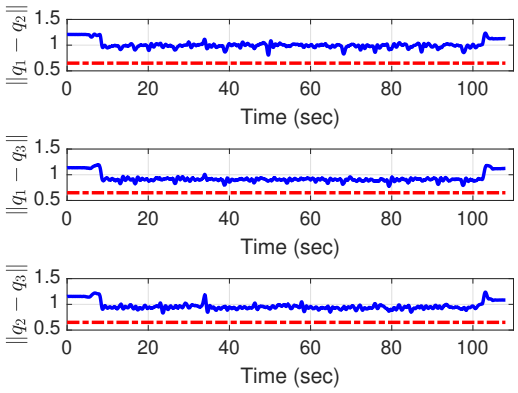

Figure 6.13: The distances between the drones while the payload was perturbed for 20 times by a wooden stick. The inter-drone damper $k_{d_{ij}} = 0.9$ eliminates the oscillations induced by the barrier terms. The drones maintain the minimum safety distance throughout the experiment.

introducing inter-drone dissipative terms ($k_{d_{ij}} = 0.9$), as it can be seen in Figure 6.13. The oscillations have diminished significantly compared to the case with $k_{d_{ij}} = 0$. In addition, the minimum safe inter-drone distances are still maintained throughout the experiment.

6.2.3 Aggressive Maneuver

Aggressive maneuvers are not usually desirable or expected in typical transportation applications. In the square trajectory following experiment the average velocity of the UAVs was $0.3\frac{m}{s}$ between any two consecutive way-points. A new experiment was carried out to test how the controller would respond to more aggressive reference trajectories.

Butterfly-shaped reference trajectories were considered for the three quad-copters as shown in Figure 6.14. The scenario for this experiment is as follows: First, the drones ascend to a desired altitude of $2.1m$. Then, they simultaneously move $-1.5m$

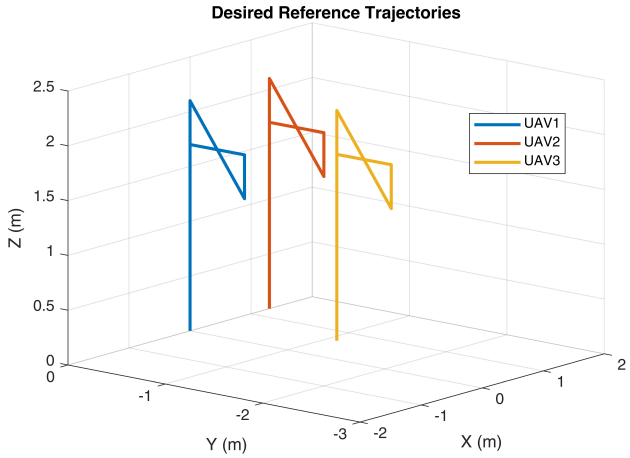

Figure 6.14: Aggressive butterfly-shaped desired trajectories for the three quad-copters.

along both x and y axis while reducing the height to a desired value of $1.7m$. While at the same x and y coordinates, they go up again to a desired altitude of $2.1m$. Next, they come back to the original locations while decreasing a desired height of $1.7m$. Finally, the cooperative aerial transportation system lands at the initial place.

Figures 6.15 and 6.16 demonstrate the desired velocity and acceleration of the flock, respectively. It can be seen that the maximum desired acceleration in this experiment was $2.25\frac{m}{s^2}$.

Figures 6.17, 6.18 and 6.19 illustrate the time history of the positions for the first, second and third quad-copters, respectively. The desired trajectories have been shown in blue color. It can be seen that the control system successfully preserved stability during the aggressive maneuver. The existing errors are mainly due to the effect of cables and gravity.

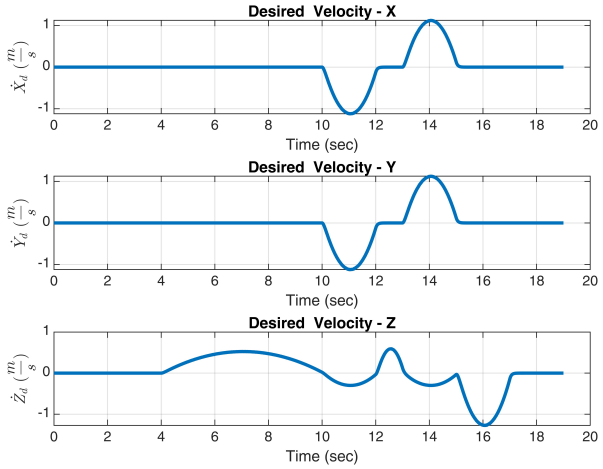

Figure 6.15: Desired velocity of the formation in the aggressive maneuver experiment.

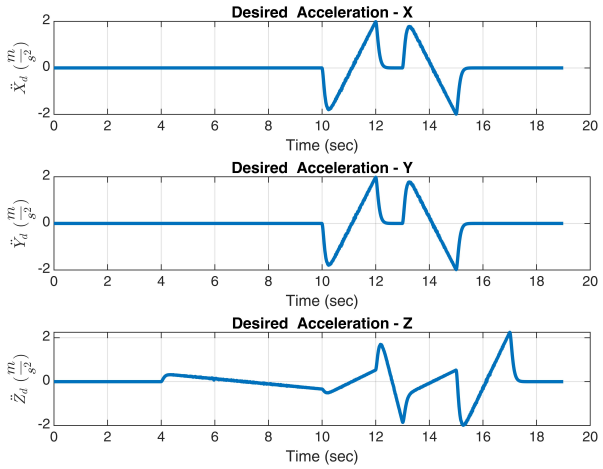

Figure 6.16: Desired acceleration of the formation in the aggressive maneuver experiment.

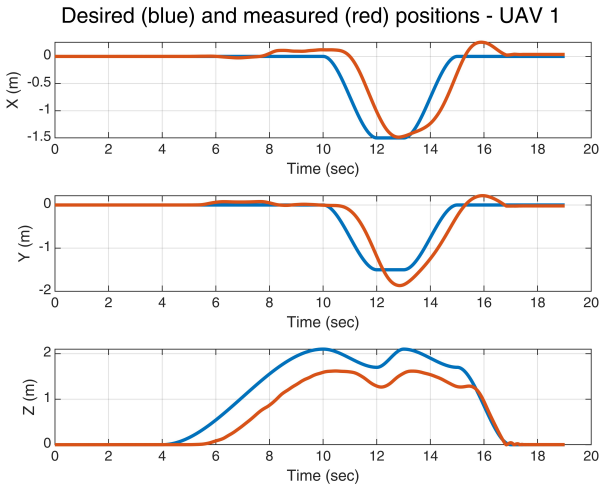

Figure 6.17: UAV 1 - Desired and measured positions in the aggressive maneuver

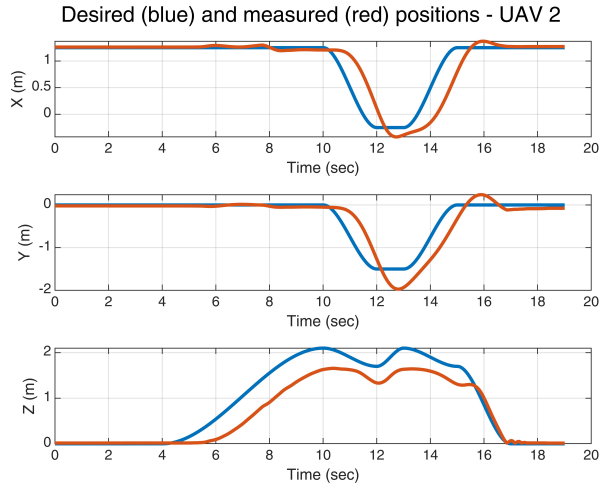

Figure 6.18: UAV 2 - Desired and measured positions in the aggressive maneuver

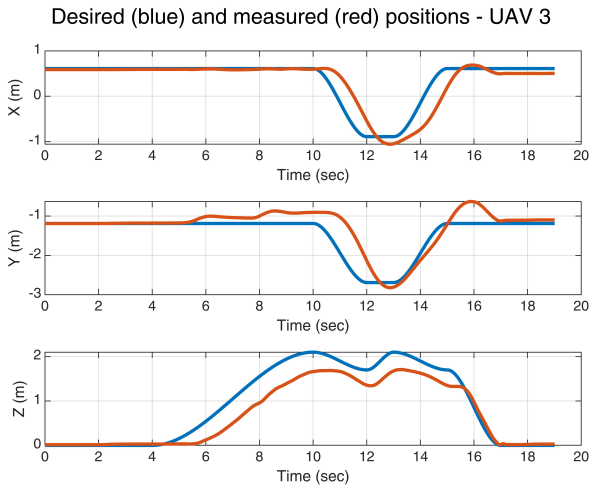

Figure 6.19: UAV 3 - Desired and measured positions in the aggressive maneuver

6.3 Summary

In this chapter, a passivity-based control approach was proposed for stable motion control of multiple quad-rotors carrying a cable-suspended payload. The controller requires no measurements from the payload and guarantees the closed-loop stability irrespective of the status of cable tensions. It also accommodates arbitrary cable attachment points between the payload and the drones. The controller combines nominal PD-type translational and attitude controllers with correction terms to maintain stability in the presence of the quad-rotors under-actuation. To this end, an energy-like storage function was defined and the dissipative terms were computed to ensure that the value of this storage function decreased over time, guaranteeing the stability of the control system. The controller was augmented with a collision avoidance term to ensure that drones keep a minimum safe distance between each other during their operation. In experiments, three conventional quad-rotors were able to stably carry a cable-suspended payload using the proposed controller. Moreover, the new controller

maintained a pre-defined minimum safe distance among the drones even when the payload was subjected to repeated disturbances; a baseline controller, used for comparison, failed to do so. Furthermore, the proposed controller preserved stability for a more aggressive maneuver.

In the next chapter, a cooperative passivity-based control strategy is introduced which is highly effective in preserving the formation shape. Interactive control actions among UAVs require transmitting of measurements. As the control law depends on measurements from the other agents, it is practical to introduce time-delay into the analysis as well. Hence, closed-loop stability has to be proven in the presence of both time-delay and under-actuation.

Chapter 7

Cooperative Control with Time Delay

The control laws presented in Chapters 4 and 5 are decentralized in the sense that the individual controller on each quad-copter relies on its measurement and can be implemented locally. The only coordination among the quad-copters is through the coordinated desired position trajectories that represent the desired formation in motion. The main advantage of this decentralized architecture is its simplicity that eliminates the need for inter-drone communication. However, external disturbances can potentially affect the formation shape more significantly because of this lack of communication. In this chapter, additional inter-drone coupling terms are introduced in the control laws to help preserve better the formation shape in the presence of disturbances. The inclusion of these coupling terms in the control law can introduce time delay in some of the feedback signals. These delays could potentially cause system instability [29]. It is therefore crucial to carefully analyze the closed-loop stability by considering the delays in the feedback loops. To this end, a formal proof of stability

has been provided, which utilizes Lyapunov-Krasovskii functionals [61] along with the theorems from cascaded systems [77]. It is noted that the work in [53] addressed the formation control problem of quad-copters with communication delays. However, the angular controller in that paper requires attitude velocity and acceleration reference commands.

7.1 Mathematical Preliminaries

Theorem 4 ([54]) *Consider the following linear system with constant time delay* $\mathfrak{T} \in \mathbb{R}^+$,

$$\dot{x} = A_1 x + A_2 x(t - \mathfrak{T}) \quad , \quad t \geq 0 \tag{7.1}$$

where $x \in \mathbb{R}^{\mathfrak{n}}$, $A_1, A_2 \in \mathbb{R}^{\mathfrak{n}\times\mathfrak{n}}$ *denote the state variables and system matrices, respectively. This time-delayed system is exponentially stable with decay rate* $\alpha > 0$ *if there exists symmetric positive definite matrices* $P, Q \in \mathbb{R}^{\mathfrak{n}\times\mathfrak{n}}$ *such that the following linear matrix inequality holds:*

$$S^*(\alpha,\mathfrak{T},A_1,A_2) \triangleq \begin{bmatrix} \bar{A}^T P + P\bar{A} + \mathfrak{T}Q & \mathfrak{T}e^{\alpha\mathfrak{T}}\bar{A}^T P A_2 \\ \mathfrak{T}e^{\alpha\mathfrak{T}} A_2^T P \bar{A} & -\mathfrak{T}Q \end{bmatrix} < 0 \tag{7.2}$$

where $\bar{A} = A_1 + \alpha I_{\mathfrak{n}} + A_2 \exp(\alpha\mathfrak{T})$ *and* $I_{\mathfrak{n}} \in \mathbb{R}^{\mathfrak{n}\times\mathfrak{n}}$ *is the identity matrix. Then, the time-delayed system in (7.1) is exponentially stable with stability degree* α.

Proof. The transformation $w(t) = \exp(\alpha t)x(t)$ turns dynamical equation (7.1) into the following system,

$$\dot{w}(t) = (A_1 + \alpha I_{\mathfrak{n}})w(t) + A_2 \exp(\alpha\mathfrak{T})w(t - \mathfrak{T}) \tag{7.3}$$

Now, consider the following Lyapunov-Krasovskii functional candidate,

$$\mathcal{V}(w_t) = L(w_t)^{\mathrm{T}} P L(w_t) + \int_{-\mathfrak{T}}^{t} \int_{t+s}^{t} w(\rho)^{\mathrm{T}} Q w(\rho) d\rho ds \tag{7.4}$$

where $L(w_t) \triangleq w(t) + \int_{t-\mathfrak{T}}^{t} A_2 \exp(\alpha\mathfrak{T})w(s)ds$. After some algebraic manipulations, the time derivative of the functional (7.4) along the trajectory of the system (7.3) can be obtained as,

$$\dot{\mathcal{V}}(w_t) = w^{\mathrm{T}}(t) S^* w(t) < 0 \tag{7.5}$$

which proves asymptotic stability of the dynamical system in (7.3). Since $\lim_{t\to\infty} w(t) = 0$, the coordinate transform $\exp(-\alpha t)w(t) = x(t)$ shows exponential stability of $x(t)$ by a decay rate α. See [54] for the details.

Lemma 1 *Consider the following time-delayed perturbed system,*

$$\dot{x} = A_1 x + A_2 x(t - \mathfrak{T}) + f(t, x) \quad , \quad t \geq 0 \quad , \quad x \in \mathcal{D} \tag{7.6}$$

where $\mathfrak{T}$ is a constant delay. Assume the origin is an exponentially stable equilibrium for the nominal system, i.e. $f(x) = 0$. Suppose the perturbation satisfies $\|f(t, x)\| \leq \varrho\|x\|$, $\varrho > 0$ in the domain of interest $\mathcal{D}$. Then, the origin is an exponentially stable equilibrium of the perturbed system for all $x \in \mathcal{D}$ if the decay rate α is sufficiently

large.

Proof. The result is a direct consequence of [39, Lemma 9.1]. The lemma proves that an exponentially stable equilibrium point shows robustness to perturbations with linear growth upper-bounds.

Lemma 2 ([32]) *For a positive definite matrix Ψ, the following inequality holds,*

$$-2a^T(t)\int_{t-d(t)}^{t} b(\tau)d\gamma - \int_{t-d(t)}^{t} b^T(\gamma)\Psi b(\gamma)d\gamma \leq \bar{d}a^T(t)\Psi^{-1}a(t) \tag{7.7}$$

where $a(t)$ and $b(t)$ are vector functions and $d(t)$ is a time-varying scalar with $0 \leq d(t) \leq \bar{d}$.

Proof. See [32].

7.2 Control Design and Stability Analysis

Throughout this chapter, the following assumptions have been made:

- The cables are attached to the COM of quad-copters.
- Each UAV establishes a communication with the other vehicles in order to send its position and velocity measurements. The ith quad-copter transmits signals with a constant time delay $\mathfrak{T}_i \in \mathbb{R}^+$.
- The aerodynamic damping forces and moments applied on the quad-copters have been compensated by adaptive control laws. See [51] for the adaptation strategy.

7.2.1 Control Laws

Consider the following position control scheme,

$$\begin{aligned}\mu_i =& m_i\ddot{q}_d - K_{d_i}\dot{\tilde{q}}_i - K_{p_i}\tilde{q}_i - \sum_{\substack{j=1\\ j\neq i}}^{n} K_{p_{ij}}\Big(\tilde{q}_i - \tilde{q}_j(t-\mathfrak{T}_j)\Big) \\ & - \sum_{\substack{j=1\\ j\neq i}}^{n} K_{d_{ij}}\Big(\dot{\tilde{q}}_i - \dot{\tilde{q}}_j(t-\mathfrak{T}_j)\Big) + m_i g z\end{aligned} \tag{7.8}$$

where the positive-definite matrices $K_{d_i}, K_{p_i}, K_{p_{ij}}, K_{d_{ij}} \in \mathbb{R}^{3\times 3}$ stand for the position and formation control gains. It is assumed that $K_{p_{ij}} = K_{p_{ji}}$ and $K_{d_{ij}} = K_{d_{ji}}$. The position error is represented by $\tilde{q}_i \triangleq q_i - q_{d_i}$ and $q_{d_i}(t) : [0,\infty) \to \mathbb{R}^3$ is the desired reference trajectory of the ith quad-copter. It is assumed that reference trajectories satisfy the following conditions:

- It is assumed that all the UAVs fly with the same velocity and acceleration profiles, i.e., $\dot{q}_{d_i} = \dot{q}_d$, $\ddot{q}_{d_i} = \ddot{q}_d$.
- The desired reference velocity consists of two parts $\dot{q}_d(t) = \mathcal{Q}_d + \dot{\mathfrak{q}}_d(t)$, a constant vector $\mathcal{Q}_d \in \mathbb{R}^3$ and an energy bounded signal $\dot{\mathfrak{q}}_d(t) \in \mathcal{L}_2$. This would imply that the desired acceleration also belongs to the same space, i.e. $\ddot{q}_d \in \mathcal{L}_2$ as well.

The proposed controller in (7.8) consists of three parts, a passivity-based controller for individual drones, a distributed inter-drone passivity-based formation control and feedforward terms to compensate gravity and desired acceleration. Implementation of the control law in (7.8) requires force generation in certain directions. However, quad-copters are under-actuated and cannot produce arbitrary forces unless aligned

with the thrust direction. This is a major limitation in conventional quad-copters which results in an under-actuation force error $\delta_i(\eta_i, \eta_{d_i}, f_i) \in \mathbb{R}^3$ defined as,

$$\delta_i(\eta_i, \eta_{d_i}, f_i) = f_i R(\eta_i) z - \mu_i \triangleq f_i \big(R(\eta_i) - R(\eta_{d_i})\big) z \tag{7.9}$$

where $\eta_{d_i} = [\phi_{d_i} \ \theta_{d_i} \ \psi_{d_i}]^{\mathrm{T}} \in \mathbb{R}^3$ is the direction of the desired force governed by the control law (7.8). A well-known solution to this problem is to utilize a cascade control structure with an outer-loop position controller and an inner-loop angular one. The outer-loop generates the desired angles η_{d_i} and passes them to the angular controller as the attitude reference commands. This requirement can be formulated as,

$$f_i R(\eta_{d_i}) z \triangleq \mu_i \tag{7.10}$$

where we solve for the thrust magnitude and the desired angles. Since Equation (7.10) is underdetermined, desired reference for yaw can be picked and controlled independently.

Now, it is necessary to design an attitude controller for following the reference attitude commands. The angular motion is not only decoupled from the rest of the dynamics, but also a fully-actuated subsystem. As a result, it is possible to design a feedback linearization controller as

$$\tau_i = \big(\Psi(\eta_i)^{\mathrm{T}}\big)^{-1} \Big(M(\eta_i) v_i + C(\eta_i, \dot{\eta}_i) \dot{\eta}_i \Big) \tag{7.11}$$

where v_i has yet to be designed. This would result in a double-integrators system $\ddot{\eta}_i = v_i$ for the angular motion.

7.2.2 Stability Analysis

Substituting the position controller (7.8) and the proposed angular feedback linearization (7.11) into the open-loop dynamics (3.2), (3.3), (3.4) and 3.5 yields,

$$\begin{aligned} m_i\ddot{\tilde{q}}_i + k_{d_i}\dot{\tilde{q}}_i + k_{p_i}\tilde{q}_i = \delta_i(\eta_i, \eta_{d_i}, f_i) + T_i R_L e_i \\ -\sum_{\substack{j=1 \\ j\neq i}}^{n} K_{p_{ij}}\Big(\tilde{q}_i - \tilde{q}_j(t-\mathfrak{T}_j)\Big) - \sum_{\substack{j=1 \\ j\neq i}}^{n} K_{d_{ij}}\Big(\dot{\tilde{q}}_i - \dot{\tilde{q}}_j(t-\mathfrak{T}_j)\Big) \end{aligned} \tag{7.12}$$

$$\ddot{\eta}_i = v_i \tag{7.13}$$

$$\begin{aligned} m_L(\ddot{q}_L - \ddot{q}_d) + D_T(\dot{q}_L - \dot{q}_d) = -\sum_{i=1}^{n} T_i R_L e_i - m_L g z \\ - m_L\ddot{q}_d - D_L\dot{q}_d \end{aligned} \tag{7.14}$$

$$J_L\dot{\omega}_L + \omega_L^{\times} J_L\omega_L + D_R\omega_L = \sum_{i=1}^{n} r_i^{\times}(-T_i e_i) \tag{7.15}$$

where the positive definite matrices $D_T, D_R \in \mathbb{R}^{3\times 3}$ are air drag coefficients for the payload. This dynamical system has the same form as the augmented system in Theorem (1) where Equations (7.12), (7.14) and (7.15) represent x dynamics and Equation (7.13) matches ζ. Hence, Theorem (1) seems appropriate for investigating closed-loop stability. The only interconnection term between the two subsystems is the under-actuation force error $\delta_i(\eta_i, \eta_{d_i}, f_i)$. Figure 7.1 summarizes the required steps to prove closed-loop stability using Theorem (1).

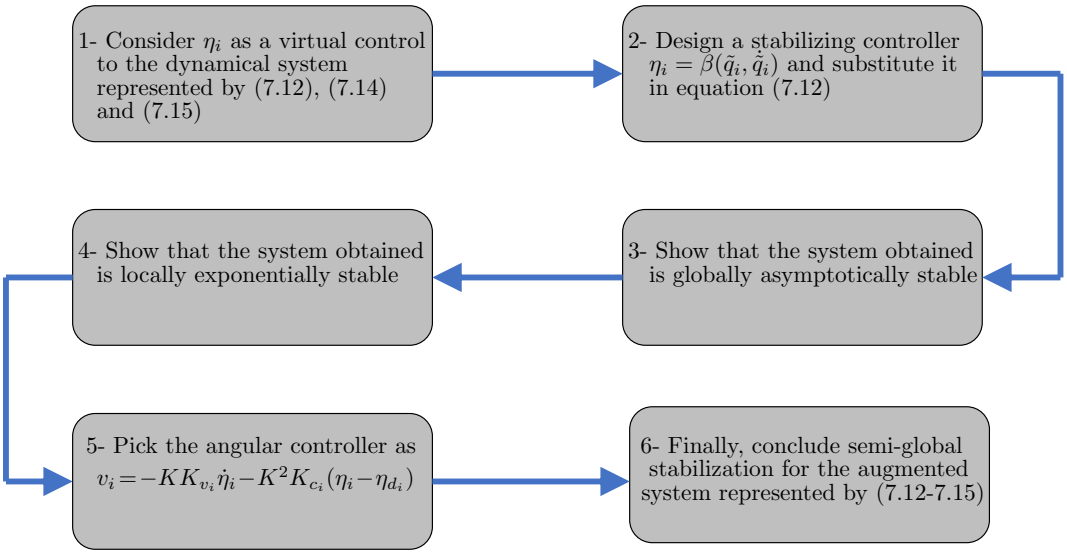

Figure 7.1: Steps taken to prove closed-loop stability using Theorem (1).

Consider η_i as a virtual control for the system dynamics (7.12). The choice $\eta_i \triangleq \eta_{d_i}$ would result in $\delta_i(\eta_{d_i}, \eta_{d_i}, f_i) = 0$ and eliminates the interconnection term. The following theorem proves global asymptotic stability of the outer-loop subsystem.

Theorem 5 *Consider the translational motion of quad-copters (7.12) with no interconnection term, i.e.* $\delta_i(\eta_i, \eta_{d_i}, f_i) = 0$ *as well as the payload dynamics (7.14) and (7.15). The system is globally asymptotically stable if there exists a solution to the following LMI:*

$$K_{d_i} - n\mathfrak{T}_i I_3 - \frac{1}{4}\sum_{\substack{j=1 \\ j\neq i}}^{n}(\mathfrak{T}_j K_{p_{ij}}^2 + K_{d_{ij}}) > 0 \ , \ \forall i = 1, ..., n \tag{7.16}$$

and $\lim_{t\to\infty} \ddot{q}_d = 0$.

proof. Consider the following Lyapunov-Krasovskii storage function $V = V_1 + V_2$,

where V_1 and V_2 are defined as

$$\begin{aligned} V_1=&\frac{1}{2}\sum_{i=1}^{n} m_i \dot{\tilde{q}}_i^{\mathrm{T}} \dot{\tilde{q}}_i + \frac{1}{2} m_L \big(\dot{q}_L - \dot{q}_d\big)^{\mathrm{T}} \big(\dot{q}_L - \dot{q}_d\big) + \frac{1}{2} \omega_L^{\mathrm{T}} J_L \omega_L \\ &+ \frac{1}{2}\sum_{i=1}^{n} \tilde{q}_i^{\mathrm{T}} K_{p_i} \tilde{q}_i + \frac{1}{4}\sum_{i=1}^{n}\sum_{\substack{j=1 \\ j\neq i}}^{n} \big(\tilde{q}_i - \tilde{q}_j\big)^{\mathrm{T}} K_{p_{ij}} \big(\tilde{q}_i - \tilde{q}_j\big) \\ &+ \big(D_T \mathcal{Q}_d + m_L g z\big)^{\mathrm{T}} \big(q_L - \frac{\sum_{i=1}^{n} q_{d_i}}{n}\big) + \kappa \end{aligned} \tag{7.17}$$

$$V_2 = n \sum_{i=1}^{n} \int_{-\mathfrak{T}_i}^{0} \int_{t+\gamma}^{t} \dot{\tilde{q}}_i(s)^{\mathrm{T}} \dot{\tilde{q}}_i(s) ds d\gamma \tag{7.18}$$

where $\kappa > 0$ adjusts the reference for gravitational potential energy. The time derivative of the storage function along the trajectories of the closed-loop system can be obtained as (see the appendix for the details),

$$\begin{aligned} \dot{V} \leq & -\sum_{i=1}^{n} \dot{\tilde{q}}_i^{\mathrm{T}} \Big(K_{d_i} - n\mathfrak{T}_i I_3 - \sum_{\substack{j=1 \\ j\neq i}}^{n} \frac{\mathfrak{T}_j}{4} K_{p_{ij}}^2 \Big) \dot{\tilde{q}}_i \\ &+ \sum_{i=1}^{n} \Big(\dot{\tilde{q}}_i^{\mathrm{T}}(t-\mathfrak{T}_i) \big(\sum_{\substack{j=1 \\ j\neq i}}^{n} \frac{K_{d_{ij}}}{4} \big) \dot{\tilde{q}}_i(t-\mathfrak{T}_i) \Big) \\ &- \omega_L^{\mathrm{T}} D_R \omega_L - (\dot{q}_L - \dot{q}_d)^{\mathrm{T}} (D_T - \frac{\epsilon I_3}{4}) (\dot{q}_L - \dot{q}_d) \\ &+ \frac{1}{\epsilon} (D_T \dot{\mathfrak{q}}_d + m_L \ddot{q}_d)^{\mathrm{T}} (D_T \dot{\mathfrak{q}}_d + m_L \ddot{q}_d) \end{aligned} \tag{7.19}$$

where $\epsilon \in \mathbb{R}^+$ is an arbitrary small positive number such that $D_T - \frac{\epsilon I_3}{4} > 0$ always holds. To show boundedness of the storage function, we transfer the analysis from power domain to energy domain by one integration. Since these physical signals are

causal and take zero values in negative times, it can be shown that,

$$\begin{aligned}
&\int_0^{t_f} \sum_{i=1}^{n} \Big(\dot{\tilde{q}}_i^{\mathrm{T}}(t-\mathfrak{T}_i)\big(\sum_{\substack{j=1\\ j\neq i}}^{n} K_{d_{ij}}\big)\dot{\tilde{q}}_i(t-\mathfrak{T}_i)\Big)dt \qquad (7.20)\\
&\quad = \int_{-\mathfrak{T}_i}^{t_f-\mathfrak{T}_i} \sum_{i=1}^{n} \Big(\dot{\tilde{q}}_i^{\mathrm{T}}(s)\big(\sum_{\substack{j=1\\ j\neq i}}^{n} K_{d_{ij}}\big)\dot{\tilde{q}}_i(s)\Big)ds\\
&\quad = \int_{0}^{t_f-\mathfrak{T}_i} \sum_{i=1}^{n} \Big(\dot{\tilde{q}}_i^{\mathrm{T}}(s)\big(\sum_{\substack{j=1\\ j\neq i}}^{n} K_{d_{ij}}\big)\dot{\tilde{q}}_i(s)\Big)ds\\
&\quad \leq \int_{0}^{t_f} \sum_{i=1}^{n} \Big(\dot{\tilde{q}}_i^{\mathrm{T}}(s)\big(\sum_{\substack{j=1\\ j\neq i}}^{n} K_{d_{ij}}\big)\dot{\tilde{q}}_i(s)\Big)ds
\end{aligned}$$

It follows from integration of inequality (7.19) from $t = 0$ to $t = t_f$ with the upper-bound given in (7.20) that,

$$\begin{aligned}
&V(t_f)+\int_0^{t_f}\sum_{i=1}^{n}\dot{\tilde{q}}_i^{\mathrm{T}}\Big(K_{d_i}-n\mathfrak{T}_i I_3-\frac{1}{4}\sum_{\substack{j=1\\ j\neq i}}^{n}(\mathfrak{T}_j K_{p_{ij}}^2+K_{d_{ij}})\Big)\dot{\tilde{q}}_i dt\\
&+\int_0^{t_f}\omega_L^{\mathrm{T}} D_R\omega_L dt+\int_0^{t_f}(\dot{q}_L-\dot{q}_d)^{\mathrm{T}}(D_T-\frac{\epsilon I_3}{4})(\dot{q}_L-\dot{q}_d)dt\\
&\leq V(0)+\mathcal{A}
\end{aligned}$$

where $\mathcal{A} \triangleq \int_0^{t_f}\frac{1}{\epsilon}(D_T\dot{\mathfrak{q}}_d + m_L\ddot{q}_d)^{\mathrm{T}}(D_T\dot{\mathfrak{q}}_d + m_L\ddot{q}_d)dt$ is bounded based on the aforementioned assumptions on the reference trajectories. If there exists a solution for the LMIs given by (7.16), then, it can be easily concluded that $V(t_f) \in \mathcal{L}_\infty$ and $\dot{\tilde{q}}_i, (\dot{q}_L - \dot{q}_d), \omega_L \in \mathcal{L}_2$. Moreover, if the system comes to a rest at the steady-state, i.e. $\lim_{t\to\infty}\ddot{q}_d = 0$, then, it follows from systems dynamics (7.12), (7.14) and (7.15) as well as Barbalat's lemma [85] that $\lim_{t\to\infty}\dot{\tilde{q}}_i, (\dot{q}_L - \dot{q}_d), \omega_L = 0$. Similar arguments

can be used to show convergence of accelerations. Since at the steady state condition

$$\lim_{t\to\infty} \tilde{q}_i(t) - \tilde{q}_j(t-\mathfrak{T}_j) = \lim_{t\to\infty} \tilde{q}_i(t) - \tilde{q}_j(t) + \int_{t-\mathfrak{T}_j}^{t} \dot{\tilde{q}}_j(\gamma) d\gamma$$
$$= \tilde{q}_i(t) - \tilde{q}_j(t)$$

then, the closed-loop system finally settles at the expected equilibrium point $\sum_{i=1}^{n} K_{p_i} \tilde{q}_i = -m_L g z - D_T \mathcal{Q}_d$. It can be seen that the inter-drone virtual spring forces are not present. This is due to the fact that they act as internal forces and have been canceled out in final static balance equation. This completes the proof for global asymptotic stability. □

The next step is to prove local exponential stability of the system without interconnection terms. This is the fourth step in terms of the block diagram in Figure 7.1. As it has been already shown that the system enjoys global asymptotic stability, it would suffice to prove that convergence rate is exponential. A worst-case analysis has been provided here, where it is assumed $\mathfrak{T}_i = \mathfrak{T}_{max} = \max\{\mathfrak{T}_1, \mathfrak{T}_2, ..., \mathfrak{T}_n\}$. This would allow for a more compact representation of system dynamics in favor of space constraints. It follows from the result of Theorem (5) that cable forces are bounded and can be seen as disturbances to translational motion of quad-copters (7.12). Consider $T_i R_L e_i \triangleq g_i(t, \tilde{q}_i, \dot{\tilde{q}}_i) + \mathcal{C}_i$ where $g(t, \tilde{q}_i, \dot{\tilde{q}}_i) : [0, \infty) \times \mathbb{R}^3 \times \mathbb{R}^3 \to \mathbb{R}^3$ is a nonlinear function upper bounded by $\|g(t, \tilde{q}_i, \dot{\tilde{q}}_i)\| \leq \varrho_i \|[\tilde{q}_i,\ \dot{\tilde{q}}_i]\|$, $\varrho_i \in \mathbb{R}^+$ and $g(t, 0, 0) = 0$. In addition, $\mathcal{C}_i \in \mathbb{R}^3$ is a constant vector such that $\sum_{i=1}^{n} \mathcal{C}_i = -m_L g z - D_L \mathcal{Q}_d$. Let us define the following state variables,

$$\mathcal{X} \triangleq [(\tilde{q}_1 - q_1^*)^{\mathrm{T}} \quad \dot{\tilde{q}}_1^{\mathrm{T}} \quad (\tilde{q}_2 - q_2^*)^{\mathrm{T}} \quad \dot{\tilde{q}}_2^{\mathrm{T}} \quad \cdots \quad (\tilde{q}_n - q_n^*)^{\mathrm{T}} \quad \dot{\tilde{q}}_n^{\mathrm{T}}]^{\mathrm{T}}$$

where $q_i^* \in \mathbb{R}^3$, $i = 1, 2, ..., n$ is the solution to the following set of linear equations, i.e. the equilibrium points,

$$\begin{cases} K_{p_1}\tilde{q}_1 + \sum\limits_{j=2}^{n} K_{p_{1j}}(\tilde{q}_1 - \tilde{q}_j) = \mathcal{C}_1 \\ K_{p_2}\tilde{q}_2 + \sum\limits_{\substack{j=1 \\ j\neq 2}}^{n} K_{p_{2j}}(\tilde{q}_2 - \tilde{q}_j) = \mathcal{C}_2 \\ \vdots \\ K_{p_n}\tilde{q}_n + \sum\limits_{j=1}^{n-1} K_{p_{nj}}(\tilde{q}_n - \tilde{q}_j) = \mathcal{C}_n \end{cases} \tag{7.21}$$

The vehicle dynamics (7.12) without the interconnection terms can be represented as,

$$\dot{\mathcal{X}}(t) = A_1\mathcal{X}(t) + A_2\mathcal{X}(t - \mathfrak{T}_{max}) + G(\mathcal{X}) \tag{7.22}$$

where $A_1 \in \mathbb{R}^{6n\times 6n}$ is the delay-free system matrix,

$$A_1 = \begin{bmatrix} \mathfrak{A}_{1_1} & 0_{6\times 6} & \cdots & 0_{6\times 6} \\ 0_{6\times 6} & \mathfrak{A}_{1_2} & \cdots & 0_{6\times 6} \\ \vdots & & \ddots & \vdots \\ 0_{6\times 6} & 0_{6\times 6} & \cdots & \mathfrak{A}_{1_n} \end{bmatrix} \tag{7.23}$$

where,

$$\mathfrak{A}_{1_i} = \begin{bmatrix} 0_{3\times 3} & I_3 \\ -K_{p_i} - \sum\limits_{\substack{j=1 \\ j\neq i}}^{n} K_{p_{ij}} & -K_{d_i} - \sum\limits_{\substack{j=1 \\ j\neq i}}^{n} K_{d_{ij}} \end{bmatrix}_{6\times 6} \tag{7.24}$$

In addition, $A_2 \in \mathbb{R}^{6n\times 6n}$ is the system matrix for delayed terms,

$$A_2 = [\mathfrak{A}_{2_{ij}}] \in \mathbb{R}^{6n\times 6n} \tag{7.25}$$

$$\mathfrak{A}_{2_{ij}} = \begin{cases} K_{p_{ij}} & \text{If } \ i = 2\mathcal{K}_1,\ j = 2\mathcal{K}_2 - 1,\ i \neq j-1 \\ K_{d_{ij}} & \text{If } \ i = 2\mathcal{K}_1,\ j = 2\mathcal{K}_2,\ i \neq j \\ 0_{3\times 3} & \text{Otherwise} \end{cases}$$

and $\mathcal{K}_1, \mathcal{K}_2 \in \{1, 2, .., n\}$. Finally, the vector $G(\mathcal{X}) \in \mathbb{R}^{6n}$ can be defined as,

$$G(\mathcal{X}) \triangleq \begin{bmatrix} 0_{1\times 3} & g_1^{\mathrm{T}} & 0_{1\times 3} & g_2^{\mathrm{T}} & \cdots & 0_{1\times 3} & g_n^{\mathrm{T}} \end{bmatrix}^{\mathrm{T}} \tag{7.26}$$

which acts as a disturbance on this network of linear time-invariant system with time delay.

The system represented by (7.22) has the same form as the general dynamics given by (7.6) in Lemma (1). Hence, it follows from Lemma (1) that the time-delayed perturbed system is exponentially stable if the nominal system (i.e. with $G(\mathcal{X}) = 0$) is exponentially stable with sufficiently large decaying rate. Exponential stability of the nominal system can be investigated through Theorem (4). Based on that, for a given stability degree $\alpha > 0$, constant time delay $\mathfrak{T}_{max} > 0$ and A_1 and A_2 defined as (7.23) and (7.25), if there exists symmetric positive definite matrices $P, Q \in \mathbb{R}^{6n\times 6n}$ such that the linear matrix inequality $S^*(\alpha, \mathfrak{T}_{max}, A_1, A_2) < 0$ is satisfied, then the nominal system is exponentially stable. This condition can be held with proper choice of control gains. Once exponential stability of the nominal system is established,

it follows from Lemma (1) that the perturbed system remains locally exponentially stable in a given compact set $\mathcal{D} \subset \mathbb{R}^{6n}$ around the origin, if the decay rate is sufficiently large. This would complete the fourth step in terms of block diagram (7.1).

The next step is to design a stabilizing controller for the angular dynamics of the quad-copters. Since the outer-loop system without the interconnection terms enjoys both GAS and LES, then it follows from Theorem (1) that the following angular controller would achieve semi-global stabilization of the equilibrium point,

$$v_i = -KK_{v_i}\dot{\eta}_i - K^2K_{c_i}(\eta_i - \eta_{d_i}) \tag{7.27}$$

where $K, K_{c_i}, K_{v_i} \in \mathbb{R}^{3\times 3}$ are positive-definite gains. The noteworthy observation for the control law (7.27) is that it does not involve the reference angular velocity and acceleration. As a result, the proposed control scheme in this chapter works only based on position and velocity measurements. These constitute the fifth and sixth steps of the block diagram in Figure 7.1 and result in the closed-loop stability of the augmented system.

7.3 Experimental Verification

To investigate the effectiveness of the proposed controller, an experiment with three quad-copters and a cable-suspended payload was conducted in an indoor environment. The implementation of the proposed approach needs communications among the UAVs. However, this would increase hardware complexity as we had to still maintain wireless communications from the ground station to each UAV. This is due to the fact that the motion capture system streams position data to the ground station. As

a result, the time delay was artificially added to the inter-drone control actions inside the code to mimic this adverse phenomena. Hence, all the outer-loop control computations were carried out in the ground station and then each quad-copter wirelessly received its desired thrust and angles.

In order to apply the proposed controller to the system, it is first essential to satisfy all the stability conditions. During this experiment, the following control gains were selected for all the quad-copters,

$$K_{p_i} = \text{diag}\Big\{9, 6, 9\Big\},$$
$$K_{d_i} = \text{diag}\Big\{3.75, 2.25, 2.25\Big\}$$

The inter-drone coupling terms were chosen as:

$$K_{p_{ij}} = \text{diag}\Big\{2.25, 2.25, 2.25\Big\},\ K_{d_{ij}} = \text{diag}\Big\{1.05, 1.05, 1.05\Big\}$$

The artificial delay inside the code was set to $\mathfrak{T}_i = 0.04$ second for all the coupling terms. In order to verify stability conditions, a couple of LMIs have to be satisfied. First, it can be shown that the LMI in (7.16) is satisfied with our choice of control gains since the following matrix,

$$K_{d_i} - n\mathfrak{T}_i I_3 - \frac{1}{4}\sum_{\substack{j=1 \\ j\neq i}}^{n}(\mathfrak{T}_j K_{p_{ij}}^2 + K_{d_{ij}}) = \text{diag}\Big\{2.7750, 1.2750, 1.2750\Big\} > 0$$

is positive-definite. The next step is to show that conditions for local exponential stability are held. This can be verified through Theorem (4). Let $\alpha = 1$ and $Q = I_{18}$, then a positive-definite P matrix can be found, to satisfy LMI (7.2). See appendix (B)

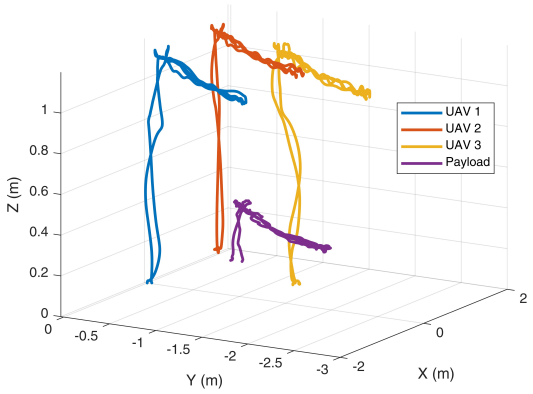

Figure 7.2: Positions of the UAVs and the payload with time-delayed coupling terms in control.

for the numerical values. This solution was obtained using MATLAB LMI toolbox.

7.3.1 Reference Following

The following scenario was considered to evaluate closed-loop stability of the system in the presence of time-delay: The quad-copters first flew to an altitude of 1.4m. They then moved diagonally for 1.5m along both x and y axes. Afterwards, they returned to their original position. This pattern of movement was repeated twice. Finally, the quad-copters landed at the starting point. Figure 7.2 illustrates the positions of quad-copters as well as the cable-suspended payload. Although the system experienced time-delay in the control loop, it could still preserve stability. Moreover, it can be seen from Figures 7.3, 7.4 and 7.5 that the the proposed controller has a satisfactory performance in terms of reference following. The position errors are mainly due to the payload and cables.

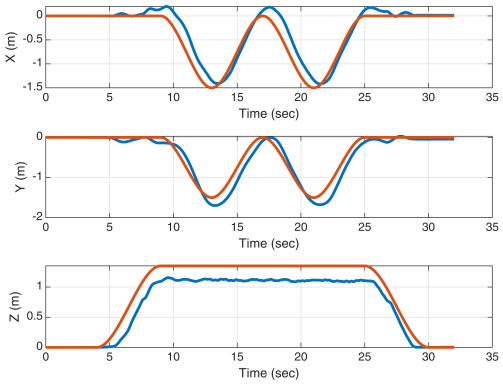

Figure 7.3: Position versus time for Quad-copter 1. The red and blue show the desired and measured signals, respectively.

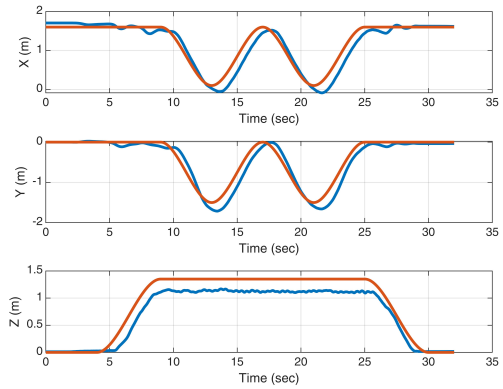

Figure 7.4: Position versus time for Quad-copter 2. The red and blue show the desired and measured signals, respectively.

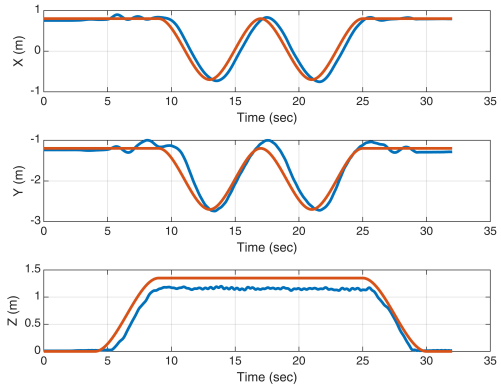

Figure 7.5: Position versus time for Quad-copter 3. The red and blue show the desired and measured signals, respectively.

7.3.2 Comparison to a Baseline Controller

The addition of the inter-drone coupling terms is expected to enhance the controller's ability to preserve the formation shape in the presence of external disturbances. In this subsection, the performance of the new controller is compared to the fully decentralized controller of Chapter 4. The following scenario was considered in this comparison: The drones flew to a hovering altitude of approximately $z = 1.15$ m. While hovering, the first quad-copter was pulled away from its position twice with the help of an extra long rope attached to it. This was done to compare the responses of the controllers to an external disturbance. A video demonstrating this experiment is available at `https://youtu.be/PVI-tvyfZ40`.

Figure 7.6 illustrates the positions of the quad-copters and the payload throughout the experiment with the distributed cooperative control law (7.8). It is clear that once the first quad-copter was perturbed, the other quad-copters moved in the same direction in order to maintain the formation shape.

Figure 7.7 depicts the positions of the drones and the payload with the fully

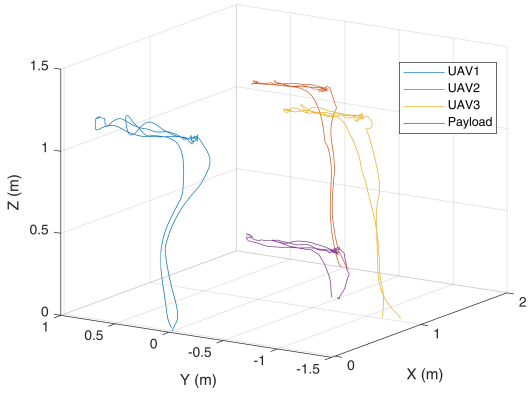

Figure 7.6: The positions of the drones and the payload with the new controller with inter-drone coupling terms. The first quad-copter was pulled away from its position twice with the aid of a rope attached to it.

decentralized controller from Chapter 4. It is clear that the controller is less effective in maintaining the formation shape. This is because the control action of each quad-copter responds only to local errors with no feedback from the other two quad-copters. The small movements of the second and third quad-copters are due to the mechanical coupling through the payload and the cables. In contrast, the inter-drone coupling terms in the new controller provide a more effective mechanism for preserving the formation shape in response to the disturbance.

7.4 Summary

In this chapter, a revised controller was introduced to help improve the system's ability to preserve the formation shape in response to external disturbances. This new controller added inter-drone coupling terms, which requires inter-drone communication of the position measurements. A comprehensive analysis of the system stability was presented, where under-actuation and communication time delay were taken into

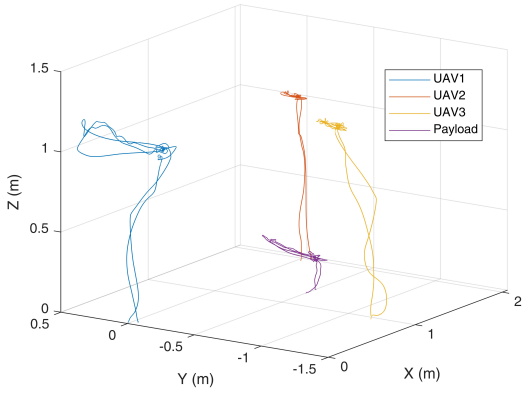

Figure 7.7: 3D positions of the aerial transport system with the fully decentralized controller of Chapter 4. An extra rope attached to UAV 1 was pulled twice during the experiment.

account. Stability conditions were derived to establish guidelines for selecting the controller gains based on the amount of time delay in the inter-drone communication links. Experiments were carried that showed that the system stability can be maintained in the presence of time delay. Moreover, as predicted, the new controller proved more effective than the one introduced in Chapter 4 in preserving the formation shape in response to an external disturbance.

Chapter 8

Formation Shape Design

The previous chapters focused on the design of controllers for multi-UAV cable-based aerial transport system. In those controllers, the reference positions for the UAVs were assumed known and provided by the user. These reference points ultimately determine the shape of the formation and the pose of the payload. However, a given payload pose may be achieved with many different formations and the question that naturally arises is which formation should be chosen.

In this chapter, we formulate an optimization problem to select the reference positions for the UAVs to minimize the total power consumed during the hovering stage of the flight. In hovering, the quad-copters mostly fight against gravity and hence minimizing their total power would minimize the lost power used to keep the payload in one position. The hovering power can be determined by a steady-state analysis, which provides a number of constraints for the optimization problem. The other constraints in the problem are the thrust limits, the kinematic constraints of the cables, and the desired minimum distance between the drones.

The payload parameters are needed in the formulation of the optimization problem. They impact the optimal formation shape. A calibration process is proposed to estimate these parameters experimentally. In this process, the quad-copters fly with the cable-suspended payload in an arbitrary formation and the sensor data is recorded. The payload parameters, i.e., the COM location of the payload (the vectors r_is in Figure 8.1) are estimated by solving a least-squares problem.

8.1 Optimal Formation Shape and Reference Trajectories

Precise control of the payload position and pose is not required in most transportation applications. Since the position of the payload is constrained by the cables, it often suffices to control the positions of the UAVs instead. However, certain applications may require the payload to follow a desired pose configuration. For instance, a bucket of water may have to be oriented in a particular way so it can be emptied to extinguish fire. In such tasks, position and orientation of the payload must be controlled. The reference positions for the UAVs can be found based on the static balance equations as well as the kinematic constraints. A minimum of three drones are required to fully control the payload position and orientation [48]. The formation solution for a given payload position/orientation is not unique. An optimization problem is formulated here to determine a unique solution.

Short flight time is a major issue in aerial transportation so power efficiency is critical in this application [62]. We seek to find a solution that would minimize the total power of the UAVs in the hovering phase. This is also the power that the vehicles

consume in steady state when moving with constant velocity (in the absence of drag forces). It follows from a similar derivation to that in [17] and Equation (7.10) that the power of a single quad-copter $\mathcal{P}_i \in \mathbb{R}$ in hovering can be calculated from,

$$\mathcal{P}_i = \xi_i f_{i_{ss}}^{1.5} = \xi_i \|\mu_{i_{ss}}\|^{1.5} \tag{8.1}$$

where $\xi_i > 0$ and the subscript "ss" stands for the steady state condition of signals. It follows from the control law (7.8) that

$$\mu_{i_{ss}} = -K_{p_i}\tilde{q}_i - \sum_{\substack{j=1 \\ j\neq i}}^{n} K_{p_{ij}}(\tilde{q}_i - \tilde{q}_j) + m_i g z \tag{8.2}$$

where the spring-type actions and gravity compensation are present.

8.1.1 Optimization Problem

The operator expresses the desired pose of the payload (q_{L_d}, R_{L_d}) for $\mathcal{N}_w \in \mathbb{N}$ waypoints. At each of these waypoints, the following optimization is solved to obtain the

formation shape as well as the UAV waypoints:

$$
\begin{aligned}
\min_{q_i, q_{d_i}, T_i} \quad & \sum_{i=1}^{n} \xi_i \|\mu_{i_{ss}}\|^{1.5} \\
\text{subject to} \quad & \mu_{i_{ss}} = \frac{T_i}{l_i}(q_i - q_{L_d} - R_{L_d} r_i) - m_i g z \ , \ i = 1, ..., n \\
& \sum_{i=1}^{n} \frac{T_i}{l_i}(q_i - q_{L_d} - R_{L_d} r_i) = -m_L g z \\
& \sum_{i=1}^{n} r_i^{\times} \left(T_i R_{L_d}^{\mathrm{T}} (q_i - q_{L_d} - R_{L_d} r_i) \right) = 0 \\
& \|q_i - q_{L_d} - R_{L_d} r_i\| \leq l_i \ , \ i = 1, ..., n \\
& \|q_i - q_j\| \geq d_{s_{ij}} \ , \ i = 1, ..., n \ , \ j = i+1, ..., n \\
& T_i \geq 0 \ , \ i = 1, ..., n \\
& \|\mu_{i_{ss}}\| \leq f_{sat_i}
\end{aligned}
\tag{8.3}
$$

where $d_{s_{ij}} \in \mathbb{R}^+$ denotes the safe distance between the ith and the jth UAVs. The thrust saturation limit is represented by $f_{sat_i} \in \mathbb{R}^+$. After solving this minimization problem for $\mathcal{N}_w$ times, the desired UAV positions q_{d_i}s are obtained at given waypoints. Provided that the time distance of the waypoints is sufficiently large, dynamically-feasible trajectories can be easily found between each two waypoints of the ith UAV since the boundary conditions are known. It should be noted that the formulation in (8.3) is a non-convex optimization problem. Hence, finding a global minimum is not guaranteed.

It is noted that the angular positions of the quad-copters are absent in the optimization formulation. This is because the cables are assumed to be attached to the COM of the quad-copters, decoupling their angular dynamics from the rest of the system dynamics. In addition, the proposed attitude controller in (7.27) guarantees that

$\lim_{t\to\infty} \eta_i = \eta_{d_i}$. This would eliminate the coupling term (7.9) in the translational motion of quad-copters in steady state.

For homogeneous UAVs and a symmetric payload (i.e., $\sum_{i=1}^{n} r_i = 0$), minimizing the cost function in optimization (8.3) has the effect of distributing the load uniformly within the feasible solution space. This would ensure that load distribution imbalances would not prematurely drain the energy supply of any UAVs and should ultimately prolong the flight time.

8.1.2 Calibration

The optimization problem in the previous section is payload-specific as it requires the mass and COM position of the payload. The mass value can be easily measured but the location of COM is trickier to find. A calibration process is proposed here that would help determine the COM of each UAV, i.e., the vectors r_is in Figure 8.1. This process involves the following steps:

1. The quad-copters fly with the payload following an arbitrary references trajectory with the only constraint that the cables must be in tension throughout this calibration flight.

2. Once in steady state, the UAV positions are recorded for each sample $\mathfrak{i} \in \{1, ..., \mathcal{N}_c\}$. A total number of $\mathcal{N}_c \in \mathbb{N}$ data samples are collected. Having the positions available, it follows from (8.2) that the steady-state control input is known. This information can be used to calculate the unit vector along each

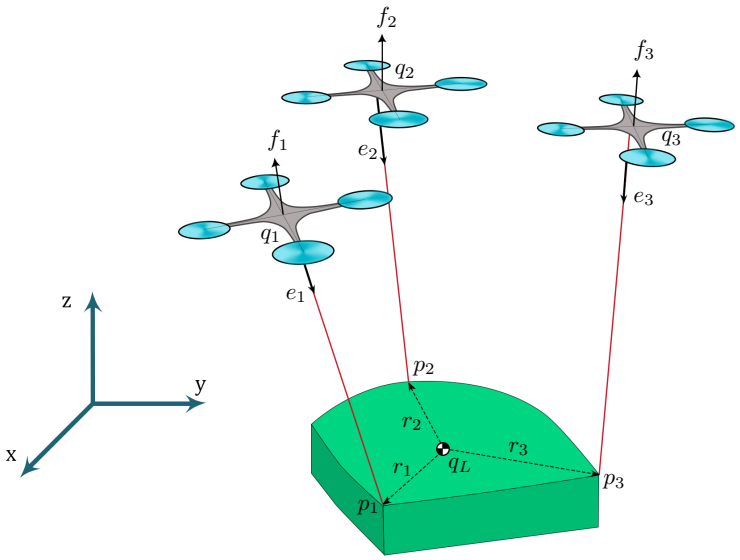

Figure 8.1: Schematic of the aerial transportation system where the cables are attached to the COM of the UAVs.

cable in the world frame as well as the tension in the cable as follows,

$$\|\mu_{i_{ss}}[\mathrm{i}] + m_i g z\| = T_i[\mathrm{i}] \ , \ i = 1, ..., n \tag{8.4}$$

$$\mu_{i_{ss}}[\mathrm{i}] + m_i g z = T_i[\mathrm{i}] R_L[\mathrm{i}] e_i[\mathrm{i}] \ , \ i = 1, ..., n \tag{8.5}$$

3. Now that the positions of the UAVs, $q_i[\mathrm{i}]$s and the unit vectors in the world frame $R_L[\mathrm{i}]e_i[\mathrm{i}]$ are known, we can find the positions of the attachment points with respect to the world frame,

$$p_i[\mathrm{i}] \triangleq q_i[\mathrm{i}] + l_i R_L[\mathrm{i}] e_i[\mathrm{i}] \tag{8.6}$$

See Figure 8.1 for more details.

4. The positions of the attachment points can be used to determine the orientation of the payload:

$$R_L[\mathfrak{i}] = \Big[a_{1_L}[\mathfrak{i}]; a_{2_L}[\mathfrak{i}]; a_{3_L}[\mathfrak{i}]\Big] \tag{8.7}$$

where $a_{1_L}[\mathfrak{i}] \triangleq \frac{p_1[\mathfrak{i}]-p_2[\mathfrak{i}]}{\|p_1[\mathfrak{i}]-p_2[\mathfrak{i}]\|}$, $a_{3_L}[\mathfrak{i}] \triangleq \frac{a_{1_L}[\mathfrak{i}]\times(p_3[\mathfrak{i}]-p_2[\mathfrak{i}])}{\|a_{1_L}[\mathfrak{i}]\times(p_3[\mathfrak{i}]-p_2[\mathfrak{i}])\|}$ and $a_{2_L}[\mathfrak{i}] = a_{3_L}[\mathfrak{i}]^{\times} a_{1_L}[\mathfrak{i}]$. Therefore, the rotation matrix of the payload is known at each sample time. This rotation matrix can be employed to obtain e_is, the unit vectors expressed in the body-fixed frame of the object.

5. With the cables in tension, one can write (see Figure 8.1),

$$r_1 - r_j = R_L^{\mathrm{T}}[\mathfrak{i}]\Big(p_1[\mathfrak{i}] - p_j[\mathfrak{i}]\Big) \quad , \quad j = \{2, 3, ..., n\} \tag{8.8}$$

In addition, the balance equation of the moment has to hold for each sample time,

$$\sum_{i=1}^{n} \Big(T_i[\mathfrak{i}]e_i[\mathfrak{i}]\Big)^{\times} r_i = 0 \tag{8.9}$$

Equations (8.8) and (8.9) for samples $\mathfrak{i} = 1$ to $\mathfrak{i} = \mathcal{N}_c$ can be written in the compact form

$$A\ [r_1^{\mathrm{T}}\ \ r_2^{\mathrm{T}}\ \ ...\ \ r_n^{\mathrm{T}}]^{\mathrm{T}} = B \tag{8.10}$$

where $A \in \mathbb{R}^{3n\mathcal{N}_c \times 3n}$. For a special case that $n = 3$, A and B can be written as,

$$A = \begin{bmatrix} I_3 & -I_3 & 0_{3\times3} \\ I_3 & 0_{3\times3} & -I_3 \\ T_1[1]e_1[1]^\times & T_2[1]e_2[1]^\times & T_3[1]e_3[1]^\times \\ \vdots & \vdots & \vdots \\ I_3 & -I_3 & 0_{3\times3} \\ I_3 & 0_{3\times3} & -I_3 \\ T_1[\mathcal{N}_c]e_1[\mathcal{N}_c]^\times & T_2[\mathcal{N}_c]e_2[\mathcal{N}_c]^\times & T_3[\mathcal{N}_c]e_3[\mathcal{N}_c]^\times \end{bmatrix}_{9\mathcal{N}_c\times9}$$

$$B = \begin{bmatrix} R_L^{\mathrm{T}}[1]\Big(p_1[1] - p_2[1]\Big) \\ R_L^{\mathrm{T}}[1]\Big(p_1[1] - p_3[1]\Big) \\ 0_{3\times1} \\ \vdots \\ R_L^{\mathrm{T}}[\mathcal{N}_c]\Big(p_1[\mathcal{N}_c] - p_2[\mathcal{N}_c]\Big) \\ R_L^{\mathrm{T}}[\mathcal{N}_c]\Big(p_1[\mathcal{N}_c] - p_3[\mathcal{N}_c]\Big) \\ 0_{3\times1} \end{bmatrix}_{9\mathcal{N}_c\times1}$$

6. The above system of equations is over-determined. A least-squares solution to the problem is given by

$$[r_1^{\mathrm{T}} \;\; r_2^{\mathrm{T}} \;\; ... \;\; r_n^{\mathrm{T}}]^{\mathrm{T}} = (A^{\mathrm{T}}A)^{-1}A^{\mathrm{T}}B \tag{8.11}$$

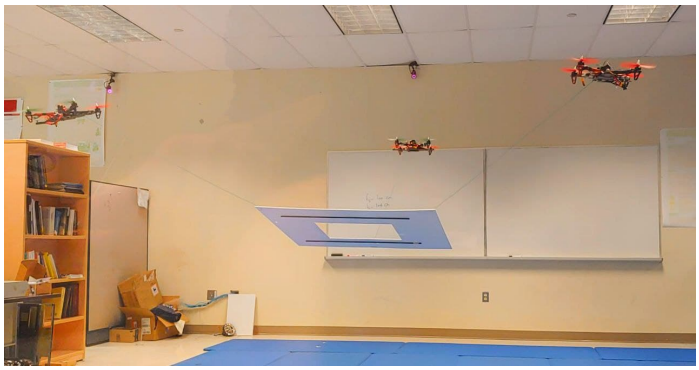

Figure 8.2: Snapshot of experiment with the whiteboard payload.

Increasing the number of samples should improve the accuracy of the estimation by reducing noise.

It is noted that the proposed calibration method requires no measurements from the payload. While the proposed strategy does not close the feedback loop over payload position measurement, it fully considers its desired pose in designing reference trajectories for the UAVs.

8.2 Experimental Results

In this section, formation shape design problem is considered for two different payloads. The first one is a whiteboard with a large effective surface area. Since the attachment points are far away, a rigid-body representation seems essential for such an object. Figure 8.2 shows a snapshot of experiment with this payload. The second payload has a small cylindrical shape. This object has been also used in previous experiments. See Figure 1.1 for more details. They both weigh around $m_L = 0.41$ kg.

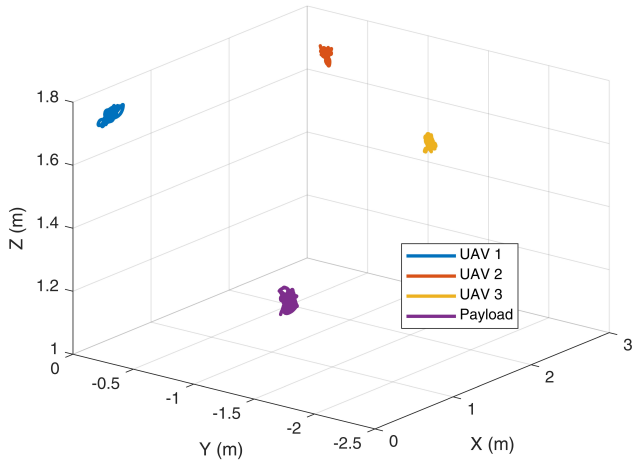

Figure 8.3: Positions of the UAVs and the cable-suspended payload during a hovering. The whiteboard payload experience significant swings and never reaches an equilibrium.

8.2.1 Whiteboard Payload

Given the relatively large dimensions of the whiteboard payload (76 cm $\times$ 100 cm), it is necessary to consider a rigid-body representation in the optimization formulation. This requires the vectors r_is in Fig. 8.1. A calibration experiment was performed on this payload. Payloads with large effective surface area are generally more prone to swing and oscillations. This turned out to be the case during calibration experiment with the whiteboard payload. Due to the swings and oscillations the payload never reached a steady state equilibrium during the calibration.

Figure 8.3 shows the positions of the quad-copters and the whiteboard in this experiment. The orientation angles of the payload are plotted in Figure 8.4. It is apparent that an equilibrium condition is never reached. The transitory oscillatory motion involves velocity and acceleration components that were ignored in deriving the calibration equations. Since the proposed calibration test only works based on

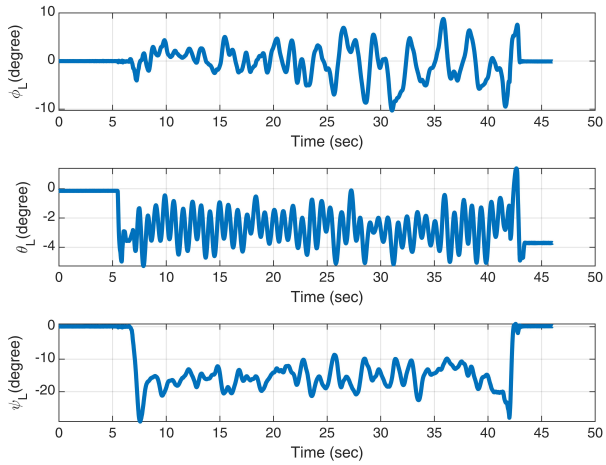

Figure 8.4: Orientation of the whiteboard payload while hovering.

position measurements, the approach cannot be effectively applied to this particular case. The effect of airflow for large surface payloads needs to be investigated in the future.

8.3 Point Mass Payload

The formation shape optimization problem can be directly applied to a point mass payload with no need for calibration. The following parameters are used in the optimization problem,

$$m_i = 0.67 \text{ kg}, \ m_L = 0.41 \text{ kg}, \ l_1 = 165 \text{ cm}, \ l_2 = 102 \text{ cm}, \ l_3 = 98 \text{ cm},$$
$$d_{s_{ij}} = 70 \text{ cm}, f_{sat_i} = 10 \text{ N}$$

The reference position for the payload is set to $q_{L_d} = [0 \ \ 0 \ \ 0.6]^{\mathrm{T}}$. The optimization problem was solved using MATLAB fimincon optimizer which returned the following

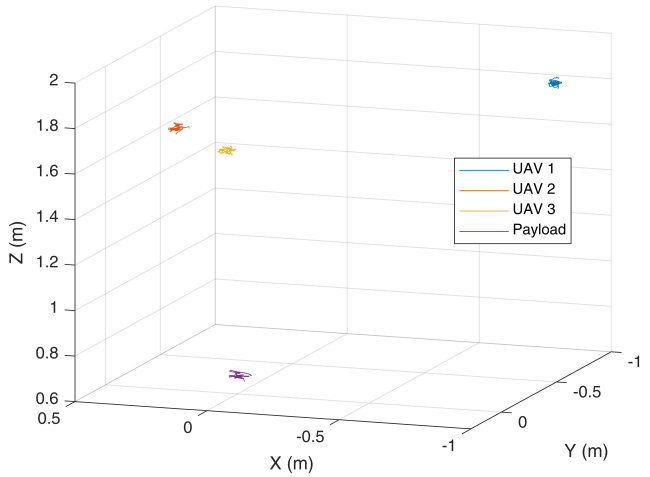

Figure 8.5: Positions of the UAVs and the cable-suspended payload while hovering for 25 seconds with the formation obtained from optimization.

solution,

$$q_{d_1} = [0.98 \quad -0.79 \quad 2.07]^{\mathrm{T}} \tag{8.12}$$

$$q_{d_2} = [-0.39 \quad -0.24 \quad 2.07]^{\mathrm{T}} \tag{8.13}$$

$$q_{d_3} = [0.16 \quad 0.43 \quad 2.07]^{\mathrm{T}} \tag{8.14}$$

It is noted that the desired altitudes of the quad-copters have been constrained to be equal due to limited space in the laboratory.

An experiment with three identical quad-copters and a cable-suspended payload was carried out where the quad-copters were commanded to hover for 25 sec at the reference positions obtained from solving the optimization problem. Figure 8.6 shows the results of this experiment. The system is mostly in steady-state condition as the payload experiences only minor swings.

It is instructive to see how closely the payload follows its reference position, q_{L_d}.

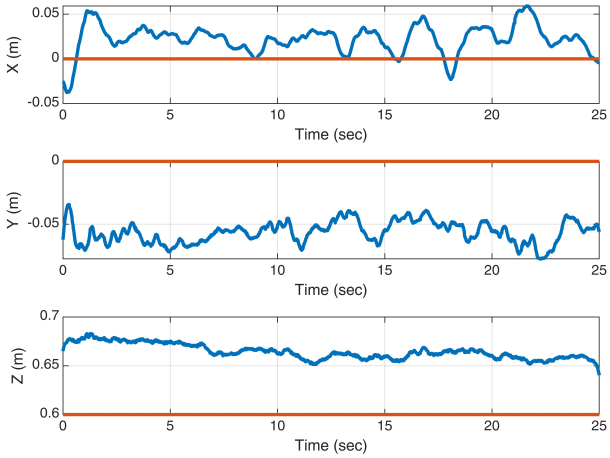

Figure 8.6: Position of the payload (blue) throughout a 25 seconds hovering experiment. The reference position (red) is $q_{L_d} = [0 \quad 0 \quad 0.6]^{\mathrm{T}}$.

Figure 8.5 depicts the measured and reference positions of the payload. The errors stem mainly from parameter errors such as errors in the cables lengths. Moreover, it is assumed that the cables are attached to the COM of the UAVs, while this may not be exactly true in the actual experiments.

Three other experiments with arbitrary formation shapes were carried out and their results were compared with those from the optimization problem solution. In each of these experiments, the quad-copter hovered for about 25 seconds in their respective formation. These triangle shapes are shown in Figure 8.7 where the star, circle and cross symbols denote the reference positions for the first, second and third UAVs, respectively.

Figure 8.8 compares the four formations in terms of total consumed power. It is clear that the formation shape obtained from the optimization problem consumes the least amount of power among the four. Table 8.1 summarizes the results in these four hovering experiments, which confirms the formation shape obtained from the

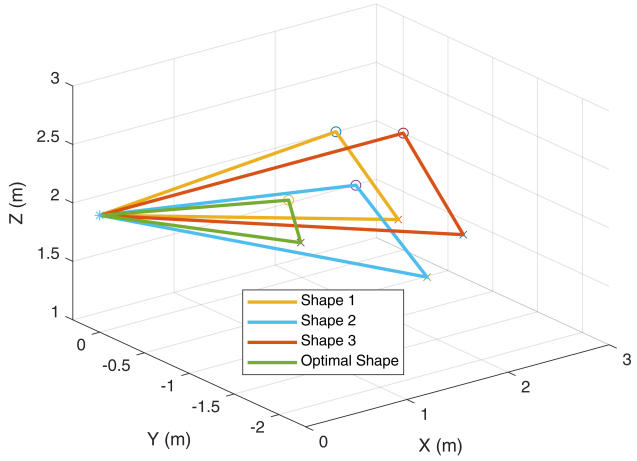

Figure 8.7: The optimal and three arbitrary reference formation shapes. The star, circle and cross symbols denote the reference positions for the first, second and third UAVs, respectively.

optimization is the most power efficient of the four.

8.4 Summary

In this chapter, an optimization problem was formulated to achieve a formation shape for the quad-copters that places the payload at a desired position and orientation,

Table 8.1: Comparison of power usage for four different formations. The last column represents an index (i.e. $\sum_{i=1}^{3} \frac{\mathcal{P}_i}{\xi} = \sum_{i=1}^{3} f_{i_{ss}}^{1.5} = \sum_{i=1}^{3} \|\mu_{i_{ss}}\|^{1.5}$) for power consumption of the system during a 25-second hovering flight.

Triangle Shapes	$q_{d_2} - q_{d_1}$	$q_{d_3} - q_{d_1}$	mean $(\sum_{i=1}^{3} \|\mu_{i_{ss}}\|^{1.5})$
Optimized Formation	$[2.6 \quad 0.3 \quad 0]^{\mathrm{T}}$	$[1.8 \quad -1.3 \quad 0]^{\mathrm{T}}$	68.95
Arbitrary Formation 1	$[2.0 \quad -0.6 \quad 0]^{\mathrm{T}}$	$[1.2 \quad -2.3 \quad 0]^{\mathrm{T}}$	71.65
Arbitrary Formation 2	$[3.0 \quad 0 \quad 0]^{\mathrm{T}}$	$[2.0 \quad -1.8 \quad 0]^{\mathrm{T}}$	72.11
Arbitrary Formation 3	$[1.38 \quad -0.55 \quad 0]^{\mathrm{T}}$	$[0.88 \quad -1.25 \quad 0]^{\mathrm{T}}$	73.88

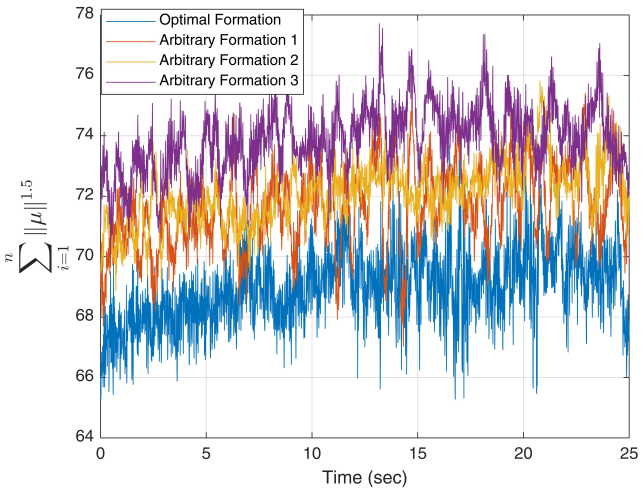

Figure 8.8: Power consumption of the four formation shapes over during a 25-second hovering flight. Note that since UAVs are identical, $\xi_1 = \xi_2 = \xi_3$.

while minimizing the total consumed power during hovering. This optimization problem requires the positions of the payload attachment points. A calibration procedure was proposed to estimate these positions from experiments in quasi-static conditions. It turned out that for light payloads with large effective surface area, quasi-static conditions are hard to achieve due to airflow interference among the quad-copters and the payload. Further research is needed to investigate this phenomenon and develop effective modeling, estimation and control strategies for such payloads. Experiments with another payload modeled as a point mass demonstrated that an optimized formation shape consumes less power than three other arbitrarily chosen formations in a hovering flight.

Chapter 9

Conclusion

This thesis was concerned with the motion control problem of an aerial transport system where multiple quad-copters cooperatively carry a cable-suspended payload. Unlike many existing methods, the proposed passivity-based controllers make no assumption about the cables being in tension. They require no measurements from the payload and consider the under-actuation of quad-copters in their design and stability analysis. A number of improvements to the controller were proposed throughout various chapters in the thesis to help avoid inter-drone collisions and reduce the effect of external disturbances. Detailed stability proofs were provided for all the control schemes. The effectiveness of the proposed controllers were evaluated in experiments carried out in an indoor setting using a motion capture system to measure the quad-copter positions.

The first method was essentially a decentralized controller for the quad-copters that exploited the passivity of the multi-body mechanical system to guarantee the system stability. The quad-copter controllers have a cascaded architecture with inner-loop attitude and outer-loop position control. Initially, the angular controller was

designed to achieve exponential convergence of the tracking errors. This attitude controller required the first and second derivatives of the desired attitude, which itself was the output of the outer-loop controller, ultimately leading to linear acceleration and jerk measurements in the control signals. A modified controller was proposed to address this issue by eliminating the derivatives of the desired attitude in the inner-loop controller. Moreover, this controller used an energy observer to estimate injected energy into the system by external disturbances and dissipated this energy via time-varying dampers. Experimental results showed a significant reduction in disturbance-induced oscillations as a result of implementing this scheme.

Next, a modified passivity-based controller was introduced that no longer required the cables being attached to the quad-copters centers of mass. In this controller, a passivity observer monitors the total energy of the system and activates a complementary damper to counter any potential active behavior. The controller was further augmented with a barrier-type controller to help avoid inter-drone collisions. Closed-loop stability was proven where safety constraints were theoretically shown to never be violated. The payload was intentionally perturbed in an experiment to demonstrate the effectiveness of the proposed method in preventing drone-to-drone collisions.

Although decentralized controllers are simple and robust, they might be challenged in preserving the formation shape in response to external perturbations acting on the system. Inter-drone control coupling terms were introduced for a better preservation of the formation shape. Implementation of this controller required communication among the drone, which could potentially be subject to time delay. The stability of the system with such delays was analyzed to obtain conditions that the controller gains need to satisfy in order to maintain stability. The under-actuation was considered in

this analysis. The robust stability of the system was demonstrated in an experiment with three quad-copters and a cable-suspended payload. Furthermore, the distributed cooperative controller was compared to the fully decentralized controller of Chapter 4 in order to highlight its improved capability in preserving the formation shape.

Finally, the thesis presented a method for designing the reference position commands for the proposed controllers. The method involves formulating an optimization problem, the goal of which is to place the payload at a desired position and orientation, while minimizing the total consumed power. This problem was formulated under quasi-static conditions, using kinematic as well as torque balance equations of constraints. Results of experiments showed that the quad-copters consumed less power in the formation determined from the solution of the optimization problem compared with three other other arbitrary formations.

9.1 Future Work

While this thesis made significant contributions towards enabling aerial transportation of cable-suspended payloads, there are still a number of avenues for future research:

- An immediate practical consideration for future work relates to the position measurements in outdoor settings. The work in this thesis was exclusively carried out in an indoor lab environment where a motion capture system provided highly accurate measurements at relatively high update rates. Real-Time Kinematic (RTK) GPS [30] technology can potentially be used to measure the

drones' positions in outdoors. This sensor would be adequate for global positioning of the drones as a group along the path. However, it may not be accurate enough to implement strategies such as inter-drone collision avoidance. To preserve the coordinated movement, the vehicles can measure their relative positions with higher accuracy using other sensors. Intel Realsense depth camera [55] can be a good candidate for this purpose. As a result, the outdoor implementation requires sensor fusion algorithms along with inter-drone communications to achieve accurate measurements in terms of both relative and global positions of the drones.

- Path and trajectory planing algorithms must be developed to allow the system operate in environments cluttered with obstacles and where flight restrictions exist. These algorithms must consider other operational constraints in planing the reference trajectories for the quad-copters that are safe and energy efficient.

- Experiments showed that light payloads with large effective surface area are prone to significant swings due to airflow interference. More work is needed to properly model these effects and to develop effective payload swing suppression strategies for such scenarios. This may require additional measurements from the payload.

- Scalibility is one of the most important features of the cooperative transportation systems. However, it is not generally straightforward to come up with the required number of drones for a practical application. In order to achieve a high level of robustness, more parameters have to be considered beyond the payload's weight. Failure of drones, payload's volume, disconnection of the cables and etc.

have to be all considered for finding the required number of drones. Given desired robustness margin, an index can be defined to find the required number of UAVs.

- Safety is a critical consideration in aerial transport systems. A drone may fail due to faults in sensors or actuators. It is crucial for the multi-drone system to be somewhat resilient to such faults and or at least avoid catastrophic failure and safely land in such emergencies. An area of interest for future research is fault detection and fault-tolerant control. Operating under fault may require re-configuring of the controller and re-designing of the formation shape on the fly.

- Many tasks are highly sensitive and fully autonomous operations may be risky in such scenarios. A human operator may have to be involved in the loop to supervise the mission and intervene in the task as needed. For instance, the cooperative aerial transportation system can be used in accident sites or search and rescue operations. An operator can guide the flock to a desired location and deliver essential services. With more than three UAVs, the operator can also control the orientation of the payload. This adds extra flexibility for the human to control the system.

Appendix A

Details on proof for Theorem 5

The time derivative of the storage function (7.17) along the system trajectories (7.12), (7.14) and (7.15) can be obtained as,

$$
\begin{aligned}
\dot{V}_1 = & \sum_{i=1}^{n} \dot{\tilde{q}}_i^{\mathrm{T}} \Big(-K_{d_i} \dot{\tilde{q}}_i - K_{p_i} \tilde{q}_i - \sum_{\substack{j=1 \\ j \neq i}}^{n} K_{p_{ij}} \big(\tilde{q}_i - \tilde{q}_j(t - \mathfrak{T}_j) \big) \\
& - \sum_{\substack{j=1 \\ j \neq i}}^{n} K_{d_{ij}} \big(\dot{\tilde{q}}_i - \dot{\tilde{q}}_j(t - \mathfrak{T}_j) \big) + T_i R_L(\eta_L) e_i \Big) \\
& + \sum_{i=1}^{n} \tilde{q}_i^{\mathrm{T}} K_{p_i} \dot{\tilde{q}}_i + \frac{1}{2} \sum_{i=1}^{n} \sum_{\substack{j=1 \\ j \neq i}}^{n} \big(\tilde{q}_i - \tilde{q}_j \big)^{\mathrm{T}} K_{p_{ij}} \big(\dot{\tilde{q}}_i - \dot{\tilde{q}}_j \big) \\
& + \big(\dot{q}_L - \dot{q}_d \big)^{\mathrm{T}} \big(- \sum_{i=1}^{n} T_i R_L(\eta_L) e_i - m_L g z - m_L \ddot{q}_d - D_T \dot{q}_d \big) \\
& + \omega_L^{\mathrm{T}} \big(- \omega_L^{\times} J_L \omega_L - D_R \omega_L - \sum_{i=1}^{n} r_i^{\times} T_i e_i \big) \\
& + \big(D_T \mathcal{Q}_d + m_L g z \big)^{\mathrm{T}} (\dot{q}_L - \dot{q}_d)
\end{aligned}
\tag{A.1}
$$

The terms related to the power of inter-drone interactions require more algebraic manipulations. Consider the power of inter-drone virtual springs, since $\sum_{i=1}^{n}\sum_{\substack{j=1\\j\neq i}}^{n}\dot{\tilde{q}}_j^{\mathrm{T}}K_{p_{ij}}\big(\tilde{q}_i-\tilde{q}_j\big)=-\sum_{i=1}^{n}\sum_{\substack{j=1\\j\neq i}}^{n}\dot{\tilde{q}}_i^{\mathrm{T}}K_{p_{ij}}\big(\tilde{q}_i-\tilde{q}_j\big)$ then, $\frac{1}{2}\sum_{i=1}^{n}\sum_{\substack{j=1\\j\neq i}}^{n}\big(\tilde{q}_i-\tilde{q}_j\big)^{\mathrm{T}}K_{p_{ij}}\big(\dot{\tilde{q}}_i-\dot{\tilde{q}}_j\big)=\sum_{i=1}^{n}\sum_{\substack{j=1\\j\neq i}}^{n}\dot{\tilde{q}}_i^{\mathrm{T}}K_{p_{ij}}\big(\tilde{q}_i-\tilde{q}_j\big)$. Adding and subtracting $\tilde{q}_i(t-\mathfrak{T}_j)$, and the fact that $\tilde{q}_j-\tilde{q}_i(t-\mathfrak{T}_j)=\int_{t-\mathfrak{T}_j}^{t}\dot{\tilde{q}}_j(\gamma)d\gamma$ results in,

$$\sum_{i=1}^{n}\sum_{\substack{j=1\\j\neq i}}^{n}\dot{\tilde{q}}_i^{\mathrm{T}}K_{p_{ij}}\Big(\tilde{q}_i-\tilde{q}_i(t-\mathfrak{T}_j)+\tilde{q}_i(t-\mathfrak{T}_j)-\tilde{q}_j\Big)= \tag{A.2}$$
$$\sum_{i=1}^{n}\sum_{\substack{j=1\\j\neq i}}^{n}\dot{\tilde{q}}_i^{\mathrm{T}}K_{p_{ij}}\Big(\tilde{q}_i-\tilde{q}_i(t-\mathfrak{T}_j)\Big)-\sum_{i=1}^{n}\sum_{\substack{j=1\\j\neq i}}^{n}\dot{\tilde{q}}_i^{\mathrm{T}}K_{p_{ij}}\int_{t-\mathfrak{T}_j}^{t}\dot{\tilde{q}}_j(\gamma)d\gamma$$

It follows from Lemma (2) that the following upper-bound exists for the second term on the right hand side of (A.2),

$$-\sum_{i=1}^{n}\sum_{\substack{j=1\\j\neq i}}^{n}\dot{\tilde{q}}_i^{\mathrm{T}}K_{p_{ij}}\int_{t-\mathfrak{T}_j}^{t}\dot{\tilde{q}}_j(\gamma)d\gamma\leq\sum_{i=1}^{n}\dot{\tilde{q}}_i^{\mathrm{T}}(t)\Big(\sum_{\substack{j=1\\j\neq i}}^{n}\frac{\mathfrak{T}_j}{4}K_{p_{ij}}^2\Big)\dot{\tilde{q}}_i(t) \tag{A.3}$$
$$+\sum_{i=1}^{n}\sum_{j=1}^{n}\int_{t-\mathfrak{T}_j}^{t}\dot{\tilde{q}}_j^{\mathrm{T}}(\gamma)\dot{\tilde{q}}_j(\gamma)d\gamma$$

The power of inter-drone virtual dampers can be rewritten as,

$$-\sum_{i=1}^{n}\sum_{\substack{j=1\\j\neq i}}^{n}\dot{\tilde{q}}_i^{\mathrm{T}}K_{d_{ij}}\Big(\dot{\tilde{q}}_i-\dot{\tilde{q}}_j(t-\mathfrak{T}_j)\Big)=-\sum_{i=1}^{n}\dot{\tilde{q}}_i^{\mathrm{T}}\Big(\sum_{\substack{j=1\\j\neq i}}^{n}K_{d_{ij}}\Big)\dot{\tilde{q}}_i \tag{A.4}$$
$$+\sum_{i=1}^{n}\dot{\tilde{q}}_i^{\mathrm{T}}\sum_{\substack{j=1\\j\neq i}}^{n}K_{d_{ij}}\dot{\tilde{q}}_j(t-\mathfrak{T}_j)$$

It follows from property $-a^{\mathrm{T}}b \leq \frac{a^{\mathrm{T}}a}{4} + b^{\mathrm{T}}b$, $\forall a, b \in \mathbb{R}^3$ and proof by induction that the following upper-bound exists for the second term on the right hand side of (A.4),

$$\sum_{i=1}^{n} \dot{\tilde{q}}_i^{\mathrm{T}} \sum_{\substack{j=1 \\ j\neq i}}^{n} K_{d_{ij}} \dot{\tilde{q}}_j(t-\mathfrak{T}_j) \leq \sum_{i=1}^{n} \dot{\tilde{q}}_i^{\mathrm{T}} \Big(\sum_{\substack{j=1 \\ j\neq i}}^{n} K_{d_{ij}} \Big) \dot{\tilde{q}}_i + \sum_{i=1}^{n} \Big(\dot{\tilde{q}}_i^{\mathrm{T}}(t-\mathfrak{T}_i) \big(\sum_{\substack{j=1 \\ j\neq i}}^{n} \frac{K_{d_{ij}}}{4} \big) \dot{\tilde{q}}_i(t-\mathfrak{T}_i) \Big) \tag{A.5}$$

Now, it follows from (A.4) and (A.5) that,

$$-\sum_{i=1}^{n} \sum_{\substack{j=1 \\ j\neq i}}^{n} \dot{\tilde{q}}_i^{\mathrm{T}} K_{d_{ij}} \Big(\dot{\tilde{q}}_i - \dot{\tilde{q}}_j(t-\mathfrak{T}_j) \Big) \leq \sum_{i=1}^{n} \Big(\dot{\tilde{q}}_i^{\mathrm{T}}(t-\mathfrak{T}_i) \big(\sum_{\substack{j=1 \\ j\neq i}}^{n} \frac{K_{d_{ij}}}{4} \big) \dot{\tilde{q}}_i(t-\mathfrak{T}_i) \Big) \tag{A.6}$$

The time derivative of the storage function in 7.18 can be found as,

$$\dot{V}_2 \leq \sum_{i=1}^{n} \dot{\tilde{q}}_i^{\mathrm{T}} (n\mathfrak{T}_i I_3) \dot{\tilde{q}}_i - \sum_{i=1}^{n} \sum_{j=1}^{n} \int_{t-\mathfrak{T}_j}^{t} \dot{\tilde{q}}_j^{\mathrm{T}}(\gamma) \dot{\tilde{q}}_j(\gamma) d\gamma \tag{A.7}$$

where we used the following two facts that $\sum_{j=1}^{n} 1 = n$ and $\sum_{j=1}^{n} \sum_{i=1}^{n} \int_{t-\mathfrak{T}_i}^{t} \dot{\tilde{q}}_i^{\mathrm{T}}(\gamma) \dot{\tilde{q}}_i(\gamma) d\gamma = \sum_{i=1}^{n} \sum_{j=1}^{n} \int_{t-\mathfrak{T}_j}^{t} \dot{\tilde{q}}_j^{\mathrm{T}}(\gamma) \dot{\tilde{q}}_j(\gamma) d\gamma$. Now, it follows the time derivatives of the storage functions (A.1), (A.7), the property $a^{\mathrm{T}}b \leq \frac{\epsilon a^{\mathrm{T}}a}{4} + \frac{b^{\mathrm{T}}b}{\epsilon}$, $\forall a, b \in \mathbb{R}^3, \epsilon \in \mathbb{R}^+$, along with the

algebraic manipulations (A.2), (A.3), (A.6) that,

$$\begin{aligned}\dot{V} \leq & -\sum_{i=1}^{n} \dot{\tilde{q}}_i^{\mathrm{T}} \Big(K_{d_i} - n\mathfrak{T}_i \mathcal{I}_3 - \sum_{\substack{j=1 \\ j\neq i}}^{n} \frac{\mathfrak{T}_j}{4} K_{p_{ij}}^2 \Big) \dot{\tilde{q}}_i \\ & + \sum_{i=1}^{n} \Big(\dot{\tilde{q}}_i^{\mathrm{T}}(t-\mathfrak{T}_i) \big(\sum_{\substack{j=1 \\ j\neq i}}^{n} \frac{K_{d_{ij}}}{4} \big) \dot{\tilde{q}}_i(t-\mathfrak{T}_i) \Big) \\ & - \omega_L^{\mathrm{T}} D_R \omega_L - (\dot{q}_L - \dot{q}_d)^{\mathrm{T}} (D_T - \frac{\epsilon I_3}{4})(\dot{q}_L - \dot{q}_d) \\ & + \frac{1}{\epsilon} (D_T \dot{\mathfrak{q}}_d + m_L \ddot{q}_d)^{\mathrm{T}} (D_T \dot{\mathfrak{q}}_d + m_L \ddot{q}_d)\end{aligned} \tag{A.8}$$

Appendix B

Numerical Value of P Matrix

Since the P matrix is symmetric, it can be rewritten as,

$$P_{18\times18} = \begin{bmatrix} P_{11} & P_{12} \\ P_{12} & P_{22} \end{bmatrix} \tag{B.1}$$

where P_{11}, P_{12} and $P_{22} \in \mathbb{R}^{9\times 9}$ and are obtained as,

$$P_{11} = \begin{bmatrix} 0.644 & 0 & 0 & 0.061 & 0 & 0 & 0.001 & 0 & 0 \\ 0 & 0.6948 & 0 & 0 & 0.0833 & 0 & 0 & 0.0225 & 0 \\ 0 & 0 & 0.713 & 0 & 0 & 0.0672 & 0 & 0 & 0.018 \\ 0.061 & 0 & 0 & 0.035 & 0 & 0 & 0.0125 & 0 & 0 \\ 0 & 0.0833 & 0 & 0 & 0.0518 & 0 & 0 & 0.0229 & 0 \\ 0 & 0 & 0.0672 & 0 & 0 & 0.0425 & 0 & 0 & 0.0149 \\ 0.001 & 0 & 0 & 0.0125 & 0 & 0 & 0.6446 & 0 & 0 \\ 0 & 0.0225 & 0 & 0 & 0.0229 & 0 & 0 & 0.6948 & 0 \\ 0 & 0 & 0.0180 & 0 & 0 & 0.0149 & 0 & 0 & 0.7137 \end{bmatrix} \tag{B.2}$$

$$P_{12} = \begin{bmatrix} 0.0125 & 0 & 0 & 0.001 & 0 & 0 & 0.0125 & 0 & 0 \\ 0 & 0.0229 & 0 & 0 & 0.0225 & 0 & 0 & 0.0229 & 0 \\ 0 & 0 & 0.0149 & 0 & 0 & 0.018 & 0 & 0 & 0.0149 \\ 0.0061 & 0 & 0 & 0.0125 & 0 & 0 & 0.0061 & 0 & 0 \\ 0 & 0.0144 & 0 & 0 & 0.0229 & 0 & 0 & 0.0144 & 0 \\ 0 & 0 & 0.0096 & 0 & 0 & 0.0149 & 0 & 0 & 0.0096 \\ 0.0610 & 0 & 0 & 0.001 & 0 & 0 & 0.0125 & 0 & 0 \\ 0 & 0.0833 & 0 & 0 & 0.0225 & 0 & 0 & 0.0229 & 0 \\ 0 & 0 & 0.0672 & 0 & 0 & 0.018 & 0 & 0 & 0.0149 \end{bmatrix} \tag{B.3}$$

$$P_{22} = \begin{bmatrix} 0.0350 & 0 & 0 & 0.0125 & 0 & 0 & 0.0061 & 0 & 0 \\ 0 & 0.0518 & 0 & 0 & 0.0229 & 0 & 0 & 0.0144 & 0 \\ 0 & 0 & 0.0425 & 0 & 0 & 0.0149 & 0 & 0 & 0.0096 \\ 0.0125 & 0 & 0 & 0.6446 & 0 & 0 & 0.0610 & 0 & 0 \\ 0 & 0.0229 & 0 & 0 & 0.6948 & 0 & 0 & 0.0833 & 0 \\ 0 & 0 & 0.0149 & 0 & 0 & 0.7137 & 0 & 0 & 0.0672 \\ 0.0061 & 0 & 0 & 0.0610 & 0 & 0 & 0.0350 & 0 & 0 \\ 0 & 0.0144 & 0 & 0 & 0.0833 & 0 & 0 & 0.0518 & 0 \\ 0 & 0 & 0.0096 & 0 & 0 & 0.0672 & 0 & 0 & 0.0425 \end{bmatrix} \tag{B.4}$$

Using MATLAB, the eigenvalues of P matrix can be found as,

$$\begin{aligned} \lambda_P = \{&0.0251, 0.0251, 0.0288, 0.0288, 0.0317, 0.0317, \\ &0.0351, 0.0484, 0.0563, 0.6473, 0.6473, 0.6587, \\ &0.6779, 0.6779, 0.6998, 0.6998, 0.7631, 0.7642\} \end{aligned}$$

Bibliography

[1] Alexis, K., Nikolakopoulos, G., and Tzes, A. (2012). Model predictive quadrotor control: attitude, altitude and position experimental studies. *IET Control Theory & Applications*, **6**(12), 1812–1827.

[2] Atashzar, S. F., Shahbazi, M., Tavakoli, M., and Patel, R. V. (2016). A passivity-based approach for stable patient–robot interaction in haptics-enabled rehabilitation systems: modulated time-domain passivity control. *IEEE Transactions on Control Systems Technology*, **25**(3), 991–1006.

[3] Barkana, I. (2014). Defending the beauty of the invariance principle. *International Journal of Control*, **87**(1), 186–206.

[4] Bernard, M., Kondak, K., Maza, I., and Ollero, A. (2011). Autonomous transportation and deployment with aerial robots for search and rescue missions. *Journal of Field Robotics*, **28**(6), 914–931.

[5] Bouffard, P., Aswani, A., and Tomlin, C. (2012). Learning-based model predictive control on a quadrotor: Onboard implementation and experimental results. In *2012 IEEE International Conference on Robotics and Automation*, pages 279–284. IEEE.

[6] Brogliato, B., Ortega, R., and Lozano, R. (1995). Global tracking controllers for flexible-joint manipulators: a comparative study. *Automatica*, **31**(7), 941–956.

[7] Cai, G., Dias, J., and Seneviratne, L. (2014). A survey of small-scale unmanned aerial vehicles: Recent advances and future development trends. *Unmanned Systems*, **2**(02), 175–199.

[8] Chen, T. and Shan, J. (2020). A novel cable-suspended quadrotor transportation system: From theory to experiment. *Aerospace Science and Technology*, **104**, 105974.

[9] Chiang, W.-C., Li, Y., Shang, J., and Urban, T. L. (2019). Impact of drone delivery on sustainability and cost: Realizing the uav potential through vehicle routing optimization. *Applied energy*, **242**, 1164–1175.

[10] Chiasson, J. (1998). A new approach to dynamic feedback linearization control of an induction motor. *IEEE Transactions on Automatic Control*, **43**(3), 391–397.

[11] Cruz, P. J. and Fierro, R. (2017). Cable-suspended load lifting by a quadrotor uav: hybrid model, trajectory generation, and control. *Autonomous Robots*, **41**(8), 1629–1643.

[12] Cruz, P. J., Oishi, M., and Fierro, R. (2015). Lift of a cable-suspended load by a quadrotor: A hybrid system approach. In *2015 American Control Conference (ACC)*, pages 1887–1892. IEEE.

[13] Diebel, J. (2006). Representing attitude: Euler angles, unit quaternions, and rotation vectors. *Matrix*, **58**(15-16), 1–35.

[14] Doumbia-Henry, C. (2020). Shipping and covid-19: protecting seafarers as front-line workers. *WMU Journal of Maritime Affairs*, **19**(3), 279–293.

[15] Doyle, J. C., Francis, B. A., and Tannenbaum, A. R. (2013). *Feedback control theory*. Courier Corporation.

[16] Dubey, P. P. and Borkar, P. (2015). Review on techniques for traffic jam detection and congestion avoidance. In *2015 2nd International Conference on Electronics and Communication Systems (ICECS)*, pages 434–440. IEEE.

[17] Dyer, E., Sirouspour, S., and Jafarinasab, M. (2019). Energy optimal control allocation in a redundantly actuated omnidirectional uav. In *2019 International Conference on Robotics and Automation (ICRA)*, pages 5316–5322.

[18] Eberts, R. (2000). Understanding the impact of transportation on economic development. *Transportation in the New Millennium*, **8**.

[19] Egeland, O. and Godhavn, J.-M. (1994). Passivity-based adaptive attitude control of a rigid spacecraft. *IEEE Transactions on Automatic Control*, **39**(4), 842–846.

[20] Ferraguti, F., Secchi, C., and Fantuzzi, C. (2013). A tank-based approach to impedance control with variable stiffness. In *2013 IEEE International Conference on Robotics and Automation*, pages 4948–4953. IEEE.

[21] Ferraguti, F., Preda, N., Manurung, A., Bonfe, M., Lambercy, O., Gassert, R., Muradore, R., Fiorini, P., and Secchi, C. (2015). An energy tank-based interactive control architecture for autonomous and teleoperated robotic surgery. *IEEE Transactions on Robotics*, **31**(5), 1073–1088.

[22] Fielding, S. and Nahon, M. (2019). Input shaped trajectory generation and controller design for a quadrotor-slung load system. In *2019 International Conference on Unmanned Aircraft Systems (ICUAS)*, pages 162–170. IEEE.

[23] Fossen, T. I. and Sagatun, S. I. (1991). Adaptive control of nonlinear underwater robotic systems. In *Proceedings. 1991 IEEE International Conference on Robotics and Automation*, pages 1687–1694 vol.2.

[24] Godbole, A. R. and Subbarao, K. (2019). Nonlinear control of unmanned aerial vehicles with cable suspended payloads. *Aerospace Science and Technology*, **93**, 105299.

[25] Guerrero, M., Mercado, D., Lozano, R., and García, C. (2015). Ida-pbc methodology for a quadrotor uav transporting a cable-suspended payload. In *2015 International Conference on Unmanned Aircraft Systems (ICUAS)*, pages 470–476. IEEE.

[26] Gwilliam, K., Kojima, M., and Johnson, T. (2004). *Reducing air pollution from urban transport*. World Bank Washington, DC.

[27] Hannaford, B. and Ryu, J.-H. (2002). Time-domain passivity control of haptic interfaces. *IEEE Transactions on Robotics and Automation*, **18**(1), 1–10.

[28] Hassanalian, M. and Abdelkefi, A. (2017). Classifications, applications, and design challenges of drones: A review. *Progress in Aerospace Sciences*, **91**, 99–131.

[29] Hatanaka, T., Chopra, N., and Spong, M. W. (2015). Passivity-based control of robots: Historical perspective and contemporary issues. In *2015 54th IEEE Conference on Decision and Control (CDC)*, pages 2450–2452. IEEE.

[30] Holman, R. A., Brodie, K. L., and Spore, N. J. (2017). Surf zone characterization using a small quadcopter: Technical issues and procedures. *IEEE Transactions on Geoscience and Remote Sensing*, **55**(4).

[31] Howell, T. A., Jackson, B. E., and Manchester, Z. (2019). Altro: A fast solver for constrained trajectory optimization. In *2019 IEEE/RSJ International Conference on Intelligent Robots and Systems (IROS)*, pages 7674–7679. IEEE.

[32] Hua, C.-C. and Liu, X. P. (2010). Delay-dependent stability criteria of teleoperation systems with asymmetric time-varying delays. *IEEE Transactions on Robotics*, **26**(5), 925–932.

[33] Jackson, B. E., Howell, T. A., Shah, K., Schwager, M., and Manchester, Z. (2020). Scalable cooperative transport of cable-suspended loads with uavs using distributed trajectory optimization. *IEEE Robotics and Automation Letters*, **5**(2), 3368–3374.

[34] Jafarinasab, M., Sirouspour, S., and Dyer, E. (2019). Model-based motion control of a robotic manipulator with a flying multirotor base. *IEEE/ASME Transactions on Mechatronics*, **24**(5), 2328–2340.

[35] Kelly, R. (1999). Regulation of manipulators in generic task space: An energy shaping plus damping injection approach. *IEEE Transactions on Robotics and Automation*, **15**(2), 381–386.

[36] Kelly, R., Davila, V. S., and Perez, J. A. L. (2006). *Control of robot manipulators in joint space*. Springer Science & Business Media.

[37] Kendoul, F. (2009). Nonlinear hierarchical flight controller for unmanned rotorcraft: design, stability, and experiments. *Journal of guidance, control, and dynamics*, **32**(6), 1954–1958.

[38] Keselman, L., Iselin Woodfill, J., Grunnet-Jepsen, A., and Bhowmik, A. (2017). Intel realsense stereoscopic depth cameras. In *Proceedings of the IEEE Conference on Computer Vision and Pattern Recognition Workshops*, pages 1–10.

[39] Khalil, H. K. and Grizzle, J. W. (2002). *Nonlinear systems*, volume 3. Prentice hall Upper Saddle River, NJ.

[40] Khosravi, M. A. and Taghirad, H. D. (2014). Dynamic modeling and control of parallel robots with elastic cables: singular perturbation approach. *IEEE Transactions on Robotics*, **30**(3), 694–704.

[41] Kim, J., Gadsden, S. A., and Wilkerson, S. A. (2019). A comprehensive survey of control strategies for autonomous quadrotors. *Canadian Journal of Electrical and Computer Engineering*, **43**(1), 3–16.

[42] Kishk, M., Bader, A., and Alouini, M.-S. (2020). Aerial base station deployment in 6g cellular networks using tethered drones: The mobility and endurance tradeoff. *IEEE Vehicular Technology Magazine*, **15**(4), 103–111.

[43] Klausen, K., Fossen, T. I., and Johansen, T. A. (2017). Nonlinear control with swing damping of a multirotor uav with suspended load. *Journal of Intelligent & Robotic Systems*, **88**(2), 379–394.

[44] Klausen, K., Meissen, C., Fossen, T. I., Arcak, M., and Johansen, T. A. (2018). Cooperative control for multirotors transporting an unknown suspended load under

environmental disturbances. *IEEE Transactions on Control Systems Technology*, **28**(2), 653–660.

[45] Kot, M. (2014). *A first course in the calculus of variations*, volume 72. American Mathematical Society.

[46] Lee, D. (2007). Passivity-based switching control for stabilization of wheeled mobile robots. In *Robotics: Science and Systems*.

[47] Lee, D. and Lui, K. Y. (2016). Passive configuration decomposition and passivity-based control of nonholonomic mechanical systems. *IEEE Transactions on Robotics*, **33**(2), 281–297.

[48] Lee, T. (2017). Geometric control of quadrotor uavs transporting a cable-suspended rigid body. *IEEE Transactions on Control Systems Technology*, **26**(1), 255–264.

[49] Lee, T., Leok, M., and McClamroch, N. H. (2010). Geometric tracking control of a quadrotor uav on se (3). In *49th IEEE conference on decision and control (CDC)*, pages 5420–5425. IEEE.

[50] Liang, X., Fang, Y., Sun, N., and Lin, H. (2017). Nonlinear hierarchical control for unmanned quadrotor transportation systems. *IEEE Transactions on Industrial Electronics*, **65**(4), 3395–3405.

[51] Liang, X., Fang, Y., Sun, N., Lin, H., and Zhao, X. (2019). Adaptive nonlinear hierarchical control for a rotorcraft transporting a cable-suspended payload. *IEEE Transactions on Systems, Man, and Cybernetics: Systems*.

[52] Liu, H., Zhao, W., Zuo, Z., and Zhong, Y. (2016). Robust control for quadrotors with multiple time-varying uncertainties and delays. *IEEE Transactions on Industrial Electronics*, **64**(2), 1303–1312.

[53] Liu, H., Ma, T., Lewis, F. L., and Wan, Y. (2019). Robust formation trajectory tracking control for multiple quadrotors with communication delays. *IEEE Transactions on Control Systems Technology*.

[54] Liu, P.-L. (2003). Exponential stability for linear time-delay systems with delay dependence. *Journal of the Franklin Institute*, **340**(6-7), 481–488.

[55] Lourenço, F. and Araujo, H. (2021). Intel realsense sr305, d415 and l515: Experimental evaluation and comparison of depth estimation. In *VISIGRAPP (4: VISAPP)*, pages 362–369.

[56] Maffezzoni, C., Schiavoni, N., and Ferretti, G. (1990). Robust design of cascade control. *IEEE Control Systems Magazine*, **10**(1), 21–25.

[57] Mas, I. and Kitts, C. (2012). Object manipulation using cooperative mobile multi-robot systems. In *Proceedings of the World Congress on Engineering and Computer Science*, volume 1.

[58] Mellinger, D. and Kumar, V. (2011). Minimum snap trajectory generation and control for quadrotors. In *2011 IEEE international conference on robotics and automation*, pages 2520–2525. IEEE.

[59] Michael, N., Fink, J., and Kumar, V. (2011). Cooperative manipulation and transportation with aerial robots. *Autonomous Robots*, **30**(1), 73–86.

[60] Mohammadi, A., Tavakoli, M., Marquez, H. J., and Hashemzadeh, F. (2013). Nonlinear disturbance observer design for robotic manipulators. *Control Engineering Practice*, **21**(3), 253–267.

[61] Mohammadi, K., Talebi, H. A., and Zareinejad, M. (2016). A novel position and force coordination approach in four channel nonlinear teleoperation. *Computers & Electrical Engineering*, **56**, 688–699.

[62] Mohammadi, K., Jafarinasab, M., Sirouspour, S., and Dyer, E. (2018). Decentralized motion control in a cabled-based multi-drone load transport system. In *2018 IEEE/RSJ International Conference on Intelligent Robots and Systems (IROS)*, pages 4198–4203. IEEE.

[63] Mohammadi, K., Sirouspour, S., and Grivani, A. (2020). Control of multiple quad-copters with a cable-suspended payload subject to disturbances. *IEEE/ASME Transactions on Mechatronics*.

[64] Mualla, Y., Najjar, A., Galland, S., Nicolle, C., Haman Tchappi, I., Yasar, A.-U.-H., and Främling, K. (2019). Between the megalopolis and the deep blue sky: Challenges of transport with uavs in future smart cities. In *Proceedings of the 18th International Conference on Autonomous Agents and MultiAgent Systems*, pages 1649–1653.

[65] Na, W. K. and Gou, B. (2008). Feedback-linearization-based nonlinear control for pem fuel cells. *IEEE Transactions on Energy Conversion*, **23**(1), 179–190.

[66] Nascimento, T. P. and Saska, M. (2019). Position and attitude control of multi-rotor aerial vehicles: A survey. *Annual Reviews in Control*, **48**, 129–146.

[67] Nonami, K., Kendoul, F., Suzuki, S., Wang, W., and Nakazawa, D. (2010). *Autonomous flying robots: unmanned aerial vehicles and micro aerial vehicles*. Springer Science & Business Media.

[68] Nuño, E., Basañez, L., and Ortega, R. (2011). Passivity-based control for bilateral teleoperation: A tutorial. *Automatica*, **47**(3), 485–495.

[69] Oh, K.-K., Park, M.-C., and Ahn, H.-S. (2015). A survey of multi-agent formation control. *Automatica*, **53**, 424–440.

[70] Ortega, R. and Spong, M. W. (1989). Adaptive motion control of rigid robots: A tutorial. *Automatica*, **25**(6), 877–888.

[71] Panagou, D., Turpin, M., and Kumar, V. (2019). Decentralized goal assignment and safe trajectory generation in multi-robot networks via multiple lyapunov functions. *IEEE Transactions on Automatic Control*.

[72] Pettersen, K. Y. (2017). Lyapunov sufficient conditions for uniform semiglobal exponential stability. *Automatica*, **78**, 97–102.

[73] Qian, L., Graham, S., and Liu, H. H.-T. (2020). Guidance and control law design for a slung payload in autonomous landing: A drone delivery case study. *IEEE/ASME Transactions on Mechatronics*, **25**(4), 1773–1782.

[74] Rezaee, H. and Abdollahi, F. (2017). Almost sure attitude consensus in multispacecraft systems with stochastic communication links. *IFAC-PapersOnLine*, **50**(1), 9392–9397.

[75] Ríos, H., Falcón, R., González, O. A., and Dzul, A. (2018). Continuous sliding-mode control strategies for quadrotor robust tracking: Real-time application. *IEEE Transactions on Industrial Electronics*, **66**(2), 1264–1272.

[76] Sanalitro, D., Savino, H. J., Tognon, M., Cortés, J., and Franchi, A. (2020). Full-pose manipulation control of a cable-suspended load with multiple uavs under uncertainties. *IEEE Robotics and Automation Letters*, **5**(2), 2185–2191.

[77] Sepulchre, R., Jankovic, M., and Kokotovic, P. V. (2012). *Constructive nonlinear control*. Springer Science & Business Media.

[78] Spong, M. W. (1994). Partial feedback linearization of underactuated mechanical systems. In *Proceedings of IEEE/RSJ International Conference on Intelligent Robots and Systems (IROS'94)*, volume 1, pages 314–321. IEEE.

[79] Spong, M. W., Hutchinson, S., Vidyasagar, M., *et al.* (2006). *Robot modeling and control*.

[80] Sreenath, K. and Kumar, V. (2013). Dynamics, control and planning for cooperative manipulation of payloads suspended by cables from multiple quadrotor robots. *Proc. Robot., Sci. Syst.*

[81] Sreenath, K., Lee, T., and Kumar, V. (2013a). Geometric control and differential flatness of a quadrotor uav with a cable-suspended load. In *52nd IEEE Conference on Decision and Control*, pages 2269–2274. IEEE.

[82] Sreenath, K., Michael, N., and Kumar, V. (2013b). Trajectory generation and

control of a quadrotor with a cable-suspended load-a differentially-flat hybrid system. In *2013 IEEE International Conference on Robotics and Automation*, pages 4888–4895. IEEE.

[83] Tang, S. and Kumar, V. (2015). Mixed integer quadratic program trajectory generation for a quadrotor with a cable-suspended payload. In *2015 IEEE international conference on robotics and automation (ICRA)*, pages 2216–2222. IEEE.

[84] Tang, S., Wüest, V., and Kumar, V. (2018). Aggressive flight with suspended payloads using vision-based control. *IEEE Robotics and Automation Letters*, **3**(2), 1152–1159.

[85] Tao, G. (1997). A simple alternative to the barbalat lemma. *IEEE Transactions on Automatic Control*, **42**(5), 698.

[86] Tee, K. P., Ge, S. S., and Tay, E. H. (2009). Barrier lyapunov functions for the control of output-constrained nonlinear systems. *Automatica*, **45**(4), 918–927.

[87] Thapa, S., Bai, H., and Acosta, J. Á. (2020). Cooperative aerial manipulation with decentralized adaptive force-consensus control. *Journal of Intelligent & Robotic Systems*, **97**(1), 171–183.

[88] Thiels, C. A., Aho, J. M., Zietlow, S. P., and Jenkins, D. H. (2015). Use of unmanned aerial vehicles for medical product transport. *Air medical journal*, **34**(2), 104–108.

[89] Utkin, V. (2015). Discussion aspects of high-order sliding mode control. *IEEE Transactions on Automatic Control*, **61**(3), 829–833.

[90] Villa, D. K., Brandão, A. S., and Sarcinelli-Filho, M. (2018). Load transportation using quadrotors: A survey of experimental results. In *2018 International Conference on Unmanned Aircraft Systems (ICUAS)*, pages 84–93. IEEE.

[91] Wehbeh, J., Rahman, S., and Sharf, I. (2020). Distributed model predictive control for uavs collaborative payload transport. In *2020 IEEE/RSJ International Conference on Intelligent Robots and Systems (IROS)*, pages 11666–11672.

[92] Yoo, W., Yu, E., and Jung, J. (2018). Drone delivery: Factors affecting the public's attitude and intention to adopt. *Telematics and Informatics*, **35**(6), 1687–1700.

[93] Zuo, Z. (2013). Adaptive trajectory tracking control design with command filtered compensation for a quadrotor. *Journal of vibration and control*, **19**(1), 94–108.